CONSERVATOIRE NATIONAL DES ARTS ET MÉTIERS | le cnam

UNIVERSITÉ FÉDÉRALE DE SANTA CATARINA | UFSC

École Doctorale du Conservatoire National des Arts et Métiers

Laboratoire CEDRIC/LAETITIA

THÈSE DE DOCTORAT

présentée par : **Bruno SENS CHANG**

soutenue le : **24 septembre 2012**

pour obtenir le grade de : **Docteur du Conservatoire National des Arts et Métiers et de l'Université Fédérale de Santa Catarina**

Spécialité : **Lasers, Métrologie et Communications**

Nouvelles Techniques de Précodage et d'Égalisation pour les Systèmes Multiporteuses

THÈSE DIRIGÉE PAR

M. Carlos Aurélio FARIA DA ROCHA	*Dr., UFSC*
M. Didier LE RUYET	*Dr., CNAM*

RAPPORTEUR

M. João Cesar MOURA MOTA	*Dr., UFC*

EXAMINATEURS

M. João Marcos TRAVASSOS ROMANO	*Dr., UNICAMP*
M. Daniel ROVIRAS	*Dr., CNAM*
Mme. Mylène PISCHELLA	*Dr., CNAM*

Acknowledgements

First, I would like to thank Thays and my family, for their love, endless support, patience and understanding. This thesis is dedicated to them.

Furthermore, I would like to express my deepest gratitude to my thesis advisors Prof. Carlos Aurélio Faria da Rocha and Prof. Didier Le Ruyet for their friendship, unwavering dedication, trust, constant support and guidance.

Besides, I would like to thank the thesis jury members Prof. João Cesar Moura Mota, Prof. João Marcos Travassos Romano, Prof. Mylène Pischella and specially Prof. Daniel Roviras for their participation which has helped to improve the quality of this work.

I have had the pleasure of having as friends and work colleagues in the Communications Research Group of UFSC and in the LAETITIA laboratory of CNAM Andrei Piccinini Legg, Diego da Silva de Medeiros, Diego Morschbacher, Haijian Zhang, Iness Ahriz, João Fernando Refosco Baggio, João Luiz Rebelatto, Mahmoud Khodjet-Kesba, Pedro Giassi Júnior, Renato Machado, Ricardo Bohaczuk Venturelli, Roberto Wanderley da Nóbrega, Rostom Zakaria, Rym Moncer, Sérgio Okida, Yahia Medjahdi and Yunlong Cai. I would like to thank them for their friendship and the always fruitful discussions.

Additionally, I gratefully acknowledge the financial support of the Brazilian National Counsil for Scientific and Technological Development (CNPq) and the Brazilian Higher Education Co-ordination Agency (CAPES).

Finally, I would like to thank all those whose names have not been cited here, but in some way aided in the realization of this thesis work.

Résumé

Dans cette thèse, de nouvelles techniques d'égalisation et de précodage pour des systèmes multiporteuses ont été proposées et analysées. D'abord, la probabilité d'erreurs des systèmes multiporteuses à base de bancs de filtres (FBMC) précodées a été analysée. Il a été montré que cette performance est très sensible à l'égalisation complète des sous-canaux. Lorsqu' il y a de l'interference inter-symbole residuelle qui vient de l'égalisation imparfaite des sous-canaux, il y a une perte de diversité ; cette diversité peut être récuperée avec l'utilisation d'un nombre de sous-canaux assez grand pour que chaque sous-canaux subisse de l'évanouissement plat ou avec l'utilisation d'un égaliseur par sous-canal avec une longueur suffisante pour compenser cette réponse en fréquence. Une approximation pour la distribution du rapport signal/bruit-plus-interfèrence (SINR) des systèmes SC-FDE qui utilisent égalisation MMSE linéaire a été ensuite proposée. Cette approximation utilise la distribution lognormal avec la plus petit distance de Kullback-Leibler vers la vraie distribution, et nous avons montré qu'elle est précise pour estimer la performance d'erreurs ; elle sert aussi comme une abstraction de ce système. Avec cette abstraction, une méthode précise pour obtenir la performance d'erreur analytique codée de ces systèmes a été proposée. Finalement, des précodeurs Tomlinson-Harashima (THP) et égaliseurs (linéaires et à retour de décision) largement linéaires pour des systèmes SC-FDE ont été proposés. Ces précodeurs et égaliseurs ont une meilleures performance comparés aux versions strictement linéaires lorsque les signaux de constellations impropres sont transmises. Aussi, le taux d'erreurs quand des égaliseurs à retour de décision sont utilisés est moins sensible à la longueur du filtre de retour. Quand des précodeurs largement linéaires sont utilisés, cette performance devient moins sensible aux erreurs d'estimation des canaux.

Mots clés : Systèmes multiporteuses, Précodage, Égalisation, Traitement largement linéaire

Abstract

In this thesis, new precoding and equalization techniques for multicarrier systems were proposed and analyzed. First, the error performance of precoded filterbank multicarrier (FBMC) systems was analyzed. It was found out that this performance is highly sensitive to complete subchannel equalization. When there is residual intersymbol interference (ISI) stemming from imperfect subchannel equalization there is a loss of diversity ; this loss can be prevented with the adoption of a number of subchannels large enough so that each subchannel suffers flat fading or with the utilization of a subchannel equalizer with sufficient length to compensate the subchannel frequency response. After that, an approximation for the signal to interference-plus-noise ratio (SINR) distribution of SC-FDE systems using linear MMSE equalization was proposed. This approximation uses the lognormal distribution with the smallest Kullback-Leibler distance to the true distribution, and was shown to be precise in the error performance sense ; it serves as a system abstraction. With this abstraction, a precise method to obtain the analytical coded error performance of these systems was proposed. Finally, widely linear Tomlinson-Harashima precoders and equalizers (linear and decision-feedback) for SC-FDE systems were proposed. These precoders and equalizers have better error performance when compared to their strictly linear versions if signals coming from an improper constellation are transmitted. Their error performance when decision-feedback equalizers are used is less sensitive to the length of the feedback filter. When widely linear precoders are used, this error performance becomes less sensitive to channel estimation errors.

Keywords : Multicarrier systems, Precoding, Equalization, Widely linear processing

Résumé des Travaux de Thèse

Chapitre 1 - Introduction

Le but de cette thèse est de proposer et d'étudier de nouvelles techniques d'égalisation et de précodage pour les systèmes multiporteuses. D'abord, nous avons étudié le taux d'erreurs des systèmes FBMC/OQAM (FilterBank MultiCarrier/OQAM) précodés. Ensuite, nous avons abordé le problème de l'aproximation du SINR des systèmes multiporteuses précodés qui utilisent l'égalisation linéaire MMSE ; une étude de leurs taux d'erreurs théoriques avec codage est aussi présentée. Finalement, nous avons examiné l'utilisation du traitement largement linéaire dans les précodeurs et égaliseurs pour les systèmes SC-FDE.

Chapitre 2 - État de l'Art

Systèmes OFDM/QAM

L'un des principaux problèmes des systèmes de communication est l'effet des trajets multiples, responsable de la selectivité en frequence. Pour éviter l'usage d'un égaliseur de grande taille dans le domaine temporel, un canal selectif en fréquence peut être partagé en plusieurs sous-canaux plus étroits qui subissent un évanouissement plat. Ces sous-canaux peuvent être égalisés avec des égaliseurs à un coefficient. Ce schéma est connu comme la technique OFDM/QAM, qui utilise la transformée de Fourier rapide pour une implementation moins complexe. En outre, un prefixe cyclique de taille plus grande que celle de la réponse impulsionnelle du canal est ajouté au bloc de symboles pour éliminer l'interference entre symboles (ISI) dans le recepteur.

Filtres prototype

Les systèmes OFDM/QAM conventionnels utilisent une fenêtre rectangulaire comme filtre pour séparer les sous-canaux. L'orthogonalité entre les filtres rectangulaires est affectée dans les systèmes pratiques par les effets du canal (l'interférence entre symboles et entre sous-canaux), *offsets* de temps et fréquence et le bruit. Une façon de surmonter ces problèmes est l'adoption de filtres de Nyquist ayant une bonne localisation en fréquence (c'est-à-dire, avec des lobes secondaires petits en fréquence), en améliorant la séparation entre les sous-canaux. La perte de puissance et de bande, conséquence de l'utilisation du préfixe cyclique, peut être éliminée en adoptant de filtres bien localisés dans le domaine du temps.

Systèmes FBMC/OQAM

L'utilisation de filtres bien localisés en temps et en fréquence, limités en bande et avec une efficacité spectrale maximale pour séparer les sous-canaux dans les systèmes OFDM/QAM conventionnels est impossible. Pour utiliser ces filtres nous devons renoncer à l'orthogonalité complexe, car les filtres bien localisés n'ont que l'orthogonalité réele.

Pour surmonter cet obstacle, la modulation OQAM peut être utilisée ; elle sépare les symboles complexes en parties réelles et imaginaires pour la transmission. Il est possible d'implémenter ce système FBMC/OQAM avec la décomposition polyphase du filtre prototype et l'IFFT ; avec cela, la complexité matérielle est réduite par rapport à une implementation directe (un filtre par chaque sous-canal).

Systèmes OFDM/QAM Précodés

Les systèmes multiporteuses subissent le problème du facteur de crête, de la faible robustesse à des trous spectraux et au *offset* de fréquence de la porteuse (CFO, en anglais). Une façon de surmonter ces obstacles en gardant l'égalisation dans le domaine de la fréquence est l'usage de la précodage linéaire. Dans les systèmes OFDM/QAM conventionnels, l'égalisation de forçage à zéro est l'optimale.Comme l'égalisation est faite bloc par bloc (avant la déprecodage) dans les systèmes OFDM/QAM précodés, les techniques de

maximum de vraisemblance peuvent avoir une complexité trop grande si le système a un nombre de sous-canaux élevé. Ainsi, des techniques d'égalisation linéaires sous-optimales sont souvent utilisées.

Égalisation Linéaire MMSE

Si le SNR est connu à la réception, l'égalisation linéaire basée dans le critere de l'erreur quadratique moyenne minimale (MMSE) peut être apliquée. Avec l'égalisation linéaire MMSE, l'ordre de diversité non-codée des systèmes OFDM/QAM précodés varie selon la taille de la réponse impulsionnelle du canal, la taille de la constellation et le nombre de sous-canaux.

Égalisation avec Retour de Décision MMSE

Un inconvenient de l'égaliseur linéaire MMSE est qu'il n'est pas capable d'éliminer complétement l'ISI. Un égaliseur avec retour de décision (DFE) peut être utilisé pour améliorer le taux d'erreurs, en utilisant les décisions précédentes pour réduire l'ISI post-curseur.

Précodage de Tomlinson-Harashima

Si l'émetteur a des informations complètes de l'état du canal, le filtre de retour du DFE peut être déplacé du récepteur vers l'émetteur pour compenser l'effet de l'ISI, en évitant la propagation des erreurs des systèmes DFE. Avec le filtre de précodage une opération modulo-$2M$ est utilisée pour limiter la puissance à la sortie du précodeur si la réponse impulsionnelle du canal a des valeurs proches de zéro.

Cette technique s'appelle précodage de Tomlinson-Harashima. Comme les décisions dans le recepteur sont instantanées dans les systèmes THP, la codage de canal peut être utilisée avec une bonne performance. Le taux d'erreurs de ces systèmes est la même que celle de systèmes qui utilisent un DFE idéal (c'est-à-dire, sans propagation d'erreur) dans le recepteur à une penalité de puissance prés (qui varie selon la constellation utilisée pour le signal).

Traitement Largement Linéaire

Les systèmes presentés jusqu'à maintenant utilisent un traitement linéaire pour obtenir l'estimation du symbole à partir du signal à l'entrée du recepteur. Pourtant, pour certains signaux, le traitement linéaire ne prend pas en compte toutes les statistiques du second ordre du signal reçu. Pour utiliser toutes ces statistiques le traitement largement linéaire a été proposé.

Chapitre 3 - Systèmes FBMC/OQAM Précodés

Introduction

Le but de ce chapitre est étudier le taux d'erreurs des systèmes FBMC/OQAM précodés, y compris le cas où l'ISI résiduelle qui vient de l'égalisation imparfaite des sous-canaux est présente dans ces systèmes lorsqu'ils utilisent l'égalisation linéaire MMSE. Il est montré que cette ISI residuelle occasionne une perte de diversité dans les systèmes FBMC/OQAM précodés. Une expression analytique du BER pour ces systèmes que prend en compte ou pas cette ISI residuelle est comparée aux resultats des simulations de Monte Carlo pour des différents modéles de canaux afin de démontrer sa précision.

Puissance de l'ISI dans les Systèmes FBMC Non-complétement Égalisés

Dans les systèmes FBMC l'égalisation n'est pas toujours parfaite, à cause de l'absence du préfixe cyclique ; donc, des intérferences residuelles peuvent être présentes. La réponse impulsionnelle réelle désirée doit être zéro en nT_s, $n \neq 0$ pour éliminer l'ISI des autres symboles transmis dans la partie réelle, lorsque la réponse impulsionnelle imaginaire désirée doit être zéro en $\frac{nT_s}{2}$, $n \neq 0$ pour éliminer l'ISI dans les symboles transmis dans la partie imaginaire. Les autres instants ne seront pas pris en compte.

Cette réponse impulsionnelle idéale resultera dans une réponse en fréquence égalisée plat du sous-canal $H_k^{eq}(f)$; ainsi, des déviations de cette réponse plat correspondront à de l'ISI supplémentaire dans le symbole détecté, parce que cette réponse en fréquence du sous-canal non-plat signifie que l'énergie du symbole a été étalée vers les autres symboles.

Donc, nous intégrons sur ce spectre résiduel du sous-canal pour déterminer la puissance

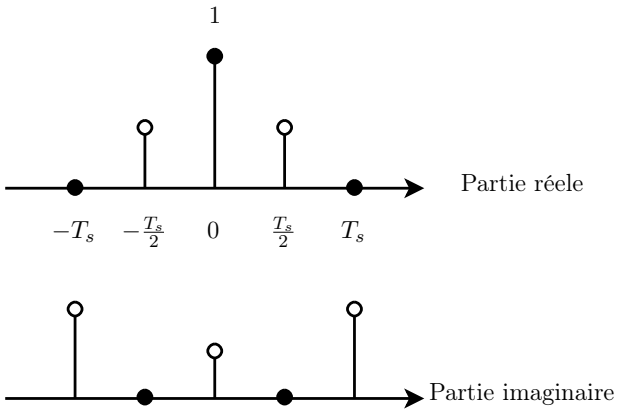

Réponse impulsionnelle complexe désirée aprés égalisation dans les systèmes FBMC.

$\sigma^2_{\text{ISI},k}$ de cette ISI supplémentaire dans le k-ème sous-canal, selon l'équation suivante.

$$\sigma^2_{\text{ISI},k} = \int_{-\infty}^{\infty} |1 - H_k^{eq}(f)|^2 df.$$

La puissance de l'ISI qui vient des sous-canaux non-complètement égalisés sera ajoutée à la variance du bruit AWGN (en considérant cette ISI comme gaussienne grâce au grand nombre de sous-canaux) pour former le SINR effectif d'un système FBMC précodé qui utilise l'égalisation MMSE. L'expression qui définit ce SINR est donnée par

$$\gamma_{\text{MMSE,ISI}} = \frac{1}{\text{MSE}_{\text{MMSE,ISI}}} - 1,$$

où

$$\text{MSE}_{\text{MMSE,ISI}} = \frac{1}{N} \sum_{n=1}^{N} \frac{1}{\zeta_k |H_n|^2 + 1}.$$

et $\zeta_k = \frac{Es}{N_0 + \sigma^2_{\text{ISI},k}}$.

Si l'égaliseur du sous-canal a une taille assez grande pour compenser la réponse en fréquence du sous-canal ou le nombre de sous-canaux est assez grand de façon que la réponse en fréquence des sous-canaux soit plat, l'équation précédente du SINR est réduite vers les équations connues de la MSE et du SINR pour les systèmes multiporteuse précodés utilisant l'égalisation linéaire MMSE.

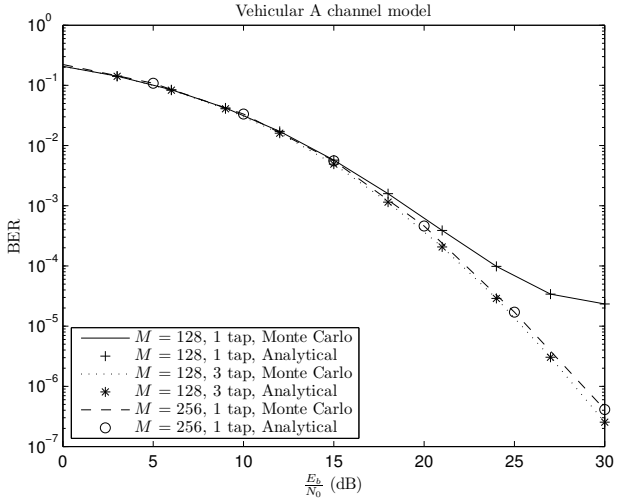

Taux d'erreurs pour les systèmes FBMC non codés précodés qui utilisent l'égalisation MMSE en transmettant à travers du modèle de canal Vehicular A.

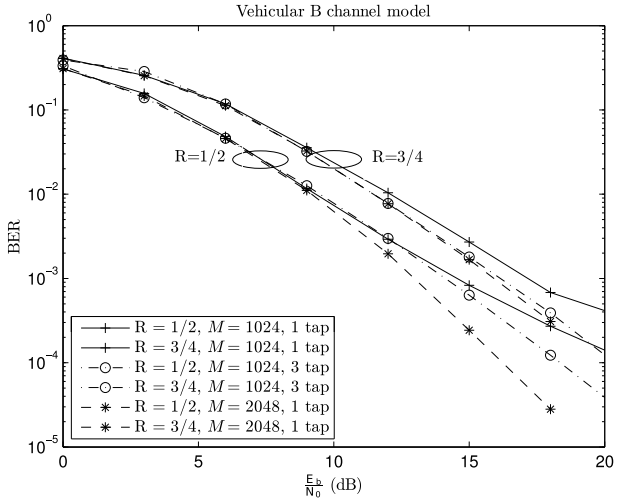

Taux d'erreurs pour les systèmes FBMC codés précodés qui utilisent l'égalisation MMSE en transmettant à travers du modèle de canal Vehicular B.

Resultats de Simulation

La première Figure montre la comparaison entre les résultats de simulation de Monte Carlo et ceux de l'approximation présentée dans ce chapitre. Les systèmes FBMC transmettent à travers un modèle de canal Vehicular A avec $N = 128, 256$. Pour ce cas, avec $N = 128$ les sous-canaux seront sélectifs en fréquence ; si $N = 256$ les sous-canaux seront

plats. Les résultats de l'approximation sont conforment avec ceux fournis par les simulations de Monte Carlo. Il est aussi possible voir que les systèmes qui utilisent des égaliseurs de sous-canal d'un coefficient ont une ordre de diversité réduite par rapport aux systèmes qui utilisent des égaliseurs de sous-canal de trois coefficients pour le même nombre de sous-canaux si les sous-canaux sont sélectifs en fréquence car l'égaliseur d'un coefficient n'est pas capable de compenser toute la sélectivité du sous-canal dans ces cas. Lorsque les sous-canaux ont une réponse en fréquence plate, l'égaliseur d'un coefficient suffit pour égaliser complètement le sous-canal et obtenir l'ordre de diversité maximum dans le scénario. Dans ce cas, l'utilisation d'égaliseurs de sous-canal avec plus de coefficients n'apporte pas de gain de performance.

Les résultats pour des systèmes qui utilisent un codage de canal avec le modèle de canal Vehicular B, avec $N = 1024, 2048$ sont présentés dans la deuxième Figure. Dans ce cas, avec $N = 1024$ on aura des sous-canaux sélectifs en fréquence, lorsque avec $N = 2048$ les sous-canaux seront plats. Les mêmes conclusions peuvent être apliquées au cas codé.

Chapitre 4 - Sur la Distribution du SINR et la Performance d'Erreur Non-codée et Codée en Systèmes SC-FDE avec Égalisation Linéaire MMSE

Dans ce chapitre, nous proposons l'adoption de la distribution lognormale avec la plus petite distance de Kullback-Leibler vers la distribution observée comme une approximation de la densité de probabilité du SINR dans un système multiporteuse précodé avec de l'égalisation linéaire MMSE. Cette approximation est précise au sens du BER même dans les valeurs élevées du SNR. Nous utilisons cette approximation lognormale pour simplifier le calcul de la performance d'erreur codée de ce système. Avec cette simplification, une expression pour la probabilité d'erreur par paire est dérivée. Cette expression pour la PEP donne des limitants proches des résultats de simulation de Monte Carlo.

Distribution du SINR

Pour le calcul du BER l'approximation doit être plus précise dans la partie gauche de la courbe du pdf, parce que cette partie va correspondre aux valeurs plus faibles du

SINR. Pour ce but, une approximation que minimise la distance de Kullback-Leibler vers la distribution du SINR est appropriée.

Il y a une connexion directe entre la minimization de la distance KL entre l'approximation et la distribution du SINR et la minimisation des erreurs avec la distance KL. Donc, avec la minimisation de la distance KL il est possible obtenir une approximation précise dans la région d'interêt pour le taux d'erreurs. Pour minimiser la distance KL entre l'approximation et le SINR une simulation de Monte Carlo est faite à chaque SNR pour chercher les paramètres de distribution qui meneront à la plus petite valeur de la distance KL pour chaque cas.

Comme la SINR d'un système multiporteuse précodé MMSE n'a que des valeurs positifs, une moyenne faible ,une forte élevée et *skew* positif, une distribution appropriée pour l' approximation peut être la distribution lognormale. Les paramètres de la distribution lognormale μ et σ peuvent être déterminés pour des modèles de canaux specifiques. L'expression compacte suivante pour la probabilité d'erreurs bit dans un système multiporteuse précodé en utilisant la distribution lognormale comme approximation pour le SINR peut être utilisée :

$$P_e \approx \frac{1}{\sqrt{\pi}} \sum_{n=1}^{K} w_n Q\left(\sqrt{\frac{E_s}{\sigma_n^2} \exp\left(\sqrt{2}\sigma x_n + \mu\right)}\right),$$

où w_n et x_n sont les paramètres d'integration de Gauss-Hermite.

Performance d'Erreur Codée

Comme le SINR non-codé d'un systéme multiporteuse précodé MMSE a été approximé par une distribution lognormale, on peut simplifier le système pour un système à porteuse unique qui transmet à travers un canal avec de l'évanouissement lognormal. On peut dériver une expression compacte pour la PEP des systèmes multiporteuses précodées en utilisant l'équation antérieure ; cette expression est donnée par

$$P_{ep}(d) \approx \frac{1}{\sqrt{\pi}} \sum_{n=1}^{N_t} w_n Q\left(\sqrt{2d\frac{E_s}{\sigma_n^2} \exp\left(\sqrt{2}\sigma x_n + \mu\right)}\right),$$

où μ et σ sont les paramètres de la distribution lognormale que minimisent la distance KL entre l'approximation lognormale et la distribution du SINR d'un système multiporteuse

précodé MMSE mais sans codage de canal. L'*union bound* pour la performance d'erreur codée est

$$P_e \leq \frac{1}{k_c} \sum_{d=d_{free}}^{\infty} w(d) P_{ep}(d).$$

Résultats de Simulation

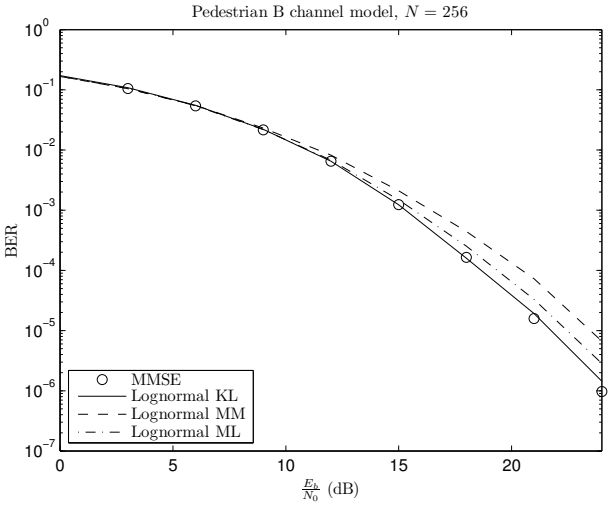

Comparaison de la performance d'erreur du SINR avec ses approximations pour le modèle de canal Pedestrian B.

La première Figure montre la probabilité d'erreur de bit du système comparée avec ses approximations pour le modèle de canal Pedestrian B. Les paramétres μ et σ en fonction du SNR et du modèle du canal sont estimés par la méthode des moments, maximum de vraisemblance et ceux qui resultent dans la plus petite distance KL vers la vraie distribution. On peut voir que l'approximation qui utilise la distance KL est la plus précise dans les SNRs élevés (> 10 dB) par rapport aux autres approximations, parce que la méthode KL assure que l'approximation sera plus proche de la vraie distribution dans la partie gauche de la pdf.

Pour valider la nouvelle méthode analytique pour la détermination de la performance codée, la deuxième Figure compare les résultats de Monte Carlo avec les résultats de l'équation de la performance codée (avec les paramétres de la distribution lognormale obtenus avec le méthode KL) pour $N = 512$, le modéle de canal Pedestrian B et les taux

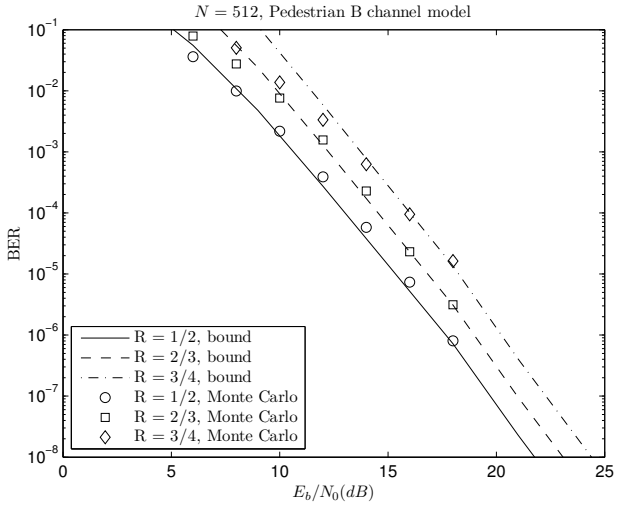

Comparaison entre les bornes et les résultats de simulation de Monte Carlo pour $N = 512$ et le modèle de canal Pedestrian B.

de code R_c 1/2, 2/3 et 3/4. Il est possible voir que les limitantes d'erreur obtenus avec l'approximation lognormale sont très proches des résultats de simulation de Monte Carlo.

Chapitre 5 - Techniques Largement Linéares MMSE de Précodage et d'Égalisation pour les Systèmes SC-FDE

Introduction

Dans ce chapitre nous proposons des systèmes SC-FDE qui utilisent de l'égalisation simple, de l'égalisation avec retour de décision et du précodage Tomlinson-Harashima MMSE largement linéaire. L'usage de l'égalisation et de la précodage largement linéaire donne une avantage de performance par rapport aux systèmes strictement linéaires quand des constellations impropres sont transmises. Des expressions pour le SINR à la sortie du récepteur sont données pour tous les cas.

Modèle du Système

Égaliseur WL-MMSE

L'égaliseur optimal $\mathbf{A}$ est donné par

$$\begin{aligned}\mathbf{A} &= \mathbf{C}_{\mathbf{RR}}^{-1}\mathbf{C}_{\mathbf{Rs}} \\ &= \begin{bmatrix} \mathbf{H}\mathbf{H}^H + \sigma_n^2\mathbf{I}_N & \mathbf{H}\mathbf{U}\mathbf{H}^T \\ \mathbf{H}^*\mathbf{U}\mathbf{H}^H & \mathbf{H}^*\mathbf{H}^T + \sigma_n^2\mathbf{I}_N \end{bmatrix}^{-1} \begin{bmatrix} \mathbf{H} \\ \mathbf{H}^*\mathbf{U} \end{bmatrix}.\end{aligned}$$

Égaliseur WL-MMSE DFE

La valeur optimale du filtre *feedforward* $\mathbf{B}$ peut être donnée par

$$\mathbf{B} = \mathbf{A}(\mathbf{I}_N + \mathbf{D}),$$

où $\mathbf{D}$ est le filtre de retour dans le domaine de la fréquence.

Les coefficients du filtre de retour $\tilde{\mathbf{d}}$ sont donnés par la solution du système linéaire

$$\mathbf{F}\tilde{\mathbf{d}} = -\mathbf{g}.$$

La matrice $\mathbf{F}$ de taille $L_{\tilde{\mathbf{d}}}$x$L_{\tilde{\mathbf{d}}}$ et le vecteur colonne $\mathbf{g}$ de taille $L_{\tilde{\mathbf{d}}}$x1 sont exprimés, respectivement, par

$$[\mathbf{F}]_{m,l} = \sum_{n=1}^{N} \frac{\exp\left(-j2\pi((n(l-m))/N)\right)}{H_{mod}(n,n) + \sigma_n^2},\ 1 \leq m, l \leq L_{\tilde{\mathbf{d}}}$$

et

$$[\mathbf{g}]_m = \sum_{n=1}^{N} \frac{\exp\left(j2\pi(nm/N)\right)}{H_{mod}(n,n) + \sigma_n^2},\ 1 \leq m \leq L_{\tilde{\mathbf{d}}}.$$

Pour initialiser le filtre de retour, les derniers $L_{\tilde{\mathbf{d}}}$ symboles de $\tilde{\mathbf{x}}_{CP}$ peuvent être utilisés. Une fois que $\tilde{\mathbf{d}}$ est determiné, $\mathbf{B}$ peut être calculé. Pour retirer toute l'ISI des symboles determinés avant, la taille du filtre de retour $L_{\tilde{\mathbf{d}}}$ doit être la même que celle du canal $L_{\tilde{\mathbf{h}}}$.

Précodeur Tomlinson-Harashima WL-MMSE

On peut démontrer que l'égaliseur $\mathbf{B}'$ et le précodeur THP $\tilde{\mathbf{d}}'$ sont les mêmes que le filtre *feedforward* et de retour d'un système SC-FDE qui utilise de l'égalisation MMSE largement linéaire avec retour de décision. Donc, les coefficients du précodeur Tomlinson-Harashima $\tilde{\mathbf{d}}'$ sont égaux a $\tilde{\mathbf{d}}$ et l'égaliseur largement linéaire MMSE $\mathbf{B}'$ est égal a $\mathbf{B}$.

Analyse de la Performance d'Erreur

SINR pour le Récepteur WL-MMSE

L'erreur moyenne quadratique $\mathrm{MSE}_{\mathrm{WL}}$ pour le système SC-FDE WL-MMSE est donnée par

$$\mathrm{MSE}_{\mathrm{WL}} = \mathbf{W^{-1}} \left(\mathbf{H}_{mod} + \sigma_n^2 \mathbf{I}_N\right)^{-1} \mathbf{W}.$$

$\mathrm{MSE}_{\mathrm{WL}}$ est bien plus petite que celle obtenue par l'égaliseur strictement linéaire. Le SINR effectif aprés la déprécodage lorsqu'on utilise un égaliseur WL-MMSE est

$$\gamma_{\text{WL-MMSE}} = \frac{1}{2}\left(\frac{\gamma N}{\mathrm{tr}[\mathrm{MSE}_{\mathrm{WL}}]} - 1\right),$$

avec

$$\mathrm{tr}[\mathrm{MSE}_{\mathrm{WL}}] = \frac{1}{2|H_1|^2 + \sigma_n^2} + \frac{1}{2|H_{N/2+1}|^2 + \sigma_n^2} + \\ + \sum_{i=2}^{N/2} \frac{2}{|H_i|^2 + |H_{N+2-i}|^2 + \sigma_n^2},$$

et $\gamma = E_s/\sigma_n^2$. La division par 2 dans l'équation du SINR est du à la décision finale du symbole qui n'utilise que l'estimation réelle.

SINR pour le Récepteur WL-MMSE DFE

La MSE du système SC-FDE WL-MMSE DFE est exprimée par

$$\mathrm{MSE}_{\text{WL-DFE}} = \exp\left(\frac{1}{N}\sum_{n=1}^{N} \log\left(\frac{1}{1+\gamma H_{mod}(n,n)}\right)\right).$$

L'erreur moyen quadratique ne prend pas en compte l'effet de la propagation de l'erreur qui peut provenir de mauvaises décisions antérieures. Cette MSE est à nouveau plus petit que celle obtenue par le système strictement linéaire.

Le SINR pour le système SC-FDE WL-MMSE est donné par

$$\gamma_{\text{WL-DFE}} = \frac{1}{2}\left(\frac{1}{\mathrm{MSE}_{\text{WL-DFE}}} - 1\right).$$

À nouveau, nous divisons par 2 pour obtenir le SINR effectif pour le système qui utilise l'égalisation largement linéaire.

SINR pour le Précodeur WL-MMSE-THP

La MSE pour le système WL-MMSE-THP SC-FDE est la même que celle d'un système WL-MMSE DFE moins un facteur η, qui représente la perte de précodage. Donc, cette MSE peut être exprimée par

$$\mathrm{MSE}_{\text{WL-THP}} = \exp\left(\frac{1}{N}\sum_{n=1}^{N}\log\left(\frac{1}{1+\frac{\gamma}{\eta}H_{mod}(n,n)}\right)\right),$$

avec $\eta = \frac{M^2}{M^2-1}$ pour des constellations unidimensionnels et $\eta = \frac{M}{M-1}$ pour des constellations bidimensionnels.

Résultats de Simulation

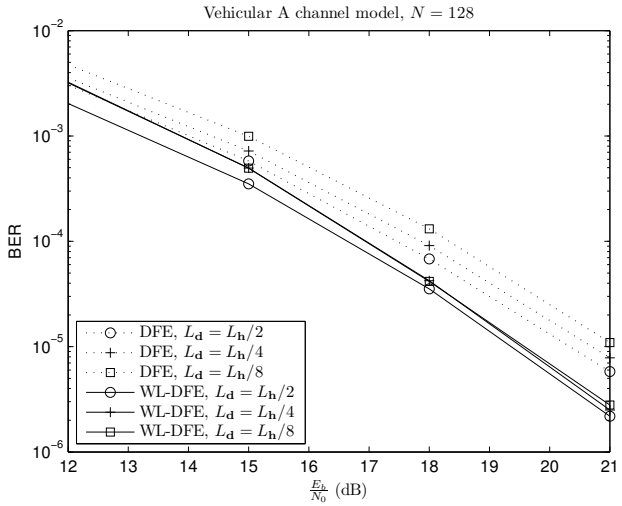

Taux d'erreurs pour $N = 128$ et le modèle de canal Vehicular A en systèmes SC-FDE DFE avec de differents tailles de $L_{\tilde{\mathbf{d}}}$.

Les systèmes avec l'égalisation et précodage largement linéaire ont un gain de performance par rapport aux leurs versions strictemente linéaires si des constellations impropres sont utilisées, grâce à l'usage complet des statistiques de second ordre du signal.

La premième figure montre l'effet de la variation de la taille du filtre de retour sur le taux d'erreurs des systèmes SC-FDE DFE. Le système largement linéaire a un taux d'erreurs moins sensible par rapport au système strictement linéaire, parce que son filtre *feedforward* est plus efficient dans l'enlèvement de l'ISI. Avec des filtres de retour plus

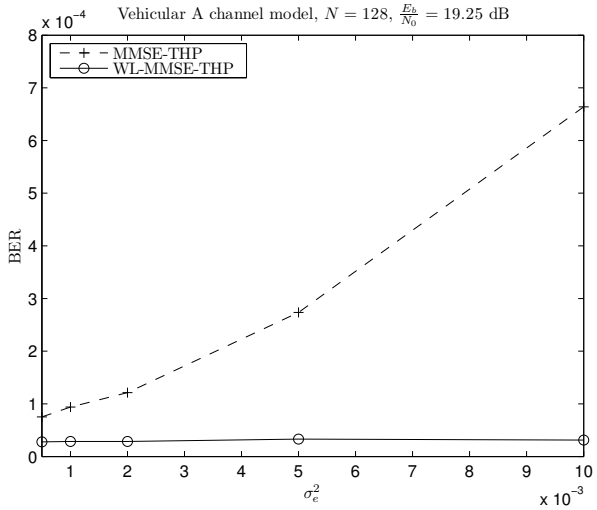

L'impact des erreur d'estimation du canal/CSI dans la performance d'erreur des systèmes THP.

courts, la complexité de calcul pour le calcul des coefficients de ce filtre est réduite.

Une comparaison de l'impact des erreurs d'estimation du canal et CSI imparfait sue le taux d'erreurs des systèmes MMSE-THP SC-FDE est présentée dans la deuxième figure pour $\frac{E_b}{N_0} = 19.25$ dB, $N = 128$ et le modèle de canal Vehicular A. L'estimation imparfaite du canal peut être exprimée comme $\mathbf{H}_e = \mathbf{H} + \mathbf{E}_\mathbf{H}$, où $\mathbf{E}_\mathbf{H}$ est la matrice d'erreurs d'estimation du canal, avec sa diagonale composée par des variables aléatoires gaussiennes, de moyenne zéro et variance σ_e^2. Cette estimation imparfaite est transmise au émetteur, qui aura une mauvaise information de l'état du canal. Lorsque les performances du système strictement linéaire deviennent pire à cause de l'augmentation de la variance d'erreur σ_e^2, le système SC-FDE précodé largement linéaire est presque insensible à l'augmentation de la variance d'erreurs de l'estimation du canal.

Chapitre 6 - Conclusions Finales

Dans cette thèse de nouvelles techniques de précodage et d'égalisation pour les systèmes multiporteuses ont été proposées, avec une analyse théorique de leurs performances. D'abord, le taux d'erreurs des systèmes FBMC/OQAM précodés a été étudié dans le Chapitre 3. Il a été montré que cette performance est très sensible à l'ISI residuelle qui provient

de l'égalisation imparfaite des sous-canaux. Une expression pour le SINR qui considère ces cas a été obtenue pour des transmissions non-codées ; cette expression fournit des résultats identiques avec ceux des simulations de Monte Carlo.

Le Chapitre 4 traite de la densité de probabilité du SINR dans un système multiporteuse précodé qui utilise l'égalisation linéaire MMSE. Nous avons proposé d'utiliser la distribution lognormale pour ce SINR comme approximation afin d'estimer le BER ; les paramétres de cette distribution doivent minimiser la distance de Kullback-Leibler vers le vrai SINR. Avec cette minimisation, nous nous assurons que cette approximation sera précise dans la partie gauche de la fonction, qui est la partie la plus importante pour le calcul du BER. Avec cette distribution lognormal comme abstration du système nous avons développé une nouvelle méthode analytique pour déterminer la performance d'erreurs pour les systèmes multiporteuses précodés qui utilisent l'égalisation linéaire MMSE et la codage de canal convolutionnel. Cette méthode donne des résultats cohérents avec ceux des simulations de Monte Carlo.

Des égaliseurs et précodeurs Tomlinson-Harashima MMSE qui utilisent le traitement largement linéaire pour les systèmes SC-FDE ont été proposés dans le Chapitre 5. Comme ces égaliseurs et précodeurs utilisent toutes les statistiques de deuxième ordre disponibles si le signal transmis est impropre, ils ont une erreur quadratique moyenne plus petite et un meilleur taux d'erreurs. Des expressions pour la MSE et le SINR de tous les égaliseurs et précodeurs proposés ont été développés ; ces expressions sont en conformité avec les résultats de simulation de Monte Carlo. Les égaliseurs à retour de décision pour les systèmes SC-FDE ont un taux d'erreurs moins sensible à la taille du filtre de retour. Les précodeurs Tomlinson-Harashima largement linéaires sont moins sensible à une information du canal erronée à l'émetteur par rapport aux versions strictement linéaires.

Contents

List of Tables

List of Figures

List of Symbols

α	Rolloff factor
δ	Kronecker delta
η	Precoding loss in Tomlinson-Harashima systems
γ	SNR
$\mathbf{H}$	Channel frequency response
$\mathbf{h}$	Channel time-domain impulse response
$\mathbf{I}_N$	Identity matrix of size NxN
$\mathbf{n}$	Noise
$\mathbf{s}$	Transmitted signal
$\mathbf{T}$	Precoding matrix
$\mathbf{W}$	Fourier matrix
σ_n^2	Noise variance
BW	Bandwidth
D	Diversity order
F	Spacing between subchannels
K	Overlapping factor
k	Subchannel index
l	Time index

L_{CP}	Cyclic prefix length
L_{PF}	Prototype filter length
L_s	Symbol length
N	Number of Subchannels
N_g	Number of subchannels not used for data transmission
PC	Pseudocovariance
T	OFDM symbol length
T_d	Channel Time Dispersion
T_s	Symbol Duration Time

List of Abbreviations

AWGN *Additional White Gaussian Noise*

BER *Bit Error Rate*

BICM *Bit Interleaved Coded Modulation*

BPSK *Binary Phase Shift Keying*

CFO *Carrier Frequency Offset*

CP *Cyclic Prefix*

DAB *Digital Audio Broadcasting*

DFE *Decision Feedback Equalizer*

DFT *Discrete Fourier Transform*

DVB-T *Digital Video Broadcasting - Terrestrial*

FB *Feedback*

FBMC *Filterbank Multicarrier*

FF *Feedforward*

FFT *Fast Fourier Transform*

ICI *Interchannel Interference*

IDFT *Inverse Discrete Fourier Transform*

IEEE *The Institute of Electrical and Electronic Engineers*

IFFT *Inverse Fast Fourier Transform*

IOTA *Isotropical Orthogonal Transform Algorithm*

ISI *Intersymbol Interference*

ITU *International Telecommunications Union*

KL *Kullback-Leibler*

LTE *Long Term Evolution*

ML *Maximum Likelihood*

MM *Moment Matching*

MMSE *Minimum Mean Square Error*

MSK *Minimum Shift Keying*

OFDM *Orthogonal Frequency Division Multiplexing*

OQAM *Offset Quadrature Amplitude Modulation*

OQPSK *Offset Quadrature Phase Shift Keying*

PAM *Phase Amplitude Modulation*

PAPR *Peak-to-average Power Ratio*

pdf *Probability distribution function*

PEP *Pairwise Error Probability*

PHYDYAS *Physical Layer for Dynamic Spectrum Access and Cognitive Radio*

PPN *Polyphase Network*

QAM *Quadrature Amplitude Modulation*

QPSK *Quadrature Phase Shift Keying*

RF *Radio frequency*

SC-FDE *Single Carrier with Frequency Domain Equalization*

SC-FDMA *Single Carrier with Frequency Domain Multiple Access*

SINR *Signal to Interference plus Noise Ratio*

SNR *Signal to Noise Ratio*

THP *Tomlinson-Harashima Precoding*

WL *Widely Linear*

ZF *Zero Forcing*

Chapter 1

Introduction

The world had 7 billion people and 5.9 billion mobile phone subscriptions in use by the end of 2011. Of those 5.9 billion subscriptions, 1.6 billion were active users of mobile browsing and 1.1 billion were smartphone users [2]. These smartphones are used for much more than calls and short messages. They have more functions, larger screens, faster processors and more connectivity options than before. Their users demand constantly faster download and upload speeds. However, the pace of battery evolution has not kept up with these demands, and battery life in these devices is sometimes measured in hours, not days.

On the other end of the spectrum, the usage of mobile phones is also widespread in poorer countries. In Kenya, for example, 40 percent of the adult population use a mobile payment system to receive their salary, buy goods and transfer money [2]. In some of these countries, power supply is not constant, and rolling blackouts can be a common occurrence. A large battery life can help the user avoid the unpleasant surprise of finding that his mobile device has no power and cannot be charged instantly. Thus, an effort to save power in every operational aspect is important to improve the user experience and battery life.

These mobile devices transmit data through multipath channels, which introduce intersymbol interference in the received data. To compensate the effect of this ISI, the adoption of multicarrier systems has increased greatly in the last few years. This is due to their efficient equalization, being able to equalize channels with a long impulse response with simple subchannel equalizers due to the use of the cyclic prefix. Nowadays, the most used multicarrier systems are the ones based on Orthogonal Frequency Division Multiplexing

and transmitting data from Quadrature Amplitude Modulation symbols (OFDM/QAM) [3; 4]. However, because these systems use the rectangular window to separate the subchannels and a cyclic prefix to make equalization easier, they have large spectral lobes outside their designated bandwidth and waste power and bandwidth to transmit redundancy. Filterbank Multicarrier systems transmitting data from Offset Quadrature Amplitude Modulation (FBMC/OQAM) [5] have been proposed to eliminate the cyclic prefix and limit this out-of-band radiation, by using a window well-localized in time and frequency to separate the subchannels. This window also allows better user separation in multiuser systems.

Both of these multicarrier systems have a major drawback : they are not suitable for the uplink of mobile devices due to their high peak-to-average power ratio (PAPR). With this high PAPR, highly linear power amplifiers are required to avoid excessive distortion. To operate in their linear region these amplifiers must be backed off from their peak power, leading to a low power efficiency (ratio of transmitted power to dc power dissipated), which places a significant burden on portable wireless terminals [6]. A way to overcome this limitation is to linearly precode the signal before transmission. These precoded systems have much lower PAPR, allowing the usage of more efficient amplifiers and improving battery life. When dealing with OFDM/QAM systems, their Discrete Fourier Transform (DFT)-precoded version is known as Single Carrier with Frequency Domain Equalization (SC-FDE) [7; 8], because the precoding DFT cancels the Inverse Fast Fourier Transform (IFFT) that is done at an OFDM/QAM transmitter. 3GPP Long Term Evolution (LTE) systems [9] use a multi-user version of SC-FDE, known as Single Carrier Frequency Domain Multiple Access (SC-FDMA) [6], for their uplink. Unlike regular multicarrier systems, where equalization is done symbol by symbol and zero-forcing equalization corresponds to the maximum-likelihood one, equalization in precoded multicarrier systems is done blockwise ; thus, maximum-likelihood detection is impractical when the system uses a high number of subchannels. Because of this, linear equalization techniques are usually employed. Improved equalization techniques can be applied to these systems to make their error performance closer to the one provided by maximum-likelihood detection.

These systems normally transmit symbols from a complex QAM constellation. QAM symbols can be described as proper, that is, they have their second-order statistics comple-

tely described by their autocovariance, which for a complex random process $\mathbf{w}$ with zero mean is expressed by $E[\mathbf{w}\mathbf{w}^H]$. However, if $\mathbf{w}$ comes from real or offset constellations (such as Binary Phase Shift Keying (BPSK) and Offset QAM (OQAM) ones) the autocovariance by itself is insufficient to describe its second-order statistics, since the pseudoautocorrelation of $\mathbf{w}$, given by $E[\mathbf{w}\mathbf{w}^T]$ is non-zero ; this type of process is called improper [10]. Widely linear (WL) processing [11; 12; 13] was proposed to take advantage of this impropriety, by processing the signal together with its conjugate version to obtain a more precise estimate.

The transmitters in these systems can also benefit from channel state information if it is available, making possible to adapt transmissions to current channel conditions and improving channel capacity [14]. This channel state information can also be useful to improve the error performance by precoding or pre-equalization [1]. However, perfect channel state information is hard to obtain at the transmitter because of the constantly changing channel conditions imposed by user and obstacle movement.

1.1 Goal

The goal of this thesis is to propose and study new equalization and precoding techniques for multicarrier systems, together with an theoretical analysis of their error performance. First, we studied the error performance of precoded FBMC/OQAM systems. After, we tackled the problem of finding a distribution for the SINR of precoded multicarrier systems using linear Minimum Mean Square Error (MMSE) equalization and studied their theoretical coded error performance. Finally, we investigated the use of widely linear processing in precoders and equalizers for SC-FDE systems.

1.2 Contributions

The contributions of this thesis are the following :

– The error performance of precoded FBMC/OQAM systems was analyzed. It was found that their diversity order is highly sensitive to incomplete equalization : when there is residual intersymbol interference stemming from incomplete subchannel equalization, this diversity order is reduced. If the number of subchannels is large en-

ough to turn the subchannel frequency responses flat or if the subchannel equalizers are large enough to compensate the selective frequency response precoded FBMC/OQAM systems have the same diversity order of SC-FDE systems using regular OFDM modulation.

- An analytical method to determine an approximation for the SINR distribution of SC-FDE systems using linear MMSE equalization and transmitting through real-life channel models was proposed. This compares with the method proposed in [15; 16], which only works when all the channel taps have equal power. With this SINR distribution, the analytical error performance of SC-FDE systems using linear MMSE equalization and convolutional channel coding was found.
- A widely linear equalizer based on the MMSE criterion in its regular and decision feedback (DFE) versions was proposed for SC-FDE systems using improper modulations, together with a widely linear Tomlinson-Harashima precoder. Since a precoder/receiver using widely linear processing makes full use of the second-order statistics made available by the transmitted signal, it has better error performance. It was found that the feedback filter length can be reduced without much impact in the error performance of SC-FDE using WL-MMSE-DFE equalizers. The semi-analytical error performance of systems using these precoders/equalizers was also analyzed. In Tomlinson-Harashima precoded systems, the error performance when using the widely linear precoder was found to be much less sensitive to imperfect channel state information in the transmitter when compared to its strictly linear version.

1.3 Publications

Based on the research work presented in this thesis the following publications were accepted or submitted.

- B. S. Chang, W. L. Lopez, and C. A. F. da Rocha, "Técnicas de Projeto para equalizadores por subcanal para sistemas FBMC/OQAM" in XXVII Simpósio Brasileiro de Telecomunicações (SBrT 2009), Blumenau, Brazil [17]
- B. S. Chang, C. A. F. da Rocha, D. Le Ruyet and D. Roviras, "On the Use of Precoding in FBMC/OQAM Systems" in The 7th International Telecommunications

Symposium (ITS 2010), Manaus, Brazil [18]

– B. S. Chang and C. A. F. da Rocha, "On the Error Performance of Precoded Filterbank Multicarrier Systems Transmitting Through Highly Frequency Selective Channels" in XXVIII Simpósio Brasileiro de Telecomunicações (SBrT 2011), Curitiba, Brazil [19]
– B. S. Chang, C. A. F. da Rocha, D. Le Ruyet and D. Roviras, "On the Distribution of the SINR in Precoded Multicarrier Systems Using Linear MMSE Equalization" in 2012 16th IEEE Mediterranean Electrotechnical Conference (MELECON 2012), Yasmine Hammamet, Tunisia [20]
– B. S. Chang, C. A. F. da Rocha, D. Le Ruyet and D. Roviras, "On the Effect of ISI in the Error Performance of Precoded FBMC/OQAM Systems" in The 18th Asia-Pacific Communications Conference (APCC 2012), Jeju Island, South Korea [21]
– B. S. Chang, C. A. F. da Rocha, D. Le Ruyet and D. Roviras, "Widely Linear MMSE Precoding and Equalization Techniques for SC-FDE Systems" in IEEE Transactions on Signal Processing, *under review*

1.4 Organization

This work is organized in five chapters after this introduction.

– Chapter 2 contains the state of the art of the subjects studied in this thesis. It first revises the basics of multicarrier systems, starting with OFDM/QAM systems. Next, FBMC/OQAM systems are introduced and a comparison is made between them. Linearly precoded multicarrier systems, together with the linear equalization techniques and the decision feedback equalizer that can be applied to them are detailed next. After that, the Tomlinson-Harashima precoder and its application to SC-FDE systems are discussed. Finally, an introduction to widely linear processing and the processing gain that can be obtained by using it is presented.
– Precoded FBMC/OQAM systems are studied in Chapter 3. We start by describing their structure. After, an error analysis in the uncoded case is done, taking into account the case where residual ISI is present after incomplete equalization and deriving a semi-analytical equation for the uncoded BER in this case. Finally, simulation

results to analyse the precision of this equation and these systems' error performance are presented.

- Chapter 4 discusses the probability density function for the SINR in a SC-FDE system using linear MMSE equalization. The lognormal distribution with the smallest Kullback-Leibler distance to the target SINR is proposed as an accurate approximation of this SINR in the sense of the BER. With this lognormal distribution, a novel way to determine the analytical error performance of these systems when they are employing convolutional channel coding is proposed.
- Widely linear MMSE equalizers and Tomlinson-Harashima precoders for SC-FDE systems are proposed in Chapter 5. This chapter starts with the derivation of the coefficients of these filters. After, an analysis of their error performance is made, with equations for the mean square error for each case provided. Finally, simulation results to validate these equations and to compare these systems with their linear counterparts are presented.
- Chapter 6 shows the concluding remarks, summarizing the main obtained results and providing suggestions for future work.

Chapter 2

State of the Art

2.1 Introduction

This chapter presents the background and the state of the art that served as basis for the research presented in this thesis. We introduce OFDM/QAM systems in Section 2.2. Section 2.3 shows prototype filters that can overcome some of the deficiencies of the rectangular windows used to separate the subchannels in OFDM/QAM systems, while introducing other characteristics of their own. In Section 2.4, multicarrier systems that can use the previously presented prototype filters are described : FBMC/OQAM ones. A comparison between the two multicarrier systems presented before in the chapter is shown in Section 2.5. Section 2.6 unveils precoded OFDM/QAM systems and the various techniques used in their equalization. After that, Tomlinson-Harasima precoding is described in Section 2.7. Finally, Section 2.8 briefly introduces widely linear processing.

2.2 OFDM/QAM Systems

One of the main problems faced by communication systems is the multipath effect, which is responsible for frequency selectivity. The several replicas of the transmitted signal received in different time instants make necessary the utilization of a long linear equalizer in the receiver to eliminate the intersymbol interference and allow reliable recovery of the transmitted information. One alternative to avoid the usage of a long equalizer is the division of a frequency-selective channel (with its time dispersion T_d larger than the

symbol duration time T_s) in N subchannels, each suffering almost flat fading (the symbol duration time NT_s is much larger than the time dispersion T_d). This way, a high data rate transmission ($\frac{1}{T_s}$) is partitioned in several parallel transmissions, each one with lower data rates ($\frac{1}{NT_s}$). In these parallel transmissions suffering from approximately flat fading, a one tap subchannel equalizer (which can be implemented by a simple multiplier) is enough to compensate the transmission channel effect, eliminating the need for a complex equalizer in the receiver.

This scheme is the technique known as OFDM/QAM [3]. Its adoption started to be widespread after the application of the fast Fourier transform to multicarrier systems [4], since its analog implementation is extremely complex. Nowadays, OFDM/QAM modulation is adopted in several standards, such as DVB-T, DAB, IEEE 802.11, among others.

OFDM/QAM symbols can be expressed by

$$\tilde{s}[n] = \sum_{k=0}^{N-1} \sum_{l=-\infty}^{\infty} a_{k,l} \tilde{g}[n - lN] e^{j\frac{2\pi}{N}kn}, \tag{2.1}$$

$$= \sum_{k=0}^{N-1} \sum_{l=-\infty}^{\infty} a_{k,l} \zeta_{k,l}[n], \tag{2.2}$$

where $\tilde{\mathbf{g}}$ is the rectangular window that separates the subchannels, with its coefficients expressed in the time domain by

$$\tilde{g}[n] = \begin{cases} \frac{1}{\sqrt{T}}, & \text{if } |n| \leq \frac{T}{2} \\ 0, & \text{if } |n| > \frac{T}{2} \end{cases} \tag{2.3}$$

with $T = \frac{1}{F} = NT_s$ is the OFDM/QAM symbol length and F is the spacing between subchannels. The synthesis basis function $\zeta_{k,l}[n]$ are given by

$$\zeta_{k,l}[n] = \tilde{g}[n - lN] e^{j\frac{2\pi}{N}kn}, \tag{2.4}$$

where $a_{k,l}$ are complex symbols from a M-QAM constellation, k is the subchannel index, l the time index, N is the number of subchannels and T is the OFDM symbol length.

We can see that $\tilde{s}[n]$ is the output of a N-point IDFT of $a_{k,l}$. With the fast Fourier transform, this IDFT can be done in a computationally efficient way.

To eliminate the intersymbol interference (ISI), a cyclic prefix of length L_{CP} is added to the OFDM/QAM symbol. If L_{CP} is equal or larger than the channel impulse response

length, the samples corrupted by ISI will be discarded, guaranteeing ISI-free received data and flat fading in every subchannel. This way, $\tilde{\mathbf{s}}$ with length $L_{\tilde{s}}$ is transformed into $\tilde{\mathbf{s}}_{CP}$, with length $L_{\tilde{s}} + L_{CP}$. $\mathbf{s}_{CP}$ can be expressed by

$$\begin{aligned}&\tilde{s}_{CP}[-L_{CP}], ..., \tilde{s}_{CP}[-L_{\tilde{s}} - 1] = \\ &\tilde{s}[L_{\tilde{s}} - L_{CP}], ..., \tilde{s}[L_{\tilde{s}} - 1], s[0], ..., \tilde{s}[L_{\tilde{s}} - 1], -L_{CP} \leq n \leq L_{\tilde{s}} - 1.\end{aligned} \tag{2.5}$$

The block diagram of an OFDM/QAM transmitter (comprising a serial to parallel conversion, the IFFT, the cyclic prefix insertion and a parallel to serial conversion) is shown in Figure 2.1.

With the cyclic prefix, the signal at the entry of the receiver $\tilde{y}[n]$ is given by

$$\tilde{y}[n] = \tilde{s}_{CP}[n] * \tilde{h}[n], \tag{2.6}$$

$$= \sum_{k=0}^{L_{CP}} \tilde{h}[k]\tilde{s}[n-k]_{L_s} \tag{2.7}$$

$$(\tilde{s}_{CP}[n-k] = \tilde{s}[n-k]_{L_{\tilde{s}}} \text{ for } 0 \leq n \leq L_{\tilde{s}} - 1), \tag{2.8}$$

$$= \tilde{s}[n] \otimes \tilde{h}[n], \tag{2.9}$$

where $[\ ]_{L_{\tilde{s}}}$ indicates a modulo-$L_{\tilde{s}}$ operation and $\otimes$ represents cyclical convolution.

It is possible to see that the cyclic prefix transforms the linear convolution of the transmitted signal with the channel impulse response $\tilde{s}_{CP}[n] * \tilde{h}[n]$ in the cyclic (also known as circular) convolution $\tilde{s}[n] \otimes \tilde{h}[n]$. This cyclic convolution will lead to a circulant channel matrix, which is diagonalized by the FFT in the receiver. With this diagonalization, flat fading in every subchannel is guaranteed, and due to this condition, one tap equalizers are enough to compensate the channel effects. These equalizers can be implemented by a simple multiplier per subchannel.

Assuming a distortion-free channel, the estimated symbol $\hat{a}_{k,l}$ at the receiver output will be equal to the transmitted symbol $a_{k,l}$ if the internal product of $\tilde{y}[n]$ and the analysis basis function $\xi_{k,l}[n]$, expressed as

$$\xi_{k,l}[n] = \tilde{g}[n - lN]e^{-j\frac{2\pi}{N}kn}, \tag{2.10}$$

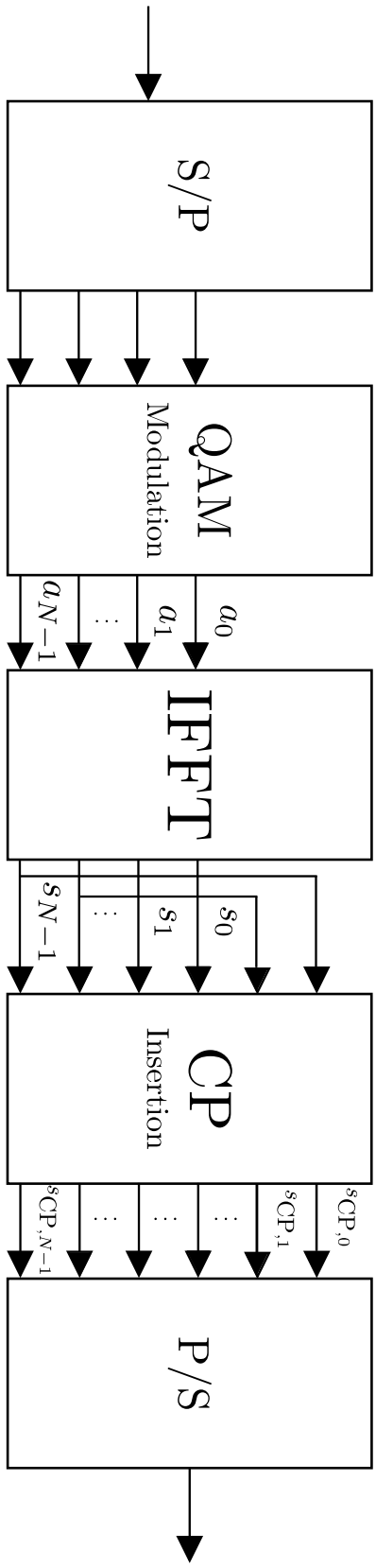

FIGURE 2.1 – An OFDM/QAM Transmitter.

constitutes an orthonormal basis of its vectorial space, in a way that

$$\left\langle \sum_{n=-\infty}^{\infty} \tilde{g}[n-lN]\tilde{g}[n-l^{'}N]e^{j\frac{2\pi}{N}(k-k^{'})(n-\frac{L_s-1}{2})} \right\rangle = \delta_{k,k'}\delta_{l,l'}, \tag{2.11}$$

where $\langle \mathbf{u}, \mathbf{v} \rangle$ is the internal product between $\mathbf{u}$ and $\mathbf{v}$, expressed by

$$\langle \mathbf{u}, \mathbf{v} \rangle = \sum_{k=-\infty}^{\infty} u^*[k]v[k], \tag{2.12}$$

and $\delta_{k,k'}$ represents the Kronecker delta.

Figure 2.2 shows an OFDM/QAM receiver, which realizes the inverse of the operations done in the transmitter plus equalization.

2.3 Prototype Filters

As stated before, conventional OFDM/QAM systems use the rectangular window $\tilde{\mathbf{g}}$ as a filter to separate the subchannels. The spectral characteristics of the rectangular window are presented in Figure 2.3.

This window allows a complex orthogonality between the synthesis/analysis basis functions $\zeta_{k,l}[n]$ and $\xi_{k,l}[n]$, which facilitates its use in the receivers. We remember that the orthogonality between two functions can be determined by the calculation of the their internal product, given in (2.12).

It can be seen in Figure 2.3 that the rectangular window has large sidelobes in its frequency response; yet, without any external interference and perfect synchronization these large sidelobes are not a problem, due to the attenuation at the crossings with other subchannels. However, this orthogonality between the basis functions is affected in practical systems by channel effects (intersymbol and interchannel interference), time and frequency offsets and noise. When using OFDM/QAM systems and the rectangular window to separate the subchannels the intersymbol interference (caused by the multipath effect) is abolished with the adoption of a cyclic prefix with sufficient length to compensate this interference. The interchannel interference and frequency offsets remain obstacles in practical conditions (due to the large sidelobes of the rectangular window's frequency response), affecting the system performance. A way to combat these problems is the adoption of Nyquist filters with good frequency localization (i.e., with small sidelobes in their frequency

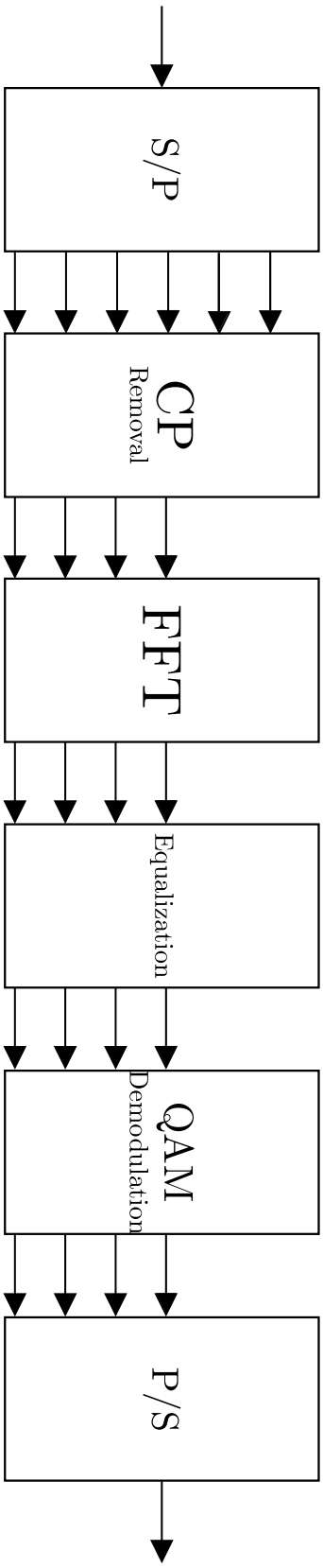

FIGURE 2.2 – An OFDM/QAM Receiver.

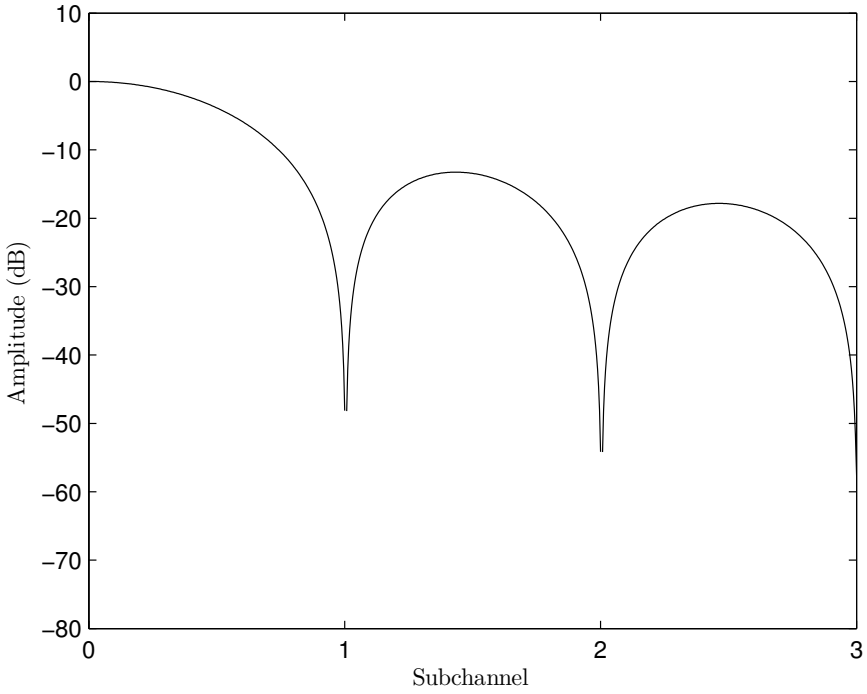

FIGURE 2.3 – Frequency response of the rectangular window.

response), improving the separation between the subchannels [22]. Power and bandwidth waste, which are consequences of the cyclic prefix, can be eliminated with the adoption of filters well localized in time.

However, if the filter is only optimized in the time domain (like conventional OFDM/QAM systems), its frequency localization will be bad, causing interchannel interference when the information is transmitted through frequency-selective channels. Perfect passband filters, on the other hand, have poor time localization, causing intersymbol interference in time-dispersive channels [22]. The raised cosine, the extended gaussian functions [23; 24] and the filter proposed for the PHYDYAS project [25] can be cited as examples of well-localized in time and frequency filters.

The raised cosine filter has the f-th element of its frequency response $\mathbf{p}$ given by

$$p(f) = \begin{cases} \frac{1}{2BW}, 0 \leq |f| < f_1 \\ \frac{1}{4BW}\left\{1 - \sin\left[\frac{\pi(|f|-BW))}{2BW-2f_1}\right]\right\}, f_1 \leq |f| < 2BW - f_1 \\ 0, |f| \geq 2BW - f_1, \end{cases} \tag{2.13}$$

with the frequency parameter f_1 and the bandwidth BW having the following relation :

$$\alpha = 1 - \frac{f_1}{BW}, \tag{2.14}$$

where α is the rolloff factor. Figures 2.4 and 2.5 show the time and frequency responses of the raised cosine filter with $\alpha = 1$.

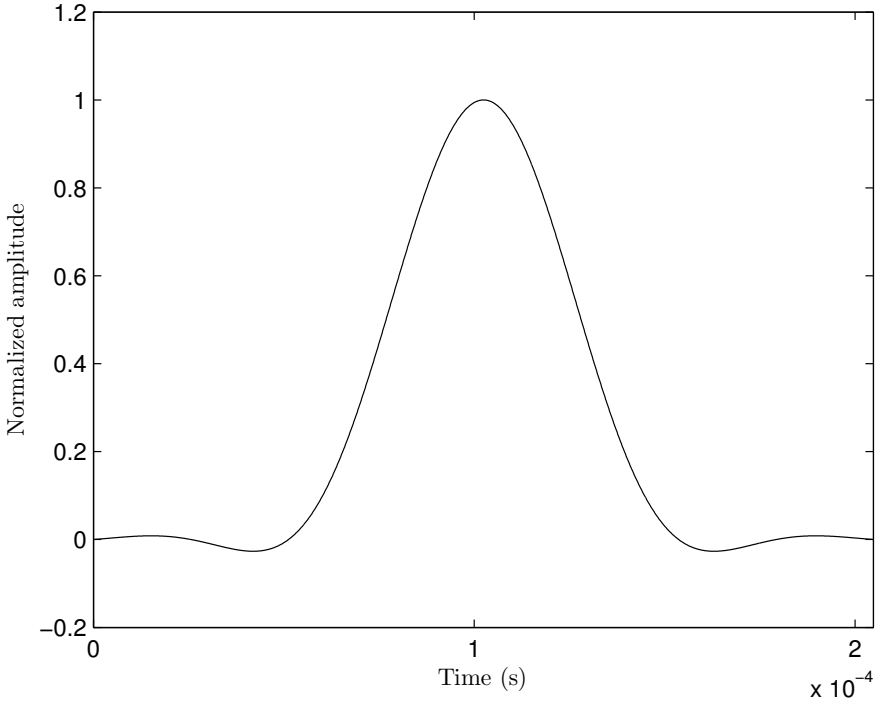

FIGURE 2.4 – Time-domain response of the raised cosine filter.

The extended gaussian functions are a result of a orthogonalization process of the gaussian function. Its time domain coefficients are

$$\begin{aligned}\tilde{z}_{\lambda,\mu_0,\tau_0}(t) = \frac{1}{2}\sum_{k=0}^{\infty}\left[g_\lambda\left(t+\frac{k}{\mu_0}\right)+g_\lambda\left(t-\frac{k}{\mu_0}\right)\right] \\ \times\sum_{l=0}^{\infty} d_{l,1/\lambda,\mu_0,\tau_0}\cos\left(2\pi l\frac{t}{\tau_0}\right),\end{aligned} \tag{2.15}$$

with λ being real-valued, d_{λ,μ_0,τ_0} coefficients found in [26], $\mu_0 = \frac{1}{2\tau_0} = F$ and $g_\lambda(t)$ being the gaussian function, expressed as

$$g_\lambda(t) = (2\lambda)^{\frac{1}{4}} e^{-\pi\lambda t^2}. \tag{2.16}$$

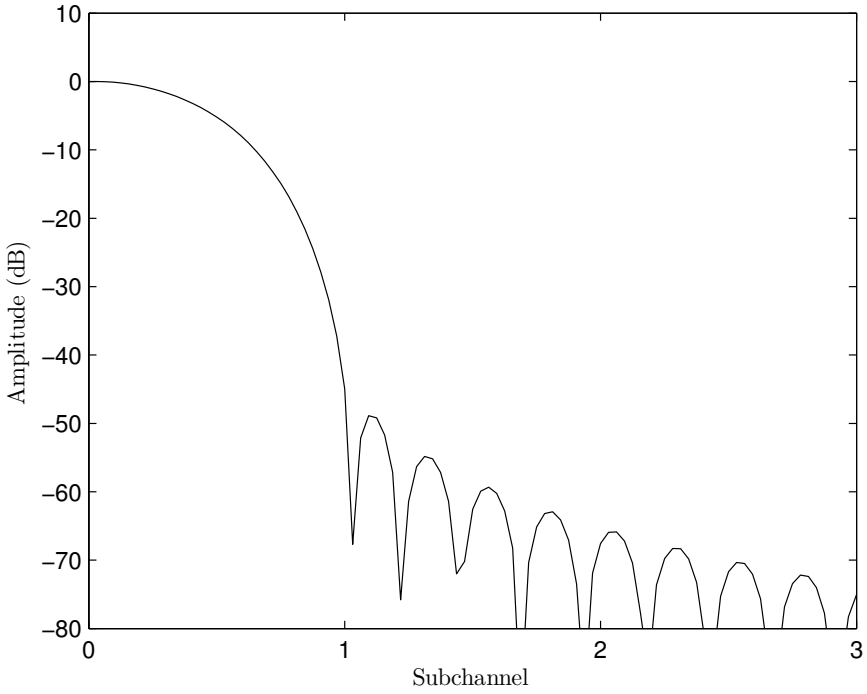

FIGURE 2.5 – Frequency-domain response of the raised cosine filter.

A special case of the extended gaussian functions is the IOTA (Isotropic Orthogonal Transform Algorithm) [27], which happens when $\lambda = 1$ and $\mu_0 = \tau_0 = \frac{1}{\sqrt{2}}$. This function has its name because its time and frequency domain responses are identical. This way, its time and frequency localization properties are also identical. They are presented, respectively in Figures 2.6 and 2.7.

The filter proposed for the PHYDYAS project has its coefficients defined as

$$F_1 = 0,97196 \tag{2.17}$$

$$F_2 = \frac{\sqrt{2}}{2} \tag{2.18}$$

$$F_3 = 0,235147 \tag{2.19}$$

$$F_k = \cos \pi \frac{k}{2K} \tag{2.20}$$

$$\tilde{f}_k = \frac{1}{2}\left[F_0 + 2\sum_{k=1}^{K-1}(-1)^k F_k\right], \tag{2.21}$$

where $\tilde{\mathbf{f}} = [\tilde{f}_1 \tilde{f}_2 \ldots \tilde{f}_{L_{PF}}]^T$ is the filter's impulse response and K is the overlapping fac-

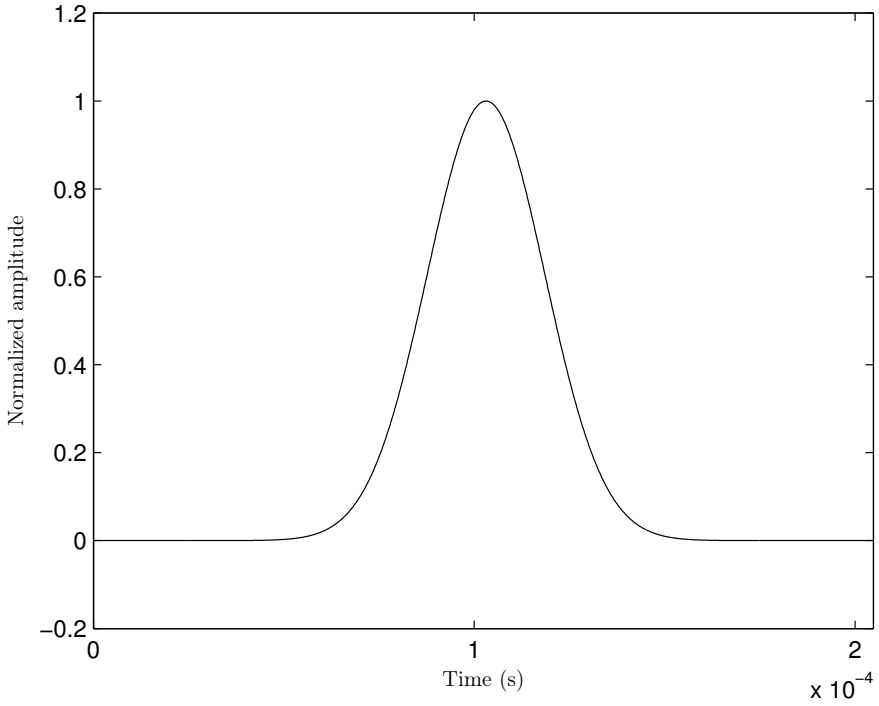

FIGURE 2.6 – Time-domain response of the IOTA filter.

tor [1]. Figures 2.8 and 2.9 show this filter's time and frequency-domain responses for an overlapping factor $K = 4$ and 512 subchannels.

It is worth saying that since well-localized in frequency filters have more compact frequency responses, each subchannel will only interfere in a meaningful way with its immediate neighbors, as it is possible to see in Figures 2.5, 2.7 and 2.9.

Since the wireless mobile channel is doubly dispersive (in time and in frequency), prototype filters must have good localization in time and in frequency. It is possible to express this localization through the Heisenberg parameter, introduced by [27] and given by

$$\xi = \frac{1}{4\pi\Delta t\Delta f}, \tag{2.22}$$

with

$$\begin{cases} \Delta t^2 = \int t^2 ||\tilde{q}(t)||^2 dt \\ \Delta f^2 = \int f^2 ||q(f)||^2 df, \end{cases} \tag{2.23}$$

1. Factor which implies that the transition phase at the output of the receiver has a length of $K - 1$ symbols

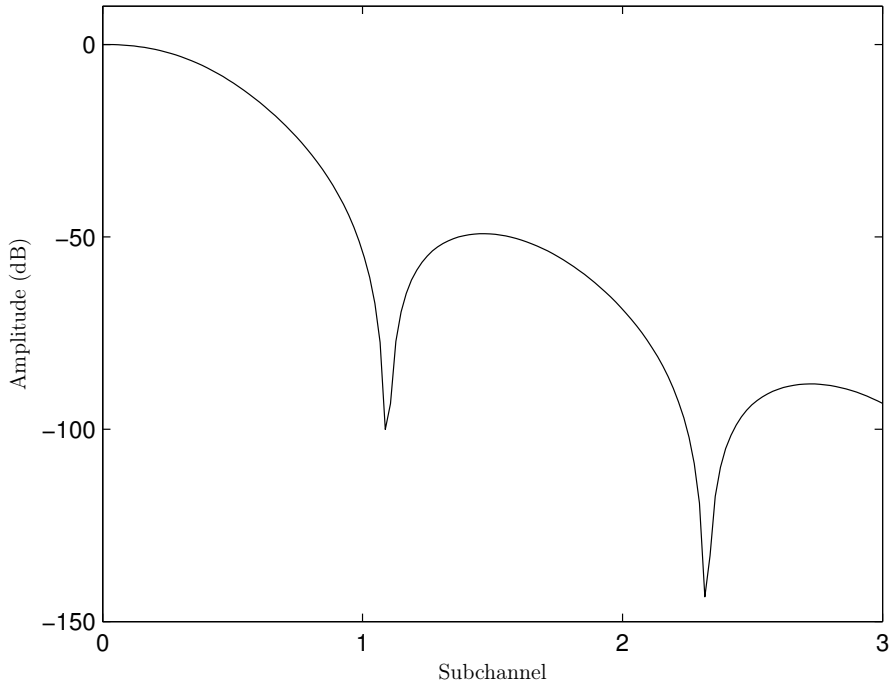

FIGURE 2.7 – Frequency-domain response of the IOTA filter.

where $\tilde{q}(t)$ and $q(f)$ are the elements of the time and frequency response of the prototype filter.

The Heisenberg parameter has its upper limit ($\xi = 1$) in the gaussian function and its lower limit ($\xi = 0$) in the rectangular window.

2.4 FBMC/OQAM Systems

It is impossible to use bandlimited and well-localized in time and frequency filters, such as the ones cited in Section 2.3, with maximal spectral efficiency ($TF = 1$) to separate the subchannels in conventional OFDM/QAM systems, because according to the Balian-Low theorem [28] these filters do not have complex orthogonality. To use these filters we have to relax the complex orthogonality constraint, since well-localized filters only have real orthogonality, expressed between $\mathbf{u}$ and $\mathbf{v}$ as

$$\langle \mathbf{u}, \mathbf{v} \rangle_{\Re} = \Re \left\{ \sum_{k=-\infty}^{\infty} u^*[k] v[k] \right\}. \tag{2.24}$$

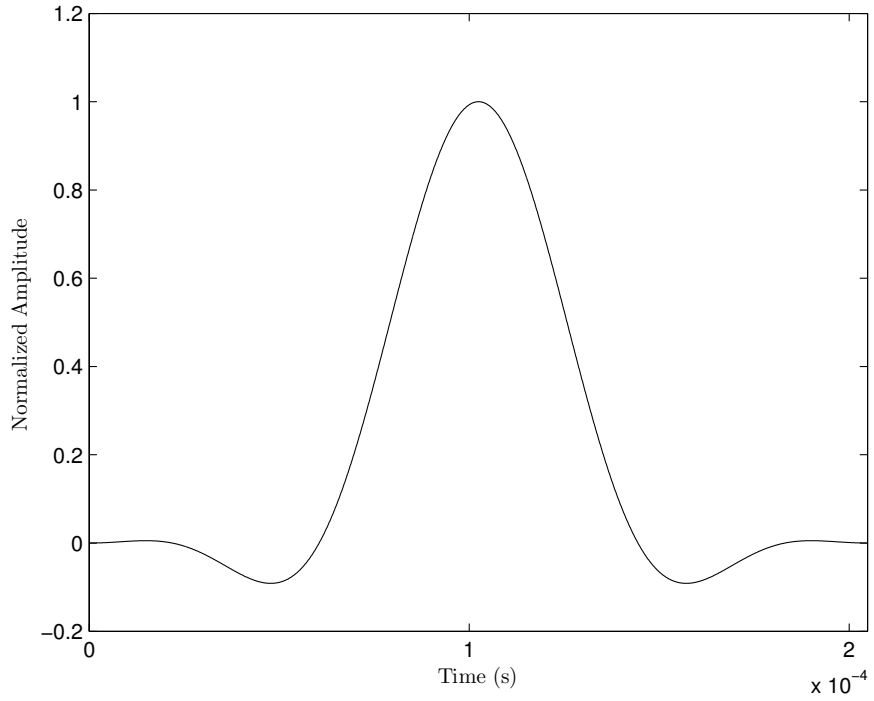

FIGURE 2.8 – Time-domain response of the PHYDYAS filter.

The time-frequency impulse response of a multicarrier system using filterbanks (with the PHYDYAS filter as the prototype filter) is presented in Table 2.1. As it is possible to see, there are interferences composed of only real or imaginary numbers. To recover information in the receiver without a lot of interference, it is necessary to transmit only the imaginary part of the symbol where the interference is a real number and vice-versa, like in the scheme presented in Figure 2.10.

This transmission scheme can be done by OQAM modulation, which separates complex symbols in its real and imaginary parts for transmission. With OQAM modulation, the

TABLE 2.1 – FBMC transmultiplexer time-frequency impulse response with the PHYDYAS prototype filter.

T/F	-3	-2	-1	0	1	2	3
-2	$0,0006$	$-0,0001$	0	0	0	$-0,0001$	$0,0006$
-1	j0,0429	-0,125	-j0,2058	0,2393	j0,2058	-0,125	-j0,0429
0	-0,0668	0,0002	0,5644	1	0,5644	0,0002	-0,0668
1	-j0,0429	-0,125	j0,2058	0,2393	-j0,2058	-0,125	j0,0429
2	0,0006	-0,0001	0	0	0	-0,0001	0,0006

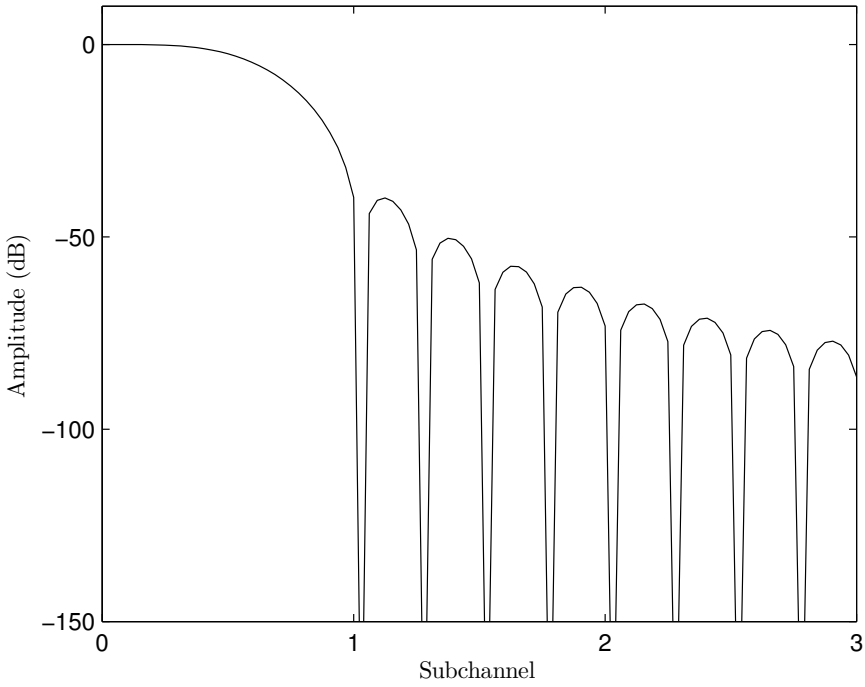

FIGURE 2.9 – Frequency-domain response of the PHYDYAS filter.

adoption of well-localized in time and frequency filters becomes possible, because this modulation transmits real symbols at two times the transmission rate of a conventional QAM modulation. A OQAM transmitted symbol can be expressed as

$$\tilde{s}_{OQAM}[n] = \sum_{k=0}^{N-1} \sum_{l=-\infty}^{\infty} b_{k,l} \tilde{q}\left[n - l\frac{N}{2}\right] e^{j\frac{2\pi}{N}k(n-\frac{L_{PF}-1}{2})} e^{j\rho_{k,l}} \tag{2.25}$$

$$= \sum_{k=0}^{N-1} \sum_{l=-\infty}^{\infty} b_{k,l} \zeta_{k,l}^{OQAM}[n], \tag{2.26}$$

with the synthesis basis function $\zeta_{k,l}^{OQAM}[n]$ given by

$$\zeta_{k,l}^{OQAM}[n] = \tilde{q}\left[n - l\frac{N}{2}\right] e^{j\frac{2\pi}{N}k(n-\frac{L_{PF}-1}{2})} e^{j\rho_{k,l}}. \tag{2.27}$$

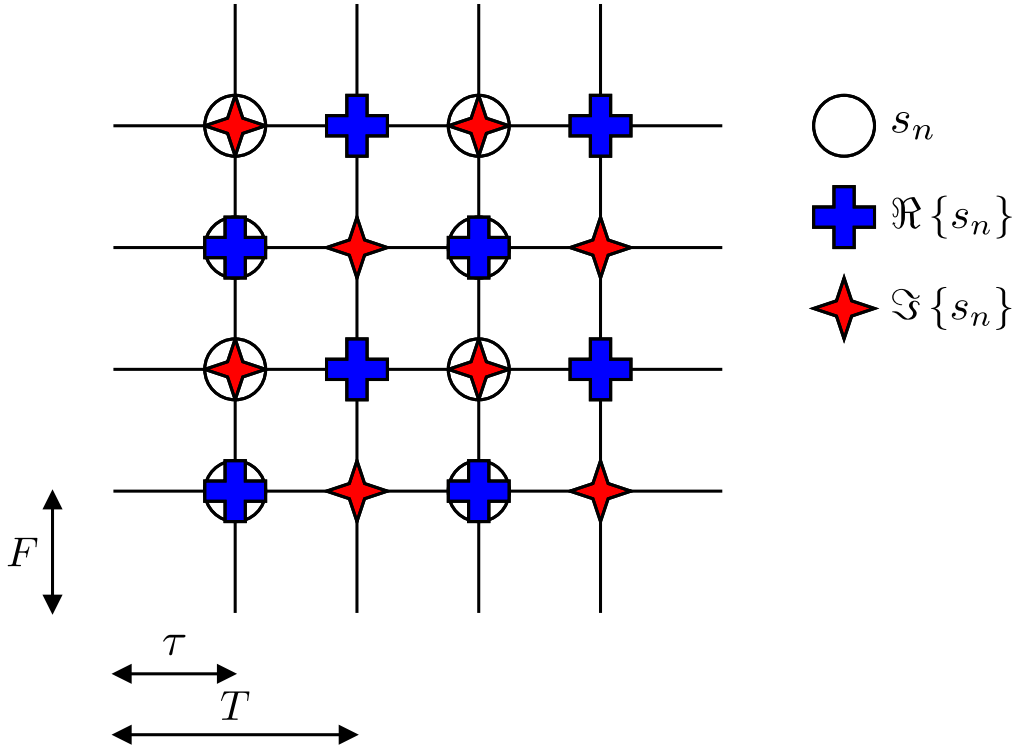

FIGURE 2.10 – The OQAM transmission scheme.

$b_{k,l}$ is given by

$$\begin{aligned} b_{2k,2l} &= a^R_{2k,l}, \\ b_{2k,2l+1} &= a^I_{2k,l}, \\ b_{2k+1,2l} &= a^I_{2k+1,l}, \\ b_{2k+1,2l+1} &= a^R_{2k+1,l}. \end{aligned} \tag{2.28}$$

As stated before, $a_{k,l} = a^R_{k,l} + ja^I_{k,l}$ are complex symbols from a QAM constellation, k the subchannel index, l the time index, N the number of subchannels, $\tilde{\mathbf{q}}$ the window separating the subchannels with length L_{PF} (the prototype filter) and $\rho_{k,l}$ is given by

$$\begin{aligned} \rho_{2k,2l} &= 0, \\ \rho_{2k,2l+1} &= \frac{\pi}{2}, \\ \rho_{2k+1,2l} &= \frac{\pi}{2}, \\ \rho_{2k+1,2l+1} &= 0. \end{aligned} \tag{2.29}$$

(2.26) can be seen as the output of a synthesis filterbank with N subchannels. This way, it is possible to implement this so-called FBMC/OQAM system with the polyphase decomposition of the prototype filter and the IFFT [29], reducing significatively the computational complexity with respect to a direct implementation (one digital filter for each subchannel). The scheme of a FBMC transmitter using the polyphase decomposition is presented in Figure 2.11.

Assuming a distortion-free channel, the estimated symbol $\hat{b}_{k,l}$ will be equal to the transmitted symbol $b_{k,l}$ if the real internal product between the received signal $y_{OQAM}[n]$ and the analysis basis function $\xi_{k,l}^{OQAM}[n]$, which is given by

$$\xi_{k,l}^{OQAM}[n] = \tilde{q}\left[n - l\frac{N}{2}\right] e^{-j\frac{2\pi}{N}k(n-\frac{L_{PF}-1}{2})} e^{j\rho_{k,l}}, \tag{2.30}$$

constitutes an orthonormal basis of its vectorial space, in a way that

$$\left\langle \sum_{n=-\infty}^{\infty} \tilde{q}\left[n - l\frac{N}{2}\right] \tilde{q}\left[n - l'\frac{N}{2}\right] e^{j\frac{2\pi}{N}(k-k')(n-\frac{L_{PF}-1}{2})} e^{j(\rho_{k',l'}-\rho_{k,l})} \right\rangle_{\Re}$$
$$= \delta_{k,k'}\delta_{l,l'}. \tag{2.31}$$

The block scheme of a FBMC receiver is presented in Figure 2.12.

2.5 Comparison Between Different Multicarrier Systems

In the previous sections, multicarrier systems based on the rectangular window, QAM modulation and the cyclic prefix (OFDM/QAM) and based on well-localized pulses, OQAM modulation and no cyclic prefix (FBMC/OQAM) were introduced. The goal of this section is to compare these systems with respect to computational and equalization complexity, bandwidth and power efficiency and error performance.

2.5.1 Equalization

Since the cyclic prefix is not present in filterbank multicarrier systems, ISI is not completely eliminated. For this reason, a one tap per subchannel equalizer is not always enough to compensate the channel effect, as is the case in OFDM/QAM systems. When the frequency selectivity of the channel is high, the usage of a multi-tap subchannel equalizer can be necessary to compensate the channel effect introduced by subchannel selectivity [30; 31].

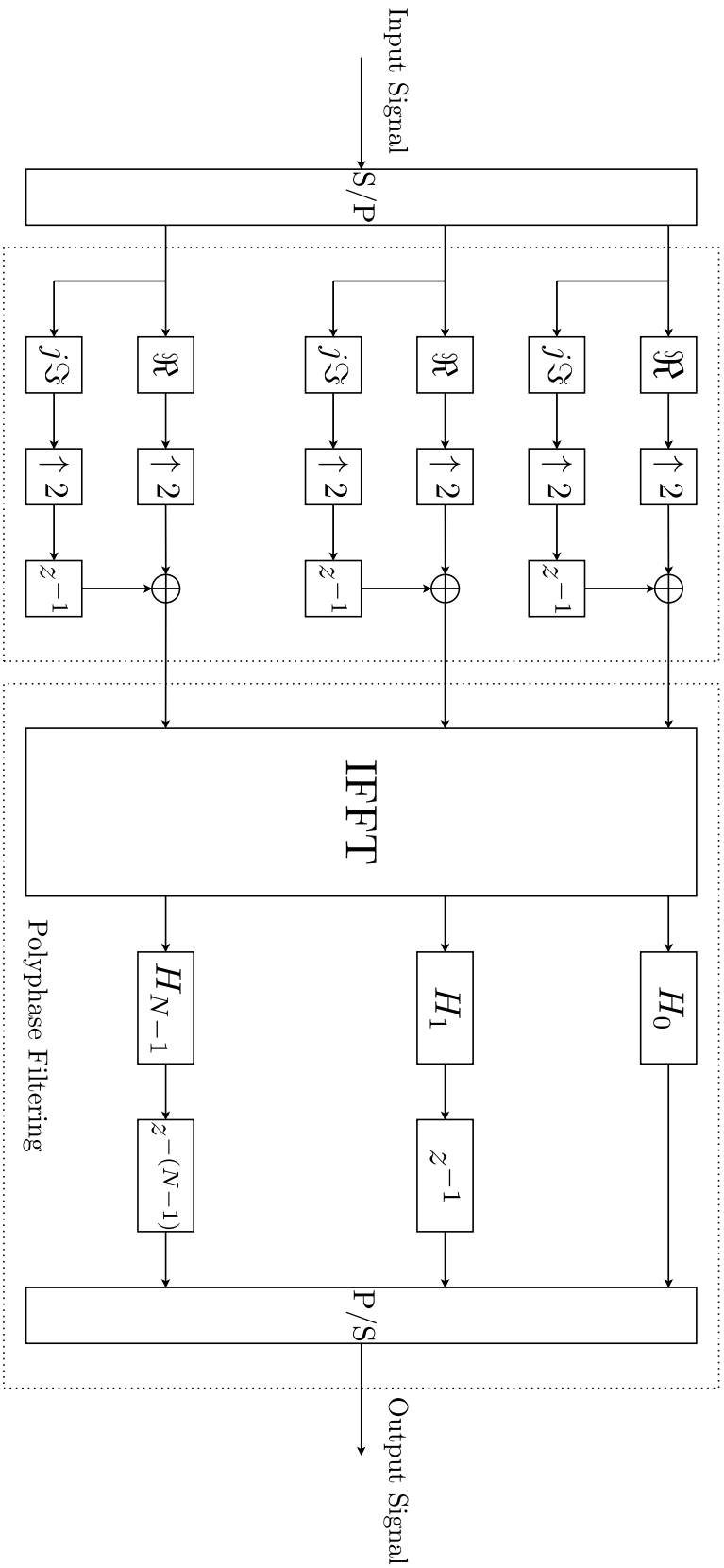

FIGURE 2.11 – A FBMC transmitter.

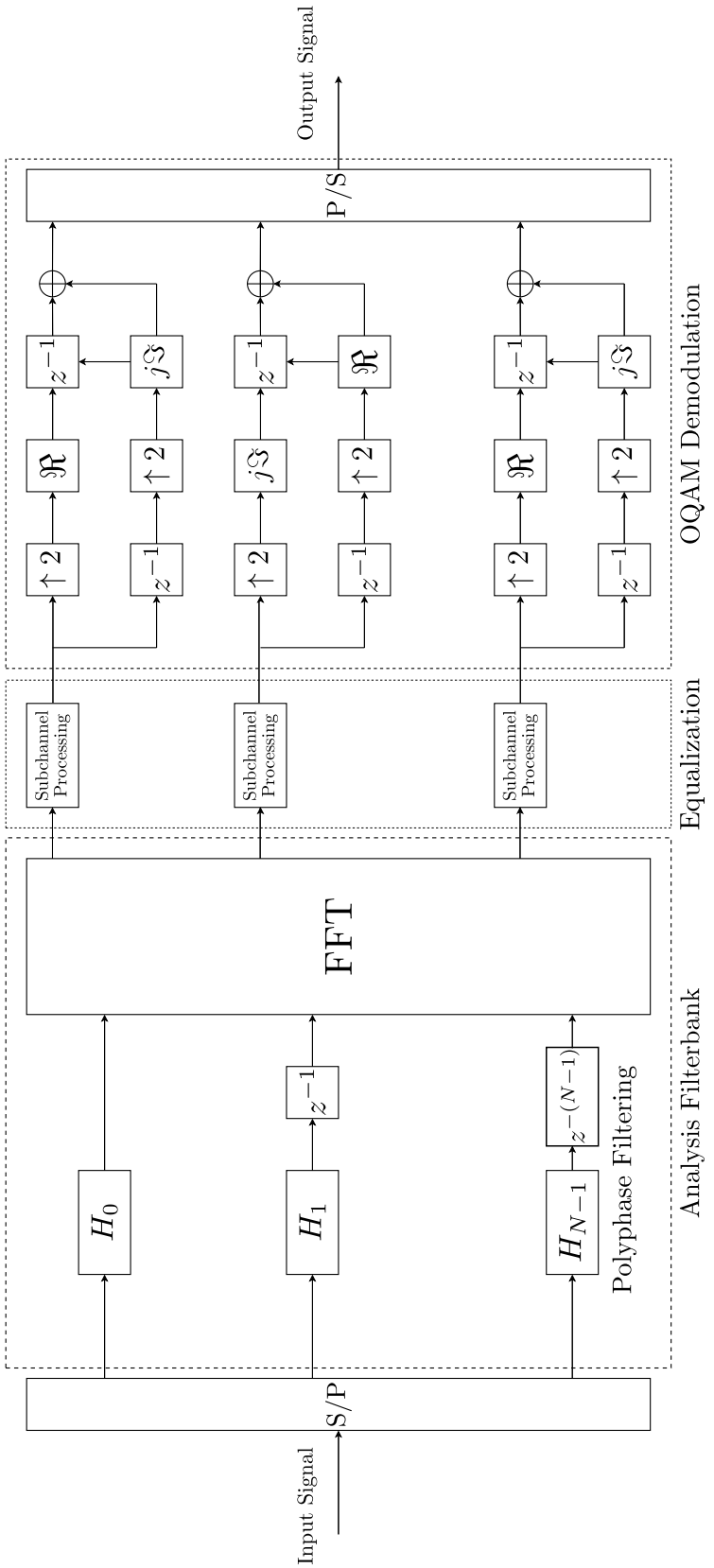

FIGURE 2.12 – A FBMC receiver.

However, since ICI is limited to the adjacent subchannel (due to the prototype filters' frequency response sidelobes), equalization complexity can be reduced. Proposals for subchannel equalizers in filterbank multicarrier systems can be found in [30; 32; 33; 17].

2.5.2 Efficiency

The introduction of the cyclic prefix in a multicarrier system brings transmission bandwidth and power waste. Bandwidth and power efficiencies η_{BW} and η_P are expressed, respectively, by

$$\eta_{BW} = \frac{N - N_g}{N + L_{CP}} \tag{2.32}$$

and

$$\eta_P = \frac{N}{N + L_{CP}}, \tag{2.33}$$

where N_g is the number of subchannels not used for data transmission.

In filterbank multicarrier systems, the cyclic prefix is not used. Therefore, there is an efficiency gain ; for this case, bandwidth and power efficiencies $\eta_{BW,FB}$ and $\eta_{P,FB}$ are expressed, respectively, by

$$\eta_{BW,FB} = \frac{N}{N + \alpha} \tag{2.34}$$

and

$$\eta_{P,FB} = \frac{N}{N} = 1, \tag{2.35}$$

with α equal to the roll-off factor of the prototype filter.

2.5.3 Computational complexity

OFDM/QAM systems operate at a symbol rate T, thus a pair of IFFT/FFTs is done at each T seconds. Since filterbank multicarrier systems transmit the real and imaginary parts of the complex symbol separately, they must operate at a $T/2$ symbol rate to transmit the same amount of data, doing two times the amount of IFFT/FFTs for the same amount of transmitted data when compared to OFDM/QAM systems. The filterbank in its polyphase implementation adds NL_{PF} multiplications, where L_{PF} is the prototype filter length. This way, the computational complexity of FBMC/OQAM is over two times higher than OFDM/QAM systems [34; 35].

2.5.4 Error Performance

The error performance of OFDM/QAM and FBMC/OQAM systems is compared in this subsection through simulation examples. The simulation parameters are

- Sampling frequency - 10 MHz
- Carrier frequency - 2,5 GHz
- Number of subchannels - 128, 256 and 1024
- 1000 independent channel realizations for each point
- Frame length - 53 OFDM symbols
- QPSK/OQPSK constellations
- PHYDYAS prototype filter for the FBMC/OQAM system
- Channel models : Vehicular A and B [36]

Alongside the one tap subchannel equalizer, multitap subchannel equalizers based on the Lagrange and geometric interpolations were used in FBMC systems [17].

For 128 subchannels and the Vehicular A channel model the results are presented in Figure 2.13. Clearly, the one tap subchannel equalizer has the worst performance in high $\frac{E_b}{N_0}$ ratios among FBMC/OQAM systems, because the subchannel frequency response is frequency selective. Thus, multi-tap subchannel equalizers are needed, but even with then the error performance is worse than the one from OFDM/QAM systems. However, this system uses a large cyclic prefix of 1/4, wasting 25 % of the bandwidth.

Figure 2.14 shows that for 256 subchannels and the Vehicular A channel model all the FBMC/OQAM subchannel equalizers have similar error performance. This result can be explained due to the fact that in this case the subchannels are nearly flat, thus a one tap subchannel equalizer is enough to compensate the channel distorsion. Again the OFDM/QAM system has the best error performance, but with a waste of more than 10 % of the bandwidth.

Finally results for 1024 subchannels and the Vehicular B channel model (which is more frequency selective than the Vehicular A one) are presented in Figure 2.15. To eliminate the ISI the OFDM/QAM system used a cyclic prefix of 1/4, which leads to a waste of 25 % of the bandwidth. Among the FBMC/OQAM systems the one using the multitap

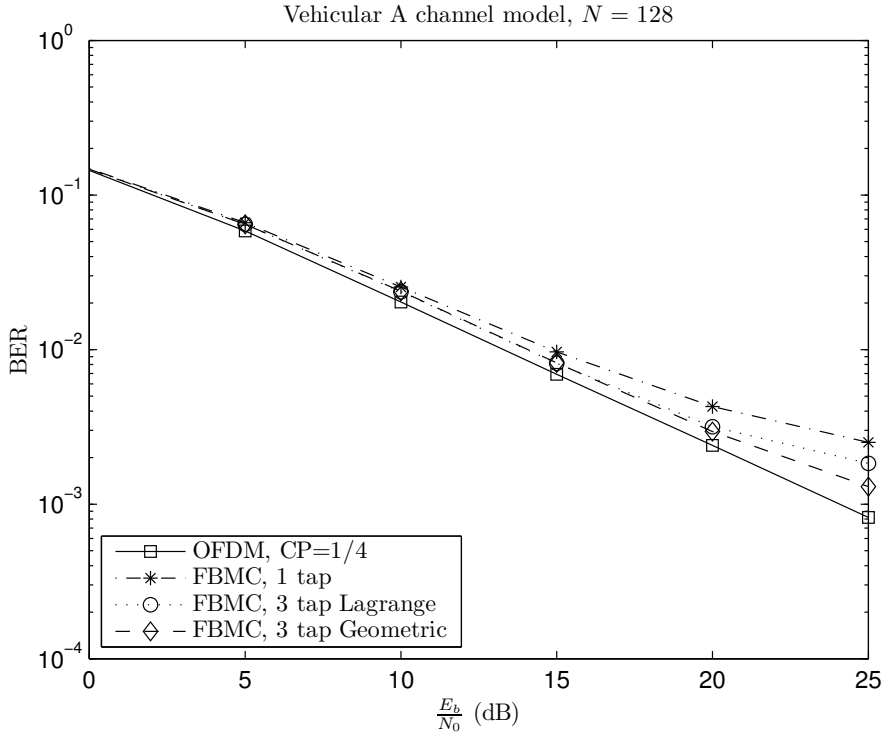

FIGURE 2.13 – Comparison between OFDM/QAM and FBMC/OQAM systems for 128 subchannels and the Vehicular A channel model.

subchannel equalizer based on geometric interpolation has the best error performance.

2.6 Precoded OFDM/QAM Systems

The multicarrier systems seen in previous sections use frequency domain equalization to simplify the equalization of channels with long impulse responses instead of long time domain equalizers. However, they suffer from high peak-to-average power ratio (PAPR), low robustness to spectral nulls in subchannels and low resistance to carrier frequency offset (CFO) [7]. One way to overcome these drawbacks, while maintaining frequency domain equalization, is the use of linear precoding [37]. This section deals only with precoded OFDM/QAM systems ; precoded FBMC/OQAM systems will be detailed in Chapter 3.

A block diagram of a precoded OFDM/QAM system is presented in Figure 2.16. In this system model, the symbols to be transmitted are precoded by an unitary matrix satisfying

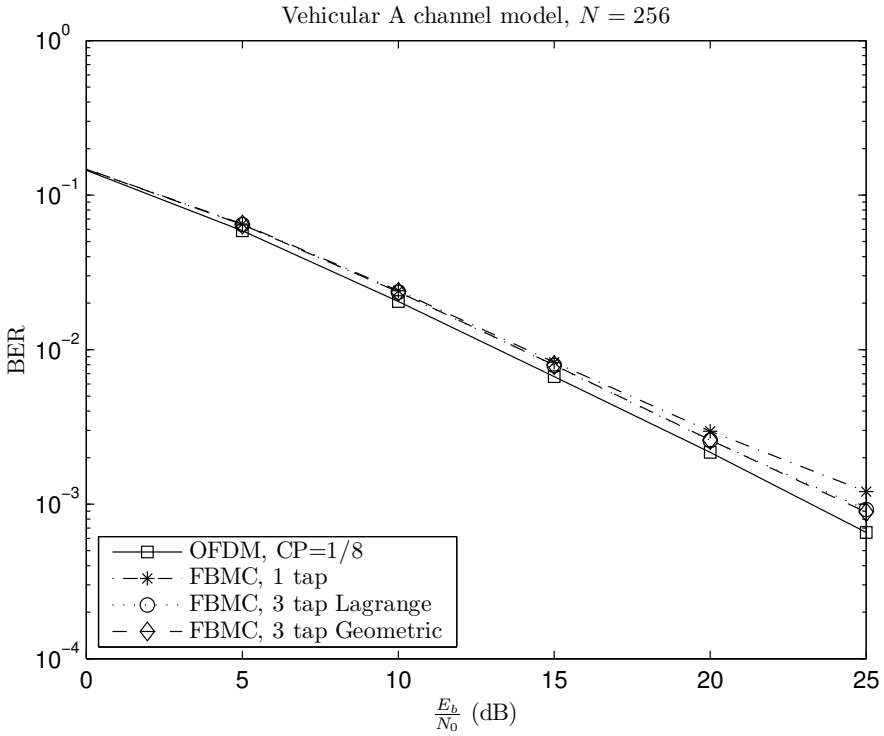

FIGURE 2.14 – Comparison between OFDM/QAM and FBMC/OQAM systems for 256 subchannels and the Vehicular A channel model.

the following condition [37] :

$$|t_{i,j}| = \frac{1}{\sqrt{N}}, 0 \leq i, j \leq N-1, \tag{2.36}$$

where $t_{i,j}$ denotes the (i,j)-th element of the precoding matrix $\mathbf{T}$. With this precoding operation, symbol power will not increase. If the matrix $\mathbf{T}$ is the normalized DFT one, this precoded multicarrier system will correspond to a SC-FDE system [7; 8], because the precoding DFT cancels the IFFT done at a OFDM/QAM transmitter. SC-FDE systems can also be seen as the switching of the IFFT from the OFDM/QAM transmitter to its receiver.

After being precoded by $\mathbf{T}$, the precoded symbols go through the usual OFDM/QAM chain. In the receiver, after equalization the combined symbols are deprecoded by the inverse precoding matrix $\mathbf{T}^{-1}$. Finally, the symbol decision is done in the time domain after deprecoding.

In regular OFDM/QAM systems, zero-forcing equalization is the optimal one, being

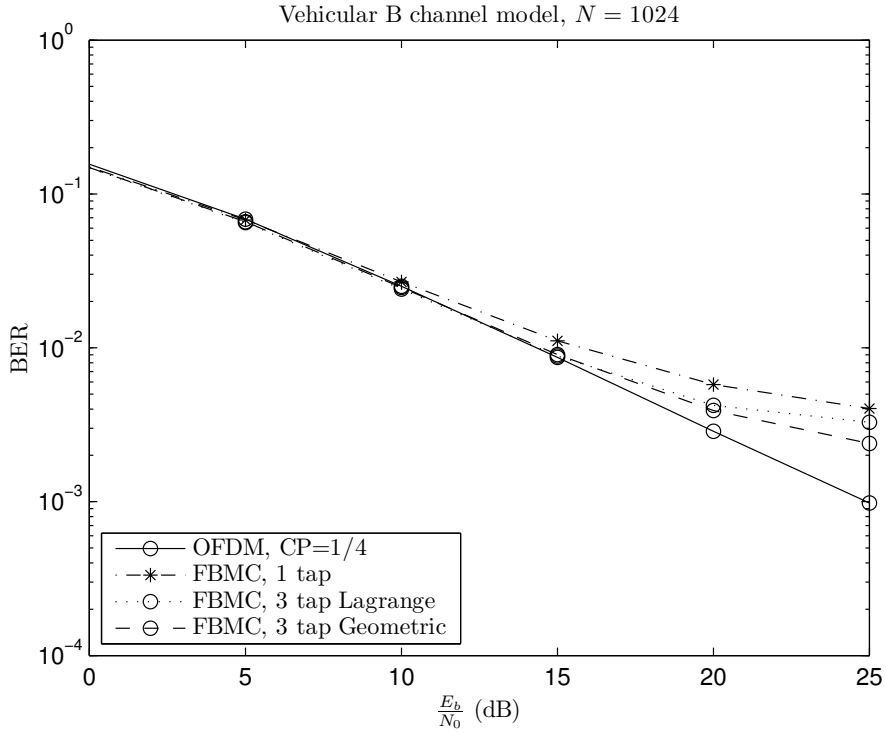

FIGURE 2.15 – Comparison between OFDM/QAM and FBMC/OQAM systems for 1024 subchannels and the Vehicular B channel model.

equivalent to maximal likelihood decoding [38]. This is because equalization is done symbol by symbol. On precoded OFDM/QAM systems, since the equalization is done block by block (before deprecoding), maximal likelihood techniques can be computationally impractical if the system has a large number of subchannels. Thus, suboptimal linear equalization techniques are usually employed. In the following, we restrict ourselves to the case where the precoding matrix $\mathbf{T}$ is the discrete Fourier matrix $\mathbf{W}$ (SC-FDE systems).

2.6.1 Linear Zero-forcing Equalization

The simplest of these techniques is zero-forcing equalization. When using ZF equalization, the equalizer $\mathbf{R}_{\text{ZF}}$ can be expressed as

$$\mathbf{R}_{\text{ZF}} = (\mathbf{H}^H\mathbf{H})^{-1}\mathbf{H}^H, \tag{2.37}$$

where $\mathbf{H}$ is the channel frequency response matrix.

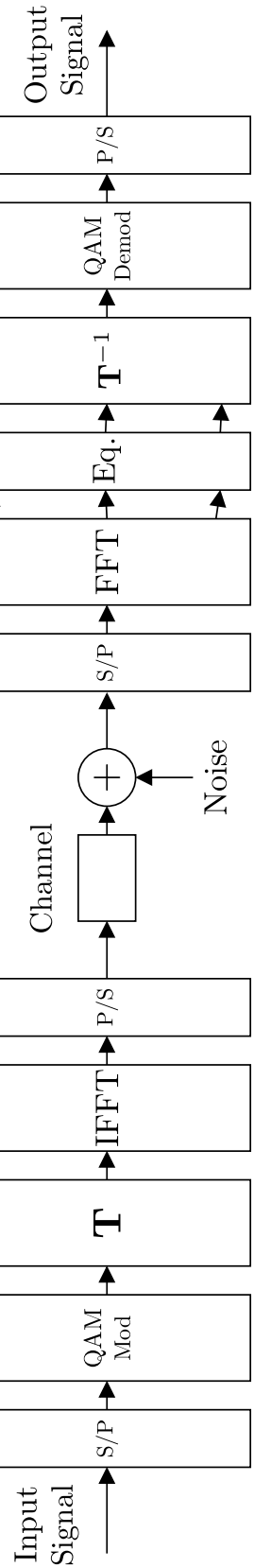

FIGURE 2.16 – A precoded OFDM/QAM system using linear equalization.

With this equalizer, the symbol estimate $\hat{\tilde{\mathbf{s}}}_{\text{ZF}}$ can be expressed as

$$\hat{\tilde{\mathbf{s}}}_{\text{ZF}} = \tilde{\mathbf{s}} + \mathbf{W}^{-1}(\mathbf{H}^H\mathbf{H})^{-1}\mathbf{H}^H\mathbf{W}\tilde{\mathbf{n}}. \tag{2.38}$$

The zero-forcing equalizer eliminates completely the ISI out of $\hat{\tilde{\mathbf{s}}}_{\text{ZF}}$; however, it amplifies the noise term.

Observing (2.38), it is possible to see that the noise correlation matrix will be circulant. Thus, the SNR after deprecoding will be the same for every symbol in the block. This SNR can be expressed as

$$\gamma_{\text{ZF}} = \frac{\gamma N}{\text{tr}((\mathbf{H}^H\mathbf{H})^{-1})}, \tag{2.39}$$

where γ is the symbol energy. Since the SNR is the same for every symbol, the BER will be too.

The maximal uncoded diversity order of a precoded OFDM/QAM system using linear zero-forcing equalization will be one, no matter what the channel impulse response length is [39]. We remember that the diversity order D for a certain system is given by

$$D = \lim_{SNR\to\infty} -\frac{\log(P_e(SNR))}{\log(SNR)}, \tag{2.40}$$

with $P_e(SNR)$ being the average error probability of a certain system as a function of the SNR.

2.6.2 Linear Minimum Mean Square Error Equalization

If the SNR is known at the receiver, linear equalization based on the minimum mean square error (MMSE) criterion can be applied. The MMSE equalizer $\mathbf{R}_{\text{MMSE}}$ is given by

$$\mathbf{R}_{\text{MMSE}} = (\mathbf{H}^H\mathbf{H} + \sigma_n^2\mathbf{I}_N)^{-1}\mathbf{H}^H. \tag{2.41}$$

The symbol estimate when using MMSE equalization is expressed as

$$\begin{aligned}\hat{\tilde{\mathbf{s}}}_{\text{MMSE}} =& \tilde{\mathbf{s}} - \sigma_n^2\mathbf{W}^{-1}(\mathbf{H}^H\mathbf{H} + \sigma_n^2\mathbf{I}_N)^{-1}\mathbf{W}\tilde{\mathbf{s}} \\ &+ \mathbf{W}^{-1}(\mathbf{H}^H\mathbf{H} + \sigma_n^2\mathbf{I}_N)^{-1}\mathbf{H}^H\mathbf{W}\tilde{\mathbf{n}}.\end{aligned} \tag{2.42}$$

Unlike when using the ZF equalizer, $\hat{\tilde{\mathbf{s}}}_{\text{MMSE}}$ contains ISI (the second term of (2.42)) alongside the noise (the third term of (2.42)). This is a characteristic of MMSE equalizers : they minimize the mean square error but do not completely eliminate the ISI.

The ISI and noise covariance matrices are again circulant ; as a consequence, the mean square error is once again the same for every symbol in the block. This mean square error in this case is given by

$$\text{MSE}_{\text{MMSE}} = \frac{1}{N}\sum_{n=1}^{N}\frac{1}{\gamma|H_n|^2+1}, \tag{2.43}$$

with H_n being the (n,n)th element of the channel frequency response matrix $\mathbf{H}$, and the unbiased signal to interference-plus-noise ratio (SINR) for this linear equalizer is

$$\gamma_{\text{MMSE}} = \frac{1}{\text{MSE}_{\text{MMSE}}} - 1. \tag{2.44}$$

With linear MMSE equalization, the uncoded diversity order of precoded OFDM/QAM systems is dependent of the channel impulse response length, the constellation size and the number of subchannels, varying between one and $L_{\tilde{\mathbf{h}}} - 1$, where $L_{\tilde{\mathbf{h}}}$ is the channel impulse response length [39]. Since this diversity order is usually higher than the one possible by using a zero-forcing equalizer, the utilization of linear MMSE equalization is preferred in precoded multicarrier systems.

2.6.3 Minimum Mean Square Error Decision Feedback Equalization

One drawback of the linear MMSE equalizer presented in Section 2.6.2 is that it is not able to completely eliminate the ISI. A decision feedback equalizer (DFE) can be used to improve the error performance, using previous decisions to reduce the postcursor ISI.

The system model of a precoded OFDM/QAM system using a MMSE DFE is shown in Figure 2.17. This equalizer consists in a frequency domain feedforward (FF) filter $\mathbf{R}_{\text{MMSE-DFE,FF}}$ and a time domain feedback (FB) filter $\tilde{\mathbf{r}}_{\text{MMSE-DFE,FB}}$. The length of the feedback filter is set to match the length of the channel impulse response in order to cancel all the ISI from the previous symbols.

To minimize the mean square error, the coefficients of the feedforward filter are [40]

$$\mathbf{R}_{\text{MMSE-DFE,FF}} = \left(\mathbf{H}^H\mathbf{H} + \sigma_n^2\mathbf{I}_N\right)^{-1}\mathbf{H}^H\left(\mathbf{I}_N - \mathbf{R}_{\text{MMSE-DFE,FB}}\right), \tag{2.45}$$

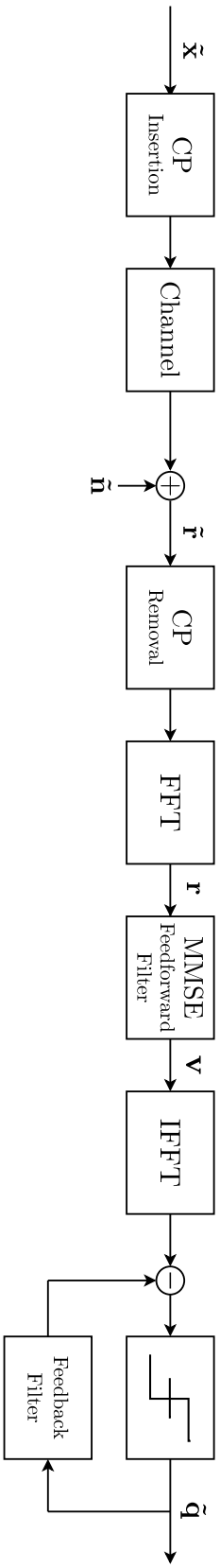

FIGURE 2.17 – A precoded OFDM/QAM system employing MMSE decision-feedback equalization.

where $\mathbf{R}_{\text{MMSE-DFE,FB}}$ is the frequency domain version of the feedback filter $\tilde{\mathbf{r}}_{\text{MMSE-DFE,FB}}$. $\tilde{\mathbf{r}}_{\text{MMSE-DFE,FB}}$ (of length $L_{\tilde{\mathbf{d}}}$) can be found by solving the following equation [40]

$$\mathbf{C}_{\text{MMSE-DFE,FB}}\tilde{\mathbf{r}}_{\text{MMSE-DFE,FB}} = \mathbf{d}_{\text{MMSE-DFE,FB}}, \tag{2.46}$$

with $\mathbf{C}_{\text{MMSE-DFE,FB}}$ being a $L_{\tilde{\mathbf{d}}}\text{x}L_{\tilde{\mathbf{d}}}$ matrix with its m,l-th element given by

$$[\mathbf{C}_{\text{MMSE-DFE,FB}}]_{m,l} = \sum_{n=1}^{N} \frac{\exp(-j2\pi(n(l-m)/N))}{|H_n|^2 + \sigma_n^2} \tag{2.47}$$

and $\mathbf{d}_{\text{MMSE-DFE,FB}}$ is a $L_{\tilde{\mathbf{d}}}\text{x}1$ vector with its m-th element given by

$$[\mathbf{d}_{\text{MMSE-DFE,FB}}]_{m} = \sum_{n=1}^{N} \frac{\exp(-j2\pi(nm)/N)}{|H_n|^2 + \sigma_n^2}. \tag{2.48}$$

When using the MMSE-DFE equalizer, the mean square error considering that previous decisions are perfect is given by [41]

$$\text{MSE}_{\text{MMSE-DFE}} = \exp\left(\frac{1}{N}\sum_{n=1}^{N}\frac{1}{1+\gamma|H_n|^2}\right). \tag{2.49}$$

2.7 Tomlinson-Harashima Precoding

While decision feedback equalizers, such as the one presented in Subsection 2.6.3, are efficient in eliminating the ISI if past symbol decisions are correct, the effect of wrong symbol decisions can be propagated to future symbols. These incorrect propagated decisions can affect significatively the final error performance, even if limited to one block as is the case in SC-FDE DFE systems. These systems also cannot use channel coding without modifications, because reliable symbol decisions in the receiver will be available only after a delay [42].

If the transmitter has complete channel state information, the feedback filter of the DFE scheme can be moved from the receiver to the transmitter to overcome the effect of the ISI, avoiding error propagation. Together with the precoding filter a modulo-$2M$ operation is employed to stop the output from increasing or diverging to infinity if the channel impulse response value is close to zero.

This scheme is known as Tomlinson-Harashima precoding [43; 44]. Since decisions are instantaneous at the receiver in Tomlinson-Harashima precoded systems, channel coding

TABLE 2.2 – Precoding loss in dB of Tomlinson-Harashima precoded systems [1].

M	2	4	8	16	32	64
η_{1D}	1.25	0.28	0.07	0.02	0.004	0.001
η_{2D}	-	1.25	0.58	0.28	0.14	0.07

can be employed with good performance. Their error performance is the same as the one from systems employing an ideal DFE (i.e., error free) in the receiver minus a power penalty, which is dependent of the signal constellation used. This power penalty is due to the modulo operation employed to limit the transmitted signal power. The power penalty for one and two-dimensional constellations is listed in Table 2.2. As seen in Table 2.2, this power penalty (precoding loss) becomes negligible as the constellation size grows [43].

Zhu et al. in [45] propose a SC-FDE system employing MMSE-based Tomlinson-Harashima precoding. The block diagram for this system is presented in Figure 2.18.

In the transmitter, together with the precoding filter a modulo-$2M$ operation is employed to stop the output from increasing or diverging to infinity by mapping the precoded symbols from a M^2-QAM constellation to the interval $(-M, M]$ if the channel impulse response has values close to zero. The precoded signal follows the same path of a SC-FDE system using linear MMSE equalization (cyclic prefix insertion, passage through the channel, cyclic prefix removal, FFT, linear MMSE equalization and IFFT). After the de-precoding IFFT, the same modulo operation is done in the receiver to obtain the symbol estimate. The coefficients for the precoding filter in this system are the same ones from the feedback filter in the MMSE-DFE equalizer ; thus, they can be found by solving (2.46). The coefficients for the equalizer in the receiver are equal to the ones from the MMSE-DFE feedforward filter, which are expressed in (2.45).

2.8 Widely Linear Processing

The systems presented up to now use linear processing to obtain the symbol estimate from the received signal in the receiver. However, for a certain category of signals, linear processing does not take into account all the available second-order statistics of the received

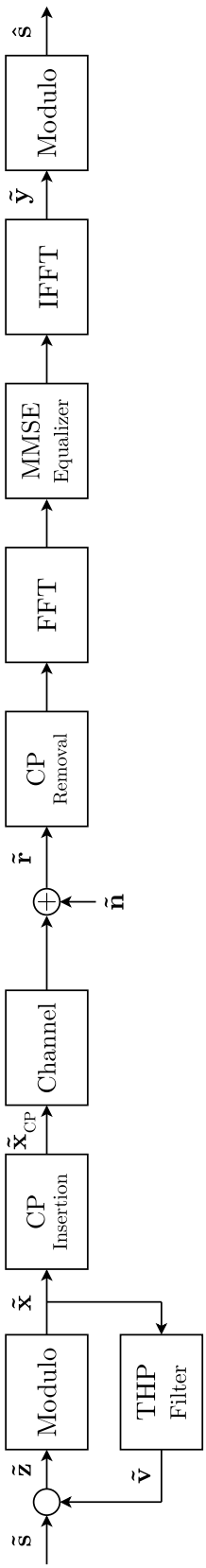

FIGURE 2.18 – A SC-FDE system employing linear MMSE equalization and Tomlinson-Harashima precoding.

signal. To use these statistics, widely linear processing was proposed [11; 12].

Let $\hat{\tilde{x}}$ be a scalar random variable to be estimated from an observation that is a random vector $\tilde{\mathbf{y}}$. $\tilde{\mathbf{y}}$ is a vector whose elements are samples from a complex random process with zero mean, that is, $E\{\tilde{\mathbf{y}}\} = 0$. This vector can be written as $\tilde{\mathbf{y}} = \tilde{\mathbf{y}}_r + j\tilde{\mathbf{y}}_i$, where $\tilde{\mathbf{y}}_r$ is the real part of $\tilde{\mathbf{y}}$ and $\tilde{\mathbf{y}}_i$ the imaginary one. As a consequence of $E\{\tilde{\mathbf{y}}\} = 0$, $E\{\tilde{\mathbf{y}}_r\} = 0$ and $E\{\tilde{\mathbf{y}}_i\} = 0$.

We can also verify that for a random variable $\tilde{y} = \tilde{y}_r + j\tilde{y}_i$ belonging to $\tilde{\mathbf{y}}$, with $\tilde{y}_r$ and $\tilde{y}_i$ independent from each other with zero mean and the same variance, $E\{\tilde{y}\tilde{y}\} = 0$.

A vector $\tilde{\mathbf{y}}$ is called a circular vector if [10]

$$PC \equiv E\left\{\tilde{\mathbf{y}}\tilde{\mathbf{y}}^T\right\} = 0, \tag{2.50}$$

where PC is the so-called pseudocovariance matrix. Together with the covariance, (2.50) defines completely the second-order statistics of $\tilde{\mathbf{y}}$. As examples of circular vectors, it is possible to cite modulated signals from complex constellations, such as M-QAM ones.

By processing the received observation $\tilde{\mathbf{y}}$ by the linear estimator $\tilde{\mathbf{f}}$ we can obtain the scalar estimate $\hat{\tilde{x}}$, resulting in

$$\hat{\tilde{x}} = \tilde{\mathbf{f}}^H\tilde{\mathbf{y}}. \tag{2.51}$$

However, if $\tilde{\mathbf{y}}$ belongs to a real or offset constellation (2.50) is no longer valid, because for these constellations the pseudocovariance is non-zero, that is

$$PC \equiv E\left\{\tilde{\mathbf{y}}\tilde{\mathbf{y}}^T\right\} \neq 0. \tag{2.52}$$

This is the case for constellations such as M-PAM (Phase Amplitude Modulation), MSK (Minimum Shift Keying), OQPSK (Offset Quadrature Phase Shift Keying)or M-OQAM (Offset Quadrature Amplitude Modulation). Thus, when the transmitted signal comes from one of these modulations the linear estimator $\tilde{\mathbf{f}}$ does not use all the available second-order statistics.

2.8.1 Widely Linear Estimator

To take into account (2.52), the received signal must be processed together with its conjugate to obtain the estimate $\tilde{\hat{x}}_{WL}$, in the following way [11] :

$$\tilde{\hat{x}}_{WL} = \tilde{\mathbf{c}}^H \tilde{\mathbf{y}}_{WL} + \tilde{\mathbf{d}}^H \tilde{\mathbf{y}}^*_{WL}, \tag{2.53}$$

where $\tilde{\mathbf{c}}$ and $\tilde{\mathbf{d}}$ are two complex vectors constituting a linear subspace over the complex field, with $\tilde{\mathbf{y}}_{WL}$ being an observation from an improper constellation.

This scheme is shown in Figure 2.19.

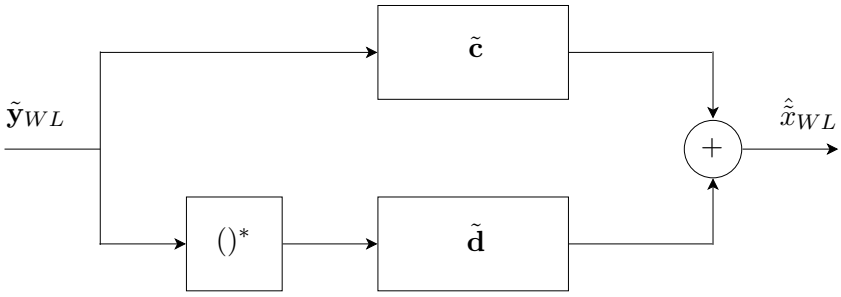

FIGURE 2.19 – A receiver using widely linear processing.

It is clear that $\tilde{\hat{x}}_{WL}$ is not a linear function of $\tilde{\mathbf{y}}_{WL}$, which is the case of $\hat{\tilde{x}}$ in (2.51). However, the order-k statistics of $\tilde{\hat{x}}_{WL}$ can be inferred from the order-k statistics of $\tilde{\mathbf{y}}_{WL}$ and $\tilde{\mathbf{y}}^*_{WL}$. This is why (2.53) is called a *wide sense linear* or *widely linear* system.

Observing (2.53), the estimation problem consists in finding the optimal values of $\tilde{\mathbf{c}}$ and $\tilde{\mathbf{d}}$ in a way that $E\left\{|\tilde{\hat{x}}_{WL} - \tilde{x}_{WL}|^2\right\}$ is minimized. The linear subspace spanned by $\tilde{\hat{x}}_{WL}$ becomes a Hilbert subspace if we define the scalar product by $< \tilde{\hat{x}}_{WL,1}, \tilde{\hat{x}}_{WL,2} > = E\left\{\tilde{\hat{x}}^*_{WL,1}\tilde{\hat{x}}_{WL,2}\right\}$. As a consequence, $\tilde{\hat{x}}_{WL}$ can be seen as a orthogonal projection of $\tilde{x}_{WL}$ in this Hilbert subspace and due to the orthogonality principle,

$$E\left\{\tilde{\hat{x}}^*_{WL}\tilde{\mathbf{y}}_{WL}\right\} = E\left\{\tilde{x}^*_{WL}\tilde{\mathbf{y}}_{WL}\right\}, \tag{2.54}$$

$$E\left\{\tilde{\hat{x}}^*_{WL}\tilde{\mathbf{y}}^*_{WL}\right\} = E\left\{\tilde{x}^*_{WL}\tilde{\mathbf{y}}^*_{WL}\right\}. \tag{2.55}$$

Substituting (2.54) and (2.55) in (2.53) we obtain

$$\Lambda\mathbf{c} + \Pi\mathbf{d} = \lambda, \tag{2.56}$$

$$\Pi^*\mathbf{c} + \Lambda^*\mathbf{d} = \varpi^*, \tag{2.57}$$

with

$$\Lambda = E\left\{\tilde{x}_{WL}\tilde{x}_{WL}^{*}\right\}, \tag{2.58}$$

$$\Pi = E\left\{\tilde{x}_{WL}\tilde{x}_{WL}^{T}\right\}, \tag{2.59}$$

$$\lambda = E\left\{\tilde{\mathbf{y}}_{WL}^{*}\tilde{x}_{WL}\right\}, \tag{2.60}$$

$$\varpi = E\left\{\tilde{\mathbf{y}}_{WL}\tilde{x}_{WL}\right\}. \tag{2.61}$$

The optimal values of $\tilde{\mathbf{c}}$ and $\tilde{\mathbf{d}}$ according to the widely linear minimum mean square error criterion are

$$\tilde{\mathbf{c}} = [\Lambda - \Pi\Lambda^{-1*}\Pi^{*}]^{-1}[\lambda - \Pi\Lambda^{-1*}\varpi^{*}], \tag{2.62}$$

$$\tilde{\mathbf{d}} = [\Lambda^{*} - \Pi^{*}\Lambda^{-1}\Pi]^{-1}[\varpi^{*} - \Pi^{*}\Lambda^{-1}\lambda], \tag{2.63}$$

and the corresponding mean square error for the widely linear estimator is

$$\epsilon_{\mathrm{WL}}^{2} = P_{\tilde{\mathbf{y}}_{WL}} - \tilde{\mathbf{c}}^{H}\lambda - \tilde{\mathbf{d}}^{H}\varpi^{*}, \tag{2.64}$$

with $P_{\tilde{\mathbf{y}}} = E\left\{|\tilde{\mathbf{y}}_{WL}|^{2}\right\}$.

The mean square error obtained when using the widely linear estimator is lower than the one from linear estimation, which is

$$\epsilon_{\mathrm{L}}^{2} = P_{\tilde{\mathbf{y}}} - \lambda^{H}\Lambda^{-1}\lambda. \tag{2.65}$$

The corresponding processing gain can be expressed by

$$\epsilon_{\delta}^{2} = \epsilon_{\mathrm{L}}^{2} - \epsilon_{\mathrm{WL}}^{2}, \tag{2.66}$$

ϵ_{δ}^{2} is also given by

$$\epsilon_{\delta}^{2} = [\varpi^{*} - \Pi^{*}\Lambda^{-1}\lambda]^{H}[\Lambda^{*} - \Pi^{*}\Lambda^{-1}\Pi]^{-1}[\varpi^{*} - \Pi^{*}\Lambda^{-1}\lambda] \geq 0. \tag{2.67}$$

2.8.2 Widely Linear Processing Gain

The gain ϵ_{δ}^{2} obtained by employing widely linear processing depends on the second-order statistics of the noise and the transmitted signal.

2.8.2.1 When both the noise and the transmitted signal are circular

The widely linear filter reduces to the strictly linear one if both the noise and the transmitted signal are circular, since $PC = 0$ and $\mathbf{s} = E\left\{\tilde{\mathbf{y}}_{WL}\tilde{x}_{WL}\right\} = 0$; thus, there is no performance advantage in using widely linear processing over strictly linear processing.

2.8.2.2 If the observed signal is circular, but $\varpi \neq 0$

In this case $PC = 0$, but $\varpi \neq 0$ since there is no information about the statistics of the transmitted signal. Thus, the optimal coefficients of the filters $\tilde{\mathbf{c}}$ and $\tilde{\mathbf{d}}$ can be expressed as

$$\tilde{\mathbf{c}} = \Lambda^{-1}\lambda, \tag{2.68}$$

$$\tilde{\mathbf{d}}^{*} = \Lambda^{-1}\varpi, \tag{2.69}$$

and the widely linear processing gain is

$$\epsilon_{\delta}^{2} = \varpi^{H}\Lambda^{-1}\varpi \geq 0. \tag{2.70}$$

2.8.2.3 If the transmitted signal is improper

However, if a improper signal is transmitted through a complex channel, the observed signal at the receiver is also complex and improper. In this case we reach easily the conclusion that $\lambda = \varpi$, which will lead to $\tilde{\mathbf{c}} = \tilde{\mathbf{d}}^{*}$. The widely linear estimator in this case will provide the following estimate $\hat{x}_{WL}$:

$$\hat{\tilde{x}}_{WL} = 2\Re\left\{\tilde{\mathbf{c}}^{H}\tilde{\mathbf{y}}\right\}. \tag{2.71}$$

This estimate is real, unlike when using strictly linear estimators, which will generate a complex estimate of this real transmitted signal. For this case, by using widely linear processing we can have up to half of the mean square error of the strictly linear estimator [46; 12]. The processing gain by using widely linear estimation is

$$\epsilon_{\delta}^{2} = \tilde{\mathbf{c}}^{H}\lambda. \tag{2.72}$$

2.9 Conclusion

This chapter has presented the background for the research work which will be presented in the next chapters of this thesis. The following chapter will deal with the application of linear precoding in FBMC/OQAM systems and their correspondent error performance.

Chapter 3

On Precoded FBMC/OQAM Systems

3.1 Introduction

Unlike precoded OFDM/QAM systems, precoded FBMC/OQAM systems are a theme not very explored in research. Few proposals have appeared so far in the literature for precoded FBMC systems ; one can be found in [47]. In this proposal, classical multicarrier, precoded multicarrier and pure single carrier transmissions can be done simultaneously, each in its group of subchannels, due to the high subchannel selectivity inherent to the FBMC systems. A proposal to minimize the transmitted symbols' PAPR in a single carrier-FBMC using a novel transmitter scheme can be found in [48]. However, the error performance of precoded FBMC systems has not been studied so far in the literature.

The objective of this chapter is to study the error performance of precoded FBMC/OQAM systems, including the case where residual ISI stemming from imperfect subchannel equalization is present in these systems when employing linear MMSE equalization. It is shown that this residual ISI causes a loss of diversity in precoded FBMC/OQAM systems. An analytical expression of the BER for these systems taking into account or not this residual ISI is compared to Monte Carlo simulations in different channel situations to demonstrate its precision.

This chapter is divided as follows : Section 3.2 presents an analysis on the error behaviour for precoded multicarrier systems with residual ISI. Simulation results for FBMC

systems and a comparison with the error approximation provided earlier in the section are presented in Section 3.3. Concluding remarks are given in Section 3.4.

3.2 BER Analysis for Precoded Filterbank Multicarrier Systems

The block diagram of a precoded FBMC/OQAM system is presented in Figure 3.1. Figure 3.1a depicts a precoded FBMC transmitter, while Figure 3.1b shows a precoded FBMC receiver. Finally, Figure 3.1c shows the complete system. In this diagram, the grey box $\mathbf{T}$ is the precoding matrix, η is the AWGN (additional white gaussian noise) with variance σ_η^2 and $\tilde{\mathbf{h}}$ is the channel impulse response for a particular channel realization. The only change with respect to a regular FBMC/OQAM system is the precoding matrix $\mathbf{T}$ in the transmitter and the deprecoding one $\mathbf{T}^{-1}$ in the receiver.

We can write the received signal $\tilde{r}^{OQAM}[n]$ as

$$\tilde{r}^{OQAM}[n] = \tilde{h}[n] * \tilde{s}^{OQAM}[n] + \eta[n] \tag{3.1}$$

$$= \tilde{y}^{OQAM}[n] + \eta[n], \tag{3.2}$$

where $*$ is the convolution operator. After demodulation, the received signal on the k-th subchannel of the l-th FBMC data block can be expressed as

$$\tilde{r}_{k,l}^{OQAM} = \Re\left\{ \sum_{n=l\frac{N}{2}}^{L_{PF}-1+l\frac{N}{2}} \xi_{k,l}^{OQAM}[n]\tilde{y}^{OQAM}[n] + \eta_{k,l} \right\} \tag{3.3}$$

$$= \hat{\tilde{r}}_{k,l}^{OQAM} + \Re\left\{\eta_{k,l}\right\}, \tag{3.4}$$

with $\hat{r}_{k,l}^{OQAM}$ being the useful signal and $\eta_{k,l}$ the filtered noise, expressed by

$$\eta_{k,l} = \sum_{n=l\frac{N}{2}}^{L_{PF}-1+l\frac{N}{2}} \eta[n]\tilde{q}\left[n - l\frac{N}{2}\right] e^{j\frac{2\pi}{N}k(n-\frac{L_{PF}-1}{2})} e^{j\rho_{k,l}}. \tag{3.5}$$

$\eta_{k,l}$ is a linear combination of Gaussian random variables ; so, it remains a Gaussian random variable with variance

$$\sigma_{\eta_{k,l}}^2 = \sigma_\eta^2 \sum_{n=l\frac{N}{2}}^{L_{PF}-1+l\frac{N}{2}} \tilde{q}\left[n - l\frac{N}{2}\right]^2 = \sigma_\eta^2, \tag{3.6}$$

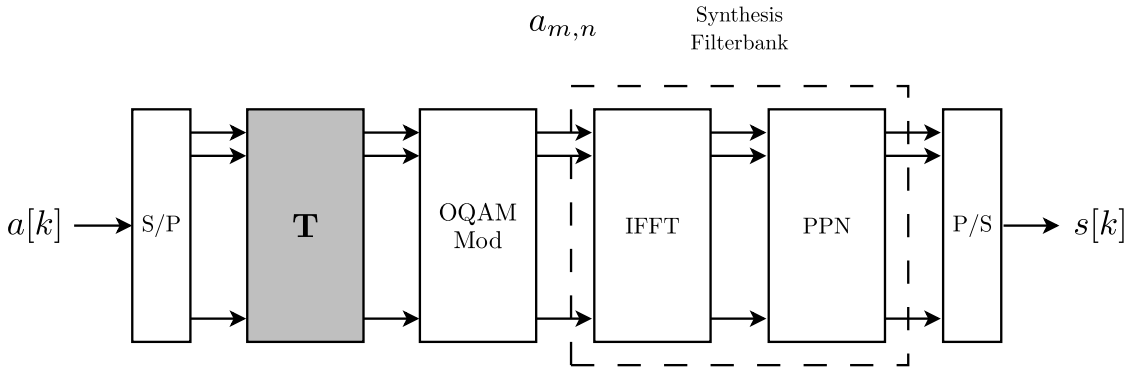

(a) A precoded FBMC transmitter

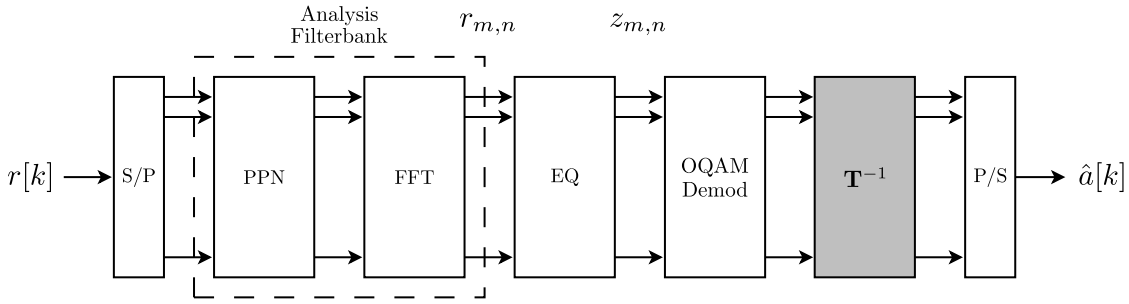

(b) A precoded FBMC receiver

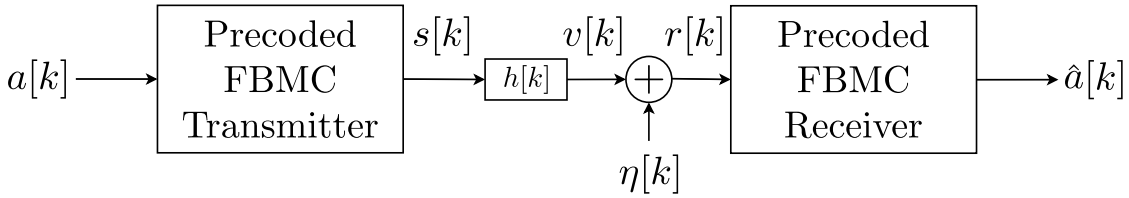

(c) The complete system

FIGURE 3.1 – A precoded FBMC/OQAM system.

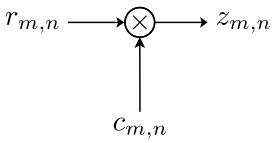

(a) One tap subchannel equalizer

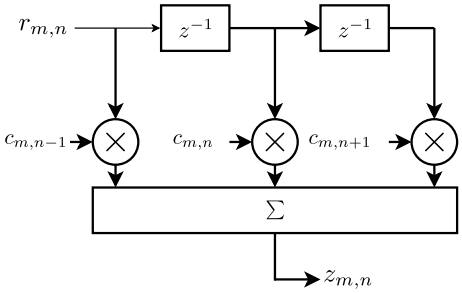

(b) Three tap subchannel equalizer

FIGURE 3.2 – Equalizers for FBMC Systems.

since the normalization of the prototype filters implies that

$$\sum_{n=l\frac{N}{2}}^{L_{PF}-1+n\frac{N}{2}} \tilde{q}^2\left[n-l\frac{N}{2}\right]=1. \tag{3.7}$$

Therefore, the noise variance will not change after the analysis filterbank, also due to the fact that the NxN DFT matrix is an unitary matrix. Thus, the analysis can proceed as in the precoded OFDM/QAM case.

The one-tap equalizer used to compensate the channel effect (see Figure 3.2a) is equal to $c_{k,l}=\frac{1}{H_k}$ for a ZF equalizer and to $c_{k,l}=\frac{\gamma H_k^*}{1+\gamma|H_k|^2}$ for the one employing the MMSE criterion, with $\gamma=\frac{E_s}{\sigma^2}$ being the SNR and H_k being the channel frequency response at the center of the k-th subchannel. A 3-tap per subchannel equalizer, which can be used to overcome frequency-selective subchannels, is presented in Figure 3.2b. The expression for its coefficients is not detailed in this section, but can be found in [30; 31].

We remind that a channel independent precoding matrix has to satisfy the following condition so that the noise variance is the same in every subchannel (Section 2.6) :

$$|t_{i,j}|=\frac{1}{\sqrt{N}}, 0\leq i,j\leq N-1, \tag{3.8}$$

where $t_{i,j}$ denotes the (i,j)-th element of the precoding matrix $\mathbf{T}$. To satisfy the condition imposed by (3.8), we can use the Discrete Fourier Transform (DFT) matrix or the

Hadamard matrix, among others.

3.2.1 ISI power in non-completely equalized FBMC systems

Up to now, we have seen that the noise variance analysis in precoded FBMC/OQAM systems can be done the same way as the OFDM/QAM ones. However, in FBMC systems equalization is not always perfect, due to the absence of the cyclic prefix ; thus, residual interferences can be present.

The effect of ICI (in absence of CFO) can be discarded in FBMC systems, because the fractionally spaced equalizer eliminates ICI from the neighbouring subchannels, and the high selectivity provided by the improved subchannel filtering eliminates the ICI from the other ones [33]. However, residual ISI can be present, due to the absence of the cyclic prefix. When the transmission channel is highly frequency-selective and the number of subchannels is low, the subchannel frequency response will also be frequency-selective, even with the subchannel pulse being optimized to minimize this selectivity.

To compensate this extra interference, equalization in FBMC systems has been dealt with in [30; 31; 33], among other works. The desired complex impulse response on each subchannel (black circles on Figure 3.3) after equalization is given in Figure 3.3. The real desired impulse response must be zero at nT_s, $n \neq 0$ in order to eliminate the ISI on the other transmitted symbols on the real part, whereas the imaginary desired impulse response must be zero at $\frac{nT_s}{2}$, $n \neq 0$ in order to eliminate the ISI on the transmitted symbols on the imaginary part. The impulse response at other instants (white circles on Figure 3.3) can have arbitrary values, because they are not taken into account for the desired equalized subchannel impulse response.

This ideal impulse response will result in a flat equalized subchannel frequency response $H_k^{eq}(f)$; thus, any deviation from the flat frequency response will correspond to extra ISI in the detected symbol, since this non-flat equalized subchannel frequency response means that the symbol energy was spread to other symbols.

So, we integrate over this residual subchannel spectrum to determine the power $\sigma^2_{\mathrm{ISI},k}$ of this extra ISI at the k-th subchannel, according to the following equation :

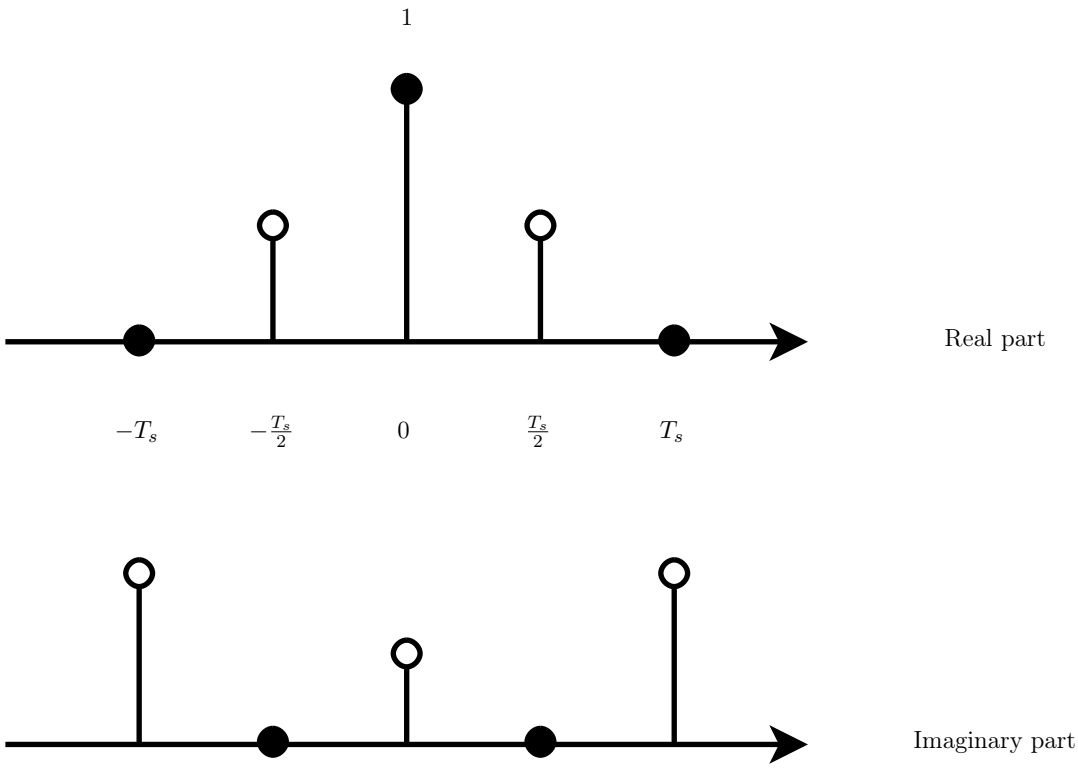

FIGURE 3.3 – Desired equalized subchannel complex impulse response in FBMC systems.

$$\sigma^2_{\text{ISI},k} = \int_{-\infty}^{\infty} |1 - H_k^{eq}(f)|^2 df. \tag{3.9}$$

When using MMSE equalization it is appropriate to use the signal to interference plus noise ratio (SINR), since there is also ISI alongside the noise. Since after deprecoding both the ISI and the noise covariance matrices are also circulant, the noise variance, SNR and BER are the same for every subchannel. The ISI power stemming from non-completely equalized subchannels will be added to the AWGN noise variance (considering this ISI as gaussian due to the large number of subchannels) to form the effective SINR, which will be, for a precoded FBMC system employing MMSE equalization,

$$\gamma_{\text{MMSE,ISI}} = \frac{1}{\text{MSE}_{\text{MMSE,ISI}}} - 1, \tag{3.10}$$

where

$$\text{MSE}_{\text{MMSE,ISI}} = \frac{1}{N} \sum_{n=1}^{N} \frac{1}{\zeta_k |H_n|^2 + 1}. \tag{3.11}$$

and $\zeta_k = \frac{Es}{N_0 + \sigma^2_{\text{ISI},k}}$.

If the subchannel equalizer has sufficient length to compensate the subchannel frequency response or the number of subchannels is large enough so the subchannel frequency response is flat, (3.10) reduces to the known MSE and SINR equations ((2.43) and (2.44)) for precoded multicarrier systems using linear MMSE equalization, which are

$$\mathrm{MSE}_{\mathrm{MMSE}} = \frac{1}{N}\sum_{n=1}^{N}\frac{1}{\gamma|H_n|^2+1}, \tag{3.12}$$

and

$$\gamma_{\mathrm{MMSE}} = \frac{1}{\mathrm{MSE}_{\mathrm{MMSE}}} - 1. \tag{3.13}$$

Finally, the overall BER P_e considering a given channel realization can be expressed as :

$$P_e = aQ\left(\sqrt{b\beta}\right). \tag{3.14}$$

where a and b are constellation-specific parameters [49], β in this equation can be β_{MMSE} or $\beta_{\mathrm{MMSE,ISI}}$ and $Q(x) = \frac{1}{\sqrt{2\pi}}\int_x^\infty e^{\frac{-t^2}{2}}dt$. To compute the overall BER an average over all the results from different channel realizations is made.

3.3 Simulation Results

In this section, simulation results of the error performance for precoded filterbank multicarrier systems are presented, comparing the results from the error approximations presented in Section 3.2 and the ones provided by Monte Carlo simulations. The simulation parameters can be found in Table 3.1. Channel estimation is assumed to be perfect and channel fading is considered to be quasistatic (time-invariant during each transmitted frame). Results were averaged over all the independent channel realizations to obtain the presented error probabilities. The multiple-tap per subchannel equalizers are the ones presented in [31], whose project is based on the frequency sampling approach, geometric interpolation and the IFFT to calculate the equalizers' coefficients.

Figure 3.4 presents the simulation results comparing the results obtained from the Monte Carlo simulations to the BER approximation presented in (2.44) (which does not take into account the residual ISI) using linear MMSE equalization, for a system with N = 1024 and the Vehicular A channel model. 1-tap and 3-tap per subchannel equalizers are

TABLE 3.1 – Simulation Parameters for Section 3.3.

Constellation	OQPSK
Sampling Frequency	10 MHz
Channel Models	ITU-T Ped. B, Veh. A, Veh. B
Number of channel realizations	5000
Minimum number of errors	200
Prototype Filter	PHYDYAS [25]
Overlapping factor K	4
Precoding matrix $\mathbf{T}$	DFT

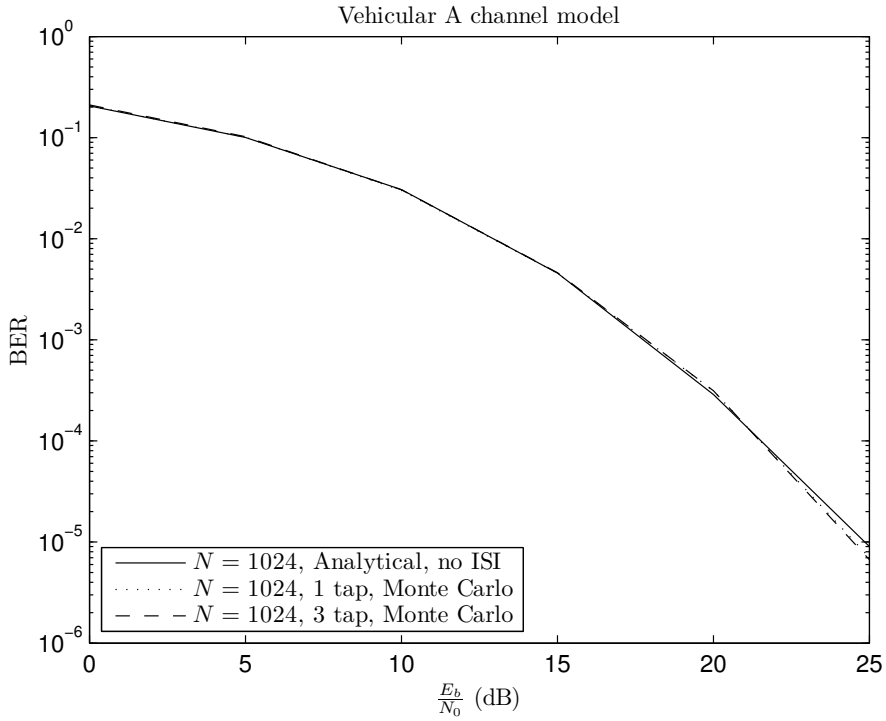

FIGURE 3.4 – Comparison between theoretical and Monte Carlo simulation results using 1024 subchannels and the Vehicular A channel model.

used. In this case, we can assume that the subchannels suffer flat fading and there is no residual ISI after equalization ; it is possible to see that the Monte Carlo simulation results are very close to the ones provided by this approximation.

For $N = 128$, Figure 3.5 compares the results from the Monte Carlo simulations to the BER approximation in (2.44) for the Vehicular A channel model. The same subchannel

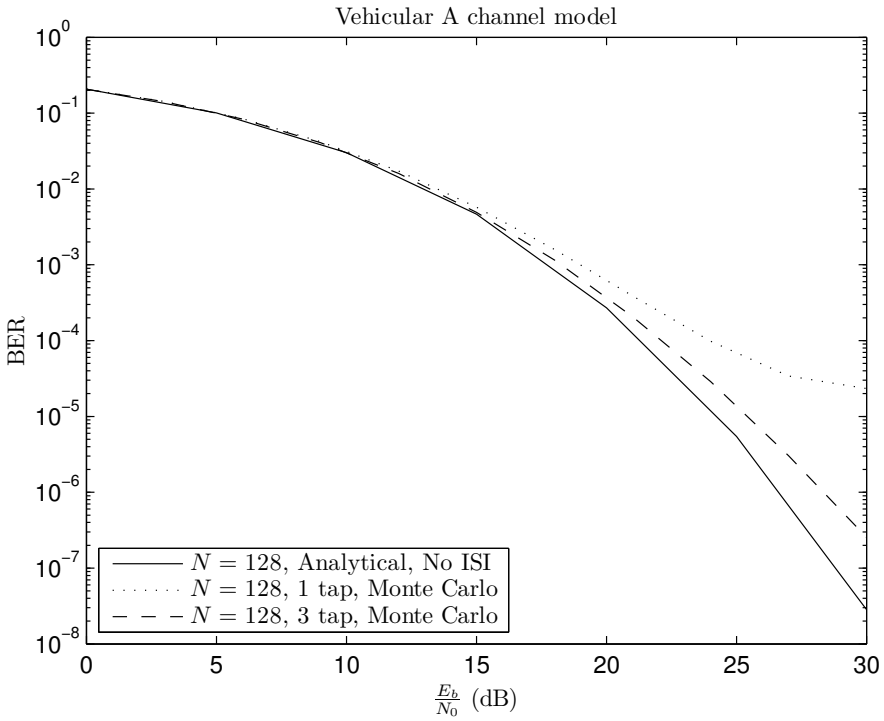

FIGURE 3.5 – Comparison between theoretical and Monte Carlo simulation results using 128 subchannels and the Vehicular A channel model.

equalizers from the previous example are used. For this case, even the multiple-tap equalizer is not enough to completely eliminate the ISI from the received data stream, because the subchannels are frequency selective. It is possible to see that in a low SNR range, the Monte Carlo simulation results are faithful to the approximation because the noise variance is higher than the one from the ISI at this stage ; however, in higher signal-to-noise ratios, their results drift from the BER approximation, due to this remaining unequalized interference being higher than the noise variance. The results from the systems using a 1-tap per subchannel equalizer are much farther from the approximation than the ones using a 3-tap per subchannel equalizer, due to its worse equalization performance.

Figure 3.6 presents the simulation results for 64 subcarriers and the ITU-T Vehicular A channel model. For this scenario, the channel is highly frequency selective (for example, if regular OFDM systems were used, the appropriate cyclic prefix size to completely eliminate the ISI would be 1/2). It is possible to see that even subchannel equalizers with a higher number of taps are not able to compensate effectively the channel selectivity, leading to

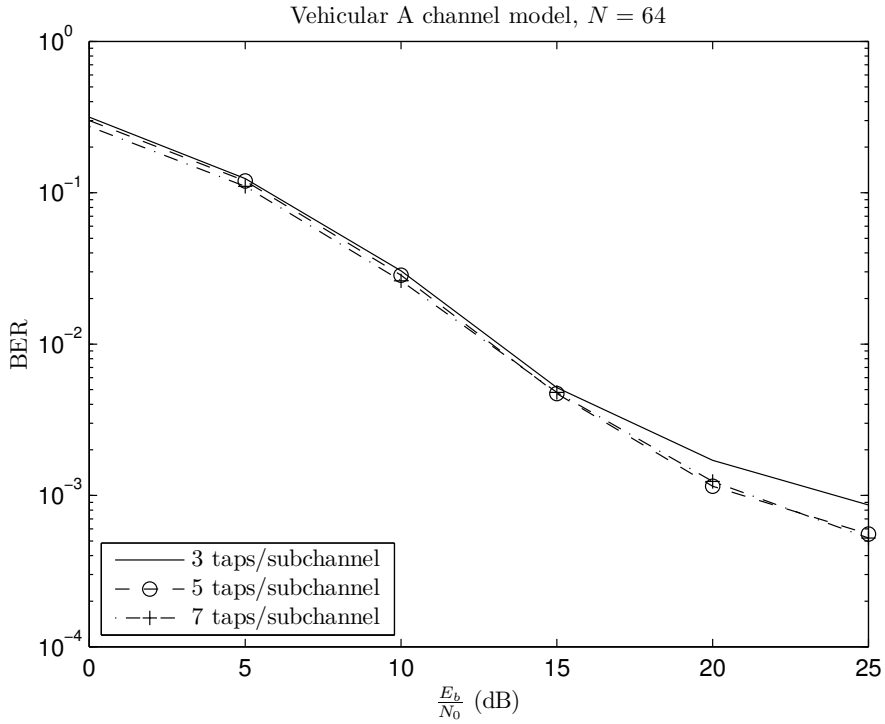

FIGURE 3.6 – Error performance for $N = 64$ and the Vehicular A channel model.

residual ISI and an error floor at a bit error rate (BER) of about 10^{-3}.

For 512 subcarriers and the Vehicular B channel model, Figure 3.7 presents the simulation results. In this scenario, the channel selectivity is similar to the one presented in Figure 3.6 (a cyclic prefix size of $1/2$ would be needed too), and the subchannel equalizers cannot eliminate all the ISI.

Figures 3.8 and 3.9 shows the comparison between the Monte Carlo simulation results and the approximation results when using the model based on (3.10), which takes into account the residual unequalized ISI present in the subchannels for the calculation of the SINR. FBMC systems are transmitting through a Vehicular A channel model with $N = 128, 256$ (in Figure 3.8) and the Pedestrian B channel model with $N = 256, 512$ (in Figure 3.9). For these cases, with $N = 128$ for the Vehicular A channel model and $N = 256$ for the Pedestrian B channel model the subchannels are going to be frequency selective. On the other hand, with $N = 256$ for the Vehicular A channel model and $N = 512$ for the Pedestrian B channel model the subchannels can be considered as flat. The

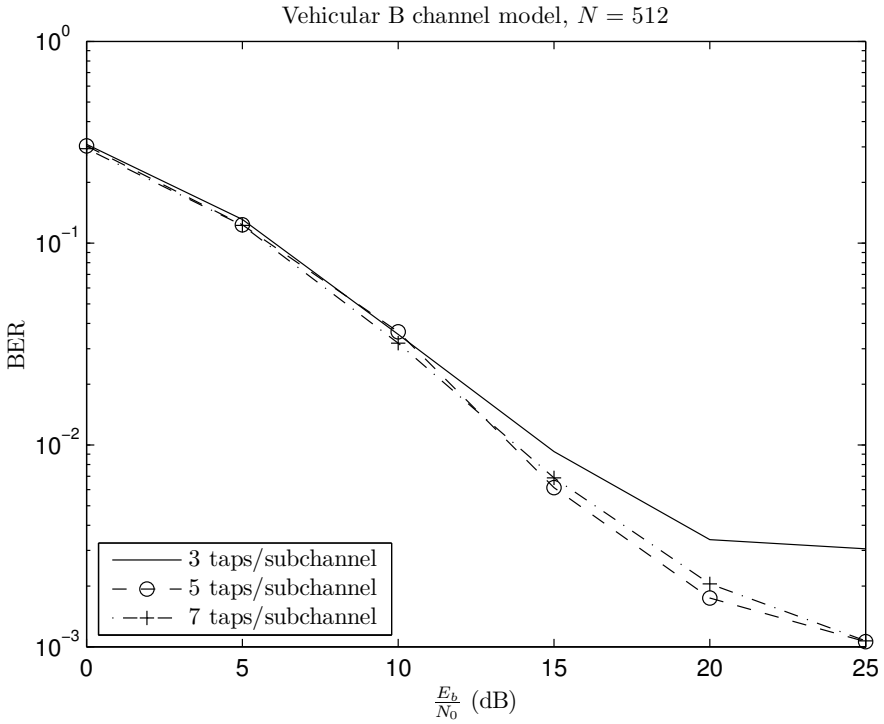

FIGURE 3.7 – Error performance for $N = 512$ and the Vehicular B channel model.

approximation results are consistent with the ones provided by Monte Carlo simulation. It is also possible to see that the systems employing a one tap per subchannel equalizer have a lower diversity order than the systems using subchannel equalizers with three taps for the same number of subchannels if the subchannels are frequency-selective ; this is because the one tap equalizer is unable to deal with the subchannel selectivity in these cases. When the subchannels have a flat frequency response, a one tap equalizer is enough to completely equalize the subchannel and obtain the maximum possible diversity in the scenario. In this case, using subchannel equalizers with three taps per subchannel does not bring a performance improvement.

In the coded simulations, a mother convolutional code of rate $1/2$ with a generating polynomial $(133, 171)_8$, a constraint length $K = 7$ and free distance $d_{free} = 10$ is used. Higher rates are obtained through puncturing. Results are presented in Figure 3.10 for systems employing convolutional coding, transmitting throught the Vehicular B channel model and with $N = 1024, 2048$. In this case, $N = 1024$ will lead to frequency-selective

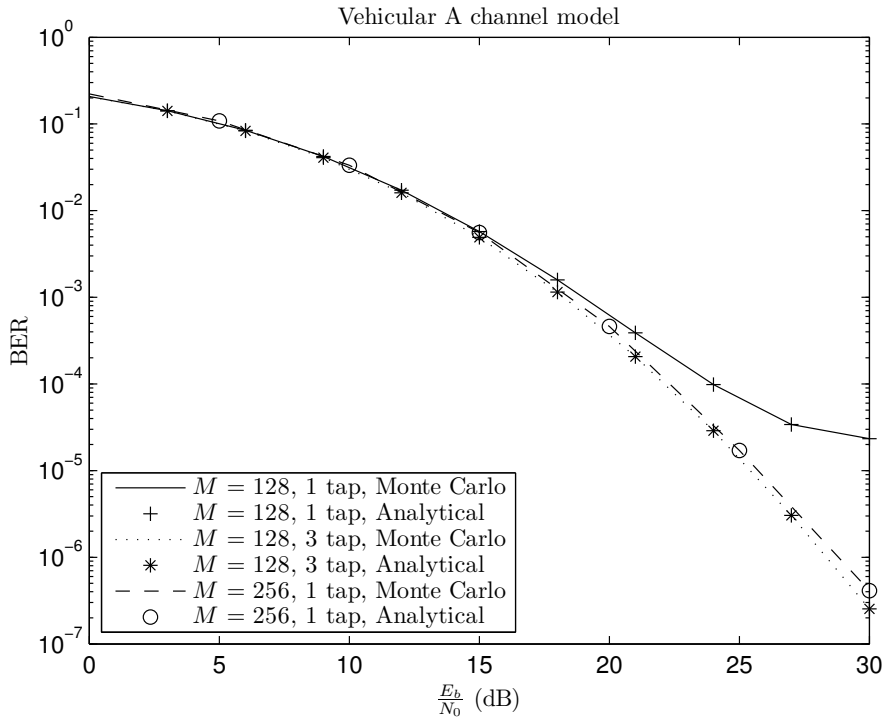

FIGURE 3.8 – Uncoded error performance for precoded FBMC systems using MMSE equalization and transmitting through the Vehicular A channel model.

subchannels, while with $N = 2048$ the subchannels will be flat. The same conclusions from the uncoded case can be drawn from the results in the coded one : the residual unequalized ISI from frequency-selective subchannels reduces the diversity order if a one tap subchannel equalizer is employed ; this diversity order can be restored with multiple tap equalizers or with an increase in the number of subchannels. With flat subchannels, a one tap equalizer is enough to remove all the ISI and obtain the maximal possible diversity.

3.4 Concluding Remarks

In this chapter the error performance of precoded FBMC systems using linear MMSE equalization was analyzed. Analytical uncoded BER performances for FBMC systems taking into account this residual ISI were derived in this section, which are precise throughout the ensemble of SNRs. It is also possible to see that the residual unequalized ISI from imperfect equalization causes a loss of diversity in the coded and uncoded cases. This loss of

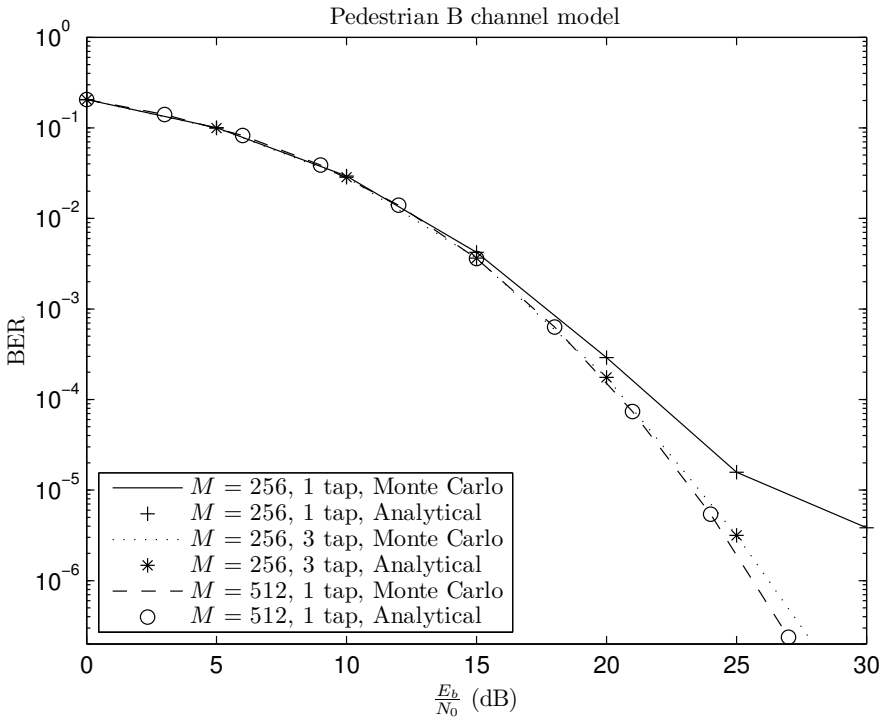

FIGURE 3.9 – Uncoded error performance for precoded FBMC systems using MMSE equalization and transmitting through the Pedestrian B channel model.

diversity can be prevented with the use of subchannel equalizers with multiple taps or with an increase in the number of subchannels ; with those measures, there will be very little to no residual ISI.

The next chapter deals with the probability density function of the SINR of a precoded multicarrier system using linear MMSE equalization and an analytical way to determine its coded performance when using convolutional coding.

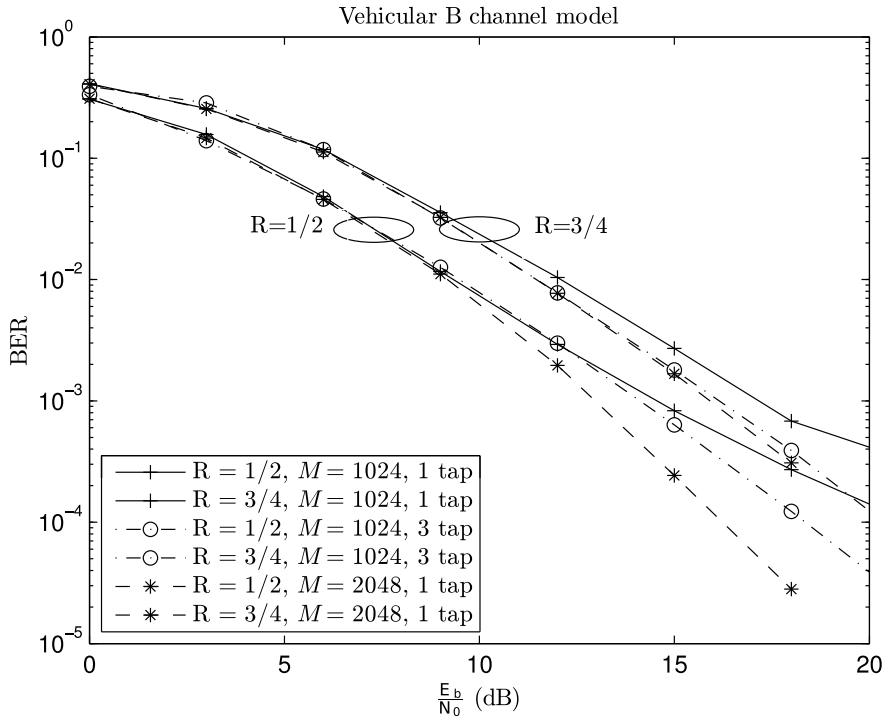

FIGURE 3.10 – Coded error performance for precoded FBMC systems using MMSE equalization and transmitting through the Vehicular B channel model.

Chapter 4

On the Distribution of the SINR and Performance in Uncoded and Coded SC-FDE Systems Using Linear MMSE Equalization

In the previous chapter we have tackled the analysis of the error probability of precoded FBMC/OQAM systems; a semi-analytical (averaging results from several channel realizations) expression for the BER of these systems was developed. However, for the direct analytical computation of the unconditional bit error probability of precoded multicarrier systems, the knowledge of the SINR distribution is necessary. [15; 16] proposed a SINR distribution for SC-FDE systems using linear MMSE equalization for channel models with equal powered taps. However, their method does not work when the channel taps do not have equal power. Thus, the distribution for precoded multicarrier systems employing MMSE equalization transmitting through real-life channel models has not been found, due to the difficulty of computing the exact probability density function (pdf) of the SINR [50].

Coding, together with interleaving, can also be applied to these systems to improve the transmission performance, resulting in the so-called Bit Interleaved Coded Modulation (BICM) [51]. In precoded multicarrier systems, since the diversity gain comes mainly from the precoding operation, coding and interleaving provide these systems with a coding gain. Numerical simulation for these systems at high SNRs is time-consuming, due to the low bit error rates at this stage; thus, an analytical analysis is desired. An analysis for block

fading channels was done in [52]. For the coded multicarrier case, but without precoding, [53; 54; 55; 56] show an analysis of their performance. In [57; 58], linear constellation precoding using subchannel grouping was applied to coded multicarrier systems, with maximum likelihood iterative decoding being used at the receiver. The use of subchannel grouping instead of full-scale (a combination of all subchannels) precoding when maximum likelihood decoding is employed is desirable, since the decoding complexity increases with the number of subchannels being grouped. As for precoded multicarrier systems using linear MMSE equalization, the obtention of a pairwise error probability (PEP), which is necessary for the analysis of their coded performance, is difficult. This is due to the inherently imperfect (non-maximum likelihood (ML)) decoding of a combination of subchannels and the noise and subchannel gains correlation introduced by this process.

In this chapter, we propose the adoption of the lognormal distribution with the smallest Kullback-Leibler distance to the observed distribution as an approximation of the probability density function of the SINR in a precoded multicarrier system employing MMSE equalization. This approximation is accurate in the sense of the BER and gives very accurate results in terms of the error probability, even at high SNR values. We use this lognormal approximation to simplify the calculation of the coded performance of this system. Due to this simplification, an expression for the PEP is derived considering the lognormal system abstraction. This PEP expression provides bounds that are close to the Monte Carlo simulation results.

This chapter is organized as follows : Section 4.1 presents the system model employed in this chapter. Section 4.2 deals with the approximation of the SINR distribution by the lognormal one with the smallest Kullback-Leibler distance to the true distribution, while the coded performance analysis employing the lognormal approximation to obtain an expression for the PEP is presented in Section 4.3. Simulation results validating this approach are presented in Section 4.4 and the concluding remarks in Section 4.5.

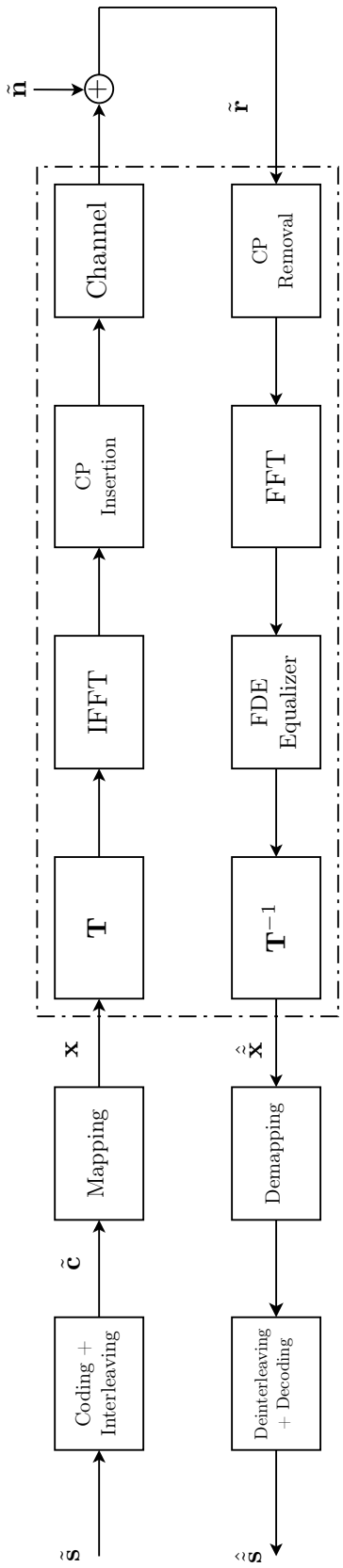

FIGURE 4.1 – A precoded multicarrier system using channel coding.

4.1 System Model

Figure 4.1 details the system model for this chapter. In this system, the sequence $\tilde{\mathbf{s}}$, of size mS is encoded by a rate R_c convolutional code with constraint length K. This codeword is bit-interleaved by an interleaver, resulting in the codeword $\tilde{\mathbf{c}}$. $\mathbf{c}$ is then Gray mapped to a block of M-QAM symbols $\tilde{\mathbf{x}} = [\tilde{x}_1\, \tilde{x}_2\, \ldots\, \tilde{x}_N]^T$ of size $N = S/R_c$, where $M = 2^m$.

After interleaving, $\tilde{\mathbf{x}}$ follows the same path detailed in Section 2.6, using linear MMSE equalization. Thus, repeating (2.43) and (2.44) we remind that the MSE and SINR for this system will be

$$\mathrm{MSE}_{\mathrm{MMSE}} = \frac{1}{N}\sum_{n=1}^{N}\frac{1}{\gamma|H_n|^2+1}, \tag{4.1}$$

and

$$\gamma_{\mathrm{MMSE}} = \frac{1}{\mathrm{MSE}_{\mathrm{MMSE}}} - 1. \tag{4.2}$$

The deprecoded sequence $\hat{\mathbf{x}}$ is demapped, deinterleaved and decoded by a soft-input soft-output (SISO) maximum likelihood Viterbi decoder, resulting in the estimated sequence $\hat{\mathbf{s}}$.

4.2 SINR Distribution

The uncoded unconditional bit error probability for a communications system transmitting through a fading channel with gain α is given by [49]

$$P_e = \int_0^\infty \xi_a Q(\sqrt{\xi_b\gamma}) p_\gamma(\gamma) d\gamma, \tag{4.3}$$

where ξ_a and ξ_b are constellation-specific parameters, $\gamma = \alpha^2 E_s/\sigma_n^2$ is the SINR and $p_\gamma(\gamma)$ is the pdf of this SINR. Looking at (4.3), it is necessary to know the pdf of γ_{MMSE} in order to compute analytically the BER of a precoded multicarrier system using linear MMSE equalization. This SINR for $N = 128$ and the Vehicular A channel model is presented in Figure 4.2.

Since it can be seen that this distribution changes for each SNR for the aforementioned

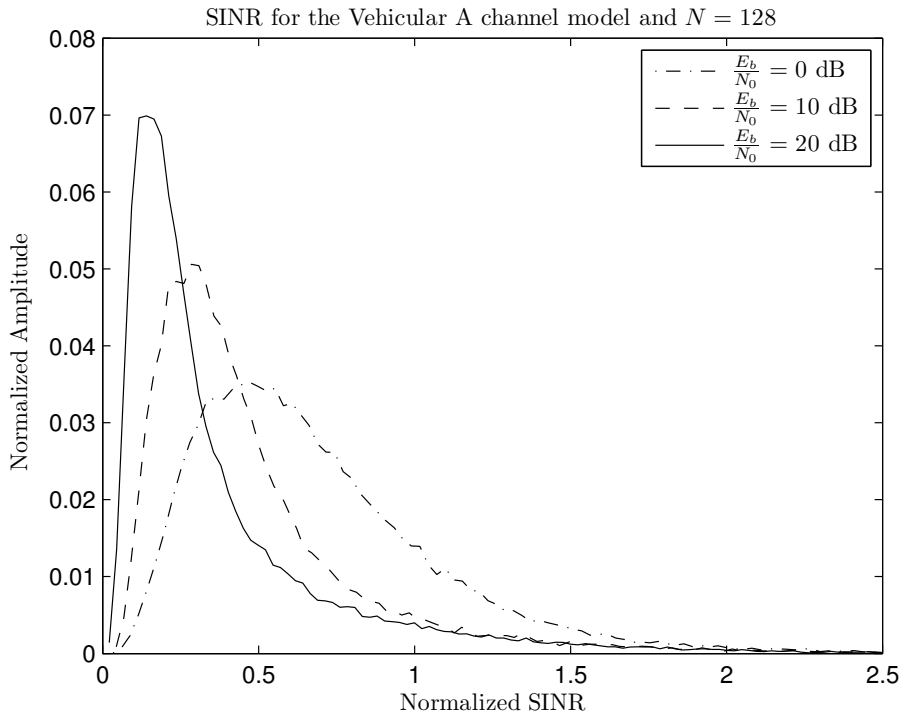

FIGURE 4.2 – SINR for a precoded multicarrier system using linear MMSE equalization, $N = 128$ and the Vehicular A channel model.

system, it is very hard to use a specific distribution that will fit to the SINR for all SNR values. For low SNRs, the SINR distribution can be approximated by various distributions, such as the Gamma one, as an example ; however, for higher SNR values, the approximation becomes very loose. For the BER computation, the approximation should be more precise in the left tail of the pdf curve. This is because this tail corresponds to low SINR values, which will contribute heavily to the overall error performance. High SINR values correspond to very low error probabilities in the Q-function curve ; thus, the other parts of the pdf curve correspond to negligible errors [59]. To achieve this goal, an approximation which will minimize the Kullback-Leibler (KL) distance to the target SINR distribution is desired. The Kullback-Leibler distance between two distributions P and Q is given as

$$D_{KL}(P||Q) = \int_{-\infty}^{\infty} p(x) \log_2 \frac{p(x)}{q(x)} dx, \tag{4.4}$$

where p and q are the probability density functions of P and Q. The KL distance (which is non-negative and zero if and only if $P = Q$) is a measure of the inefficiency of assuming

that the distribution is Q when the true distribution is P [60]. Also called relative entropy, it is a measure of the distance between two distributions, but it is not a true distance because it is not symmetric and does not satisfy the triangle inequality.

There is a direct connection between the minimization of the KL distance between an approximation and the target distribution and the minimization of the effect of the KL tail components [61]. A good fit in the tails of the pdf is needed so that the tail components effect is minimized. Thus, with the minimization of the KL distance it is possible to obtain a precise approximation in the region of interest for the bit error probability case. To minimize the KL distance between the approximation and the SINR, a Monte Carlo simulation is done at each SNR to search for the distribution parameters that will lead to the smallest possible value of the KL distance.

Since the SINR of a precoded multicarrier system using MMSE equalization has only positive values, low mean, high variance and positive skew, a suitable distribution for a fit could be the lognormal distribution [62]. It was seen in our tests that by using the lognormal distribution it is possible to obtain a smaller KL distance to the true SINR distribution when compared to other distributions.

The lognormal distribution has its probability density function given by

$$f_X(x,\mu,\sigma) = \frac{1}{x\sigma\sqrt{2\pi}} \exp -\frac{(\ln x - \mu)^2}{2\sigma^2} \text{ for } \{x > 0\}, \tag{4.5}$$

where μ and σ are the mean and standard deviation, respectively, of a variable whose logarithm is normally distributed.

μ and σ can be found for specific channel models. Figures 4.3,4.4 and Tables 4.1,4.2 specify them for some of the ITU-T channel models. They were found to minimize the KL distance between the approximation and the SINR specified by (2.44). 30000 channel realizations were made to generate this SINR.

Using Craig's formula for the Q function, which is [63]

$$Q(x) = \frac{1}{\pi} \int_0^{\frac{\pi}{2}} \exp\left(\frac{-x^2}{2\sin^2\theta}\right) d\theta, \tag{4.6}$$

(4.3) can be rewritten, for the lognormal distribution presented in (4.5) and a QPSK

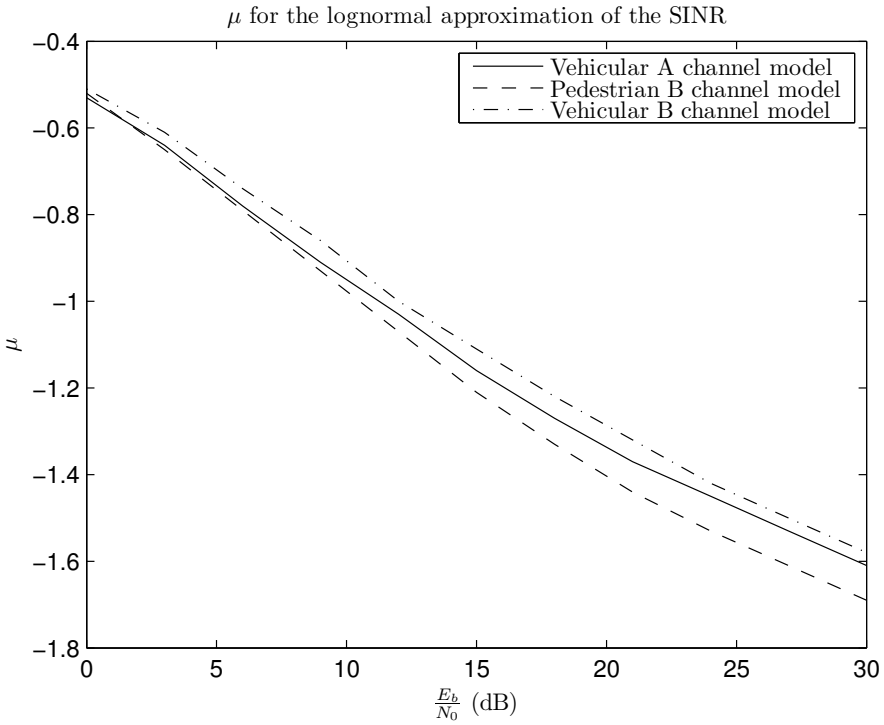

FIGURE 4.3 – μ for some ITU-T channel models.

TABLE 4.1 – μ for some ITU-T channel models.

$\frac{E_b}{N_0}$ (dB)	0	3	6	9	12	15
Veh. A	-0.53	-0.64	-0.78	-0.91	-1.03	-1.16
Ped. B	-0.52	-0.65	-0.79	-0.93	-1.07	-1.21
Veh. B	-0.51	-0.61	-0.74	-0.86	-1	-1.11

$\frac{E_b}{N_0}$ (dB)	18	21	24	27	30
Veh. A	-1.27	-1.37	-1.45	-1.53	-1.61
Ped. B	-1.33	-1.44	-1.53	-1.61	-1.69
Veh. B	-1.22	-1.32	-1.42	-1.5	-1.58

constellation, as

$$P_e = \frac{1}{\pi}\int_0^{\frac{\pi}{2}}\left[\int_0^{\infty}\exp\left(\frac{-\gamma}{2\sin^2\theta}\right)\frac{1}{\sqrt{2\pi\sigma^2\gamma}}\exp\left(-\frac{(\ln\gamma-\mu)^2}{2\sigma^2}\right)d\gamma\right]d\theta, \tag{4.7}$$

since $\xi_a = \xi_b = 1$ for a QPSK constellation.

By the variable substitution $x = \frac{\ln\gamma-\mu}{\sqrt{2\sigma^2}}$, (4.7) can be rewritten as

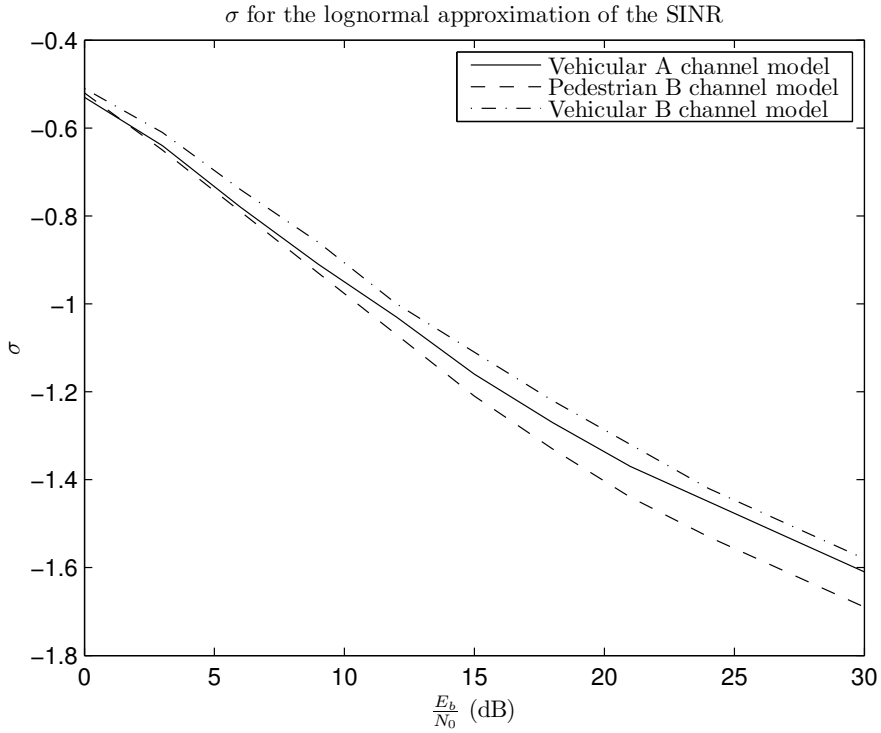

FIGURE 4.4 – σ for some ITU-T channel models.

TABLE 4.2 – σ for some ITU-T channel models.

$\frac{E_b}{N_0}$ (dB)	0	3	6	9	12	15
Veh. A	0.52	0.54	0.56	0.59	0.63	0.66
Ped. B	0.45	0.45	0.48	0.5	0.52	0.55
Veh. B	0.56	0.58	0.6	0.63	0.67	0.71

$\frac{E_b}{N_0}$ (dB)	18	21	24	27	30
Veh. A	0.7	0.74	0.79	0.82	0.86
Ped. B	0.59	0.62	0.66	0.7	0.73
Veh. B	0.74	0.79	0.82	0.86	0.90

$$P_e = \frac{1}{\pi}\int_0^{\frac{\pi}{2}}\left[\frac{1}{\sqrt{\pi}}\int_0^{\infty}\left(\exp\left(-\frac{\frac{E_s}{\sigma_n^2}\exp\left(\sqrt{2}\sigma x+\mu\right)}{2\sin^2\theta}\right)\right)\exp(-x^2)dx\right]d\theta. \tag{4.8}$$

The inner integral in (4.8) can be calculated by a quadrature Gauss-Hermite integration, which results in

$$\sum_{n=1}^{K} w_n \exp\left(-\frac{\exp(\frac{E_s}{\sigma_n^2}\sqrt{2}\sigma x_n + \mu)}{2\sin^2\theta}\right), \tag{4.9}$$

where w_n and x_n are, respectively, the weights and the abcissas of the Hermite polynomial and K is the desired series precision. Values of w_n, x_n and K can be found in [64].

Thus, the following closed-form expression for the bit error probability in a precoded multicarrier system using the lognormal approximation can be used :

$$P_e \approx \frac{1}{\sqrt{\pi}} \sum_{n=1}^{K} w_n \left[\frac{1}{\pi}\int_0^{\frac{\pi}{2}} \exp\left(-\frac{\frac{E_s}{\sigma_n^2}\exp(\sqrt{2}\sigma x_n + \mu)}{2\sin^2\theta}\right) d\theta\right] \tag{4.10}$$

$$\approx \frac{1}{\sqrt{\pi}} \sum_{n=1}^{K} w_n Q\left(\sqrt{\frac{E_s}{\sigma_n^2}\exp\left(\sqrt{2}\sigma x_n + \mu\right)}\right). \tag{4.11}$$

4.3 Coded Performance

The direct derivation of the pairwise error probability of a precoded multicarrier system employing MMSE equalization is very difficult, due to the subchannel gains and noise correlation introduced by the imperfect (non-ML) decoding of a combination of all subcarriers. Since the uncoded SINR of a precoded system employing MMSE equalization was approximated by a lognormal distribution in the previous section, we can simplify the highlighted part of the system model presented in Figure 4.1 to the one presented in Figure 4.5. Thus, the analysis of the coded performance of a precoded multicarrier system employing MMSE equalization can be reduced to the much simpler analysis of the coded performance of a single carrier system transmitting through a lognormal fading channel (because if $\gamma = \alpha^2 E_s/\sigma_n^2$ has a lognormal distribution, α has the same distribution).

A tight BER union upper bound for this system employing a convolutional code (with a rate $R_c = k_c/n_c$ obtained by puncturing a rate $1/2$ mother code, with a minimum Hamming distance d_{free}) is given by [49]

$$P_e \leq \frac{1}{k_c} \sum_{d=d_{free}}^{\infty} w(d) P_{ep}(d|\gamma), \tag{4.12}$$

where $w(d)$ is the input weight of all error events at Hamming distance d and $P_{ep}(d|\gamma)$ is the average pairwise error probability (PEP) conditional on the lognormal SINR γ between

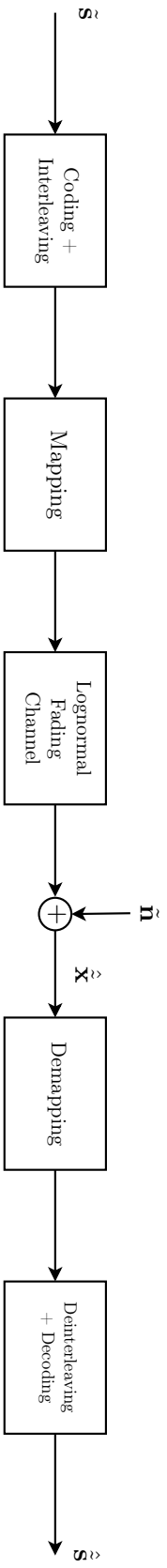

FIGURE 4.5 – A coded precoded multicarrier system using the lognormal approximation.

the codewords having Hamming distance d between them, expressed by [52]

$$P_{ep}(d|\gamma) = Q\left(\sqrt{2d\gamma}\right). \tag{4.13}$$

Values for $w(d)$ at various code rates can be found in [65]. Without loss of generality, we consider that these two codewords only differ in their first d bits. The unconditional pairwise error probability can be obtained by averaging the conditional PEP over the probability density function of the SINR, yielding

$$P_{ep}(d) = \int P_{ep}(d|\gamma) f(\gamma) d\gamma. \tag{4.14}$$

Thus, we can use the process shown in Section 4.2 to derive a closed-form solution for (4.14), which can be expressed as

$$P_{ep}(d) \approx \frac{1}{\sqrt{\pi}} \sum_{n=1}^{N_t} w_n Q\left(\sqrt{2d\frac{E_s}{\sigma_n^2}\exp\left(\sqrt{2}\sigma x_n + \mu\right)}\right), \tag{4.15}$$

where μ and σ are the lognormal distribution parameters which were found to minimize the Kullback-Leibler distance between the lognormal approximation and the true SINR distribution from a uncoded precoded multicarrier system employing MMSE equalization. We remind that these parameters were presented in Tables 4.1 and 4.2 for some channel models.

The union bound for the coded error performance can be obtained by remplacing (4.14) in (4.12), resulting in

$$P_e \leq \frac{1}{k_c} \sum_{d=d_{free}}^{\infty} w(d) P_{ep}(d). \tag{4.16}$$

4.4 Simulation Results

In this section, simulation results to validate the approach presented in the previous sections in different situations are presented. The simulation parameters used are depicted in Table 4.3. In the coded simulations, a mother convolutional code of rate 1/2 with a generating polynomial $(133, 171)_8$, a constraint length $K = 7$ and free distance $d_{free} = 10$ is used. Higher rates are obtained through puncturing. Table 4.4 contains the weights at each Hamming distance for the code rates used in this section. Only the 6 first Hamming

TABLE 4.3 – Simulation parameters for Section 4.4.

Constellation	QPSK
Sampling Frequency	10 MHz
Channel Models	ITU-T Pedestrian B, Vehicular A
Number of channel realizations	20000

TABLE 4.4 – Error event weights.

R_c	d_{free}	$w(d)$, $d = d_{free}, d_{free}+1, \ldots, d_{free}+5$
1/2	10	[11 0 38 0 193 0]
2/3	6	[1 16 48 158 642 2435]
3/4	5	[8 31 160 892 4512 23297]

distances were considered, because their impact appears at low SNR [65]. The cyclic prefix size is the minimum sufficient to eliminate the interblock interference and the power loss caused by the redundance introduced by the cyclic prefix is taken into account in the SNR calculation. Channel estimation in the receiver is assumed to be perfect, channel fading is considered to be quasistatic (time-invariant during each transmitted block) and other system imperfections are not taken into account in our simulations.

For a SNR of 25 dB, a comparison of the observed SINR distribution (obtained with 20000 channel realizations) with the lognormal approximation with the smallest Kullback-Leibler distance to the observed distribution is presented in Figure 4.6 for the ITU-T Pedestrian B channel model and in Figure 4.7 for the ITU-T Vehicular A channel model. To validate this approach, the results from lognormal distributions whose parameters were estimated using up to second-order moment matching (MM) and maximum likelihood (ML) estimation are also presented. These figures are shown with the x axis in logarithmic scale to make it easier to visualize the beginning of the probability density function curve. It is possible to see that the approximation using the Kullback-Leibler distance to estimate its parameters matches more closely the target distribution than the other ones in the beginning of the pdf curve for both cases.

In order to show the effect of the left tail of the pdf function on the bit error probability,

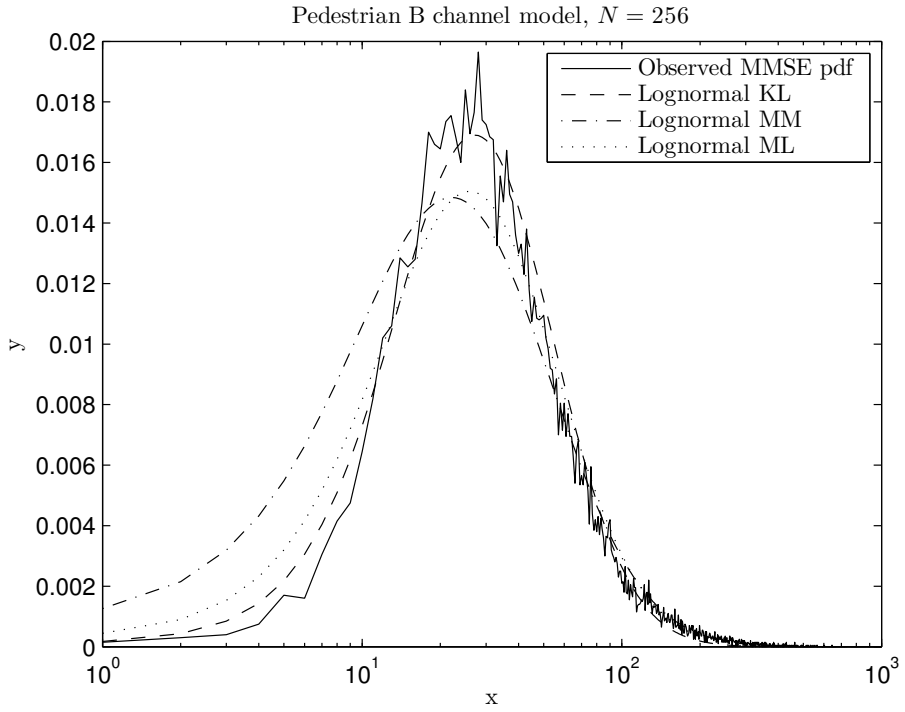

FIGURE 4.6 – A comparison of the true SINR distribution with the approximations at SNR = 25 dB for the Pedestrian B channel model.

Figure 4.8 presents the bit error probability when taking into account into the calculation different percentages of the left tail of the SINR's probability density function curve. For this simulation, the Vehicular A channel model was used. As stated before and validated by the results seen in this Figure, only the lowest SINR values (the beginning of the pdf curve) are important when calculating the bit error probability at high SNR values, due to the fact that the rest of the pdf curve will correspond to very high SINR values, which in turn will lead to a near-zero bit-error rate.

Figures 4.9 and 4.10 shows the system's bit error probability (an average from all channel realizations) compared to its approximations, for the Pedestrian B and Vehicular A channel models respectively. (4.11) is used to calculate the bit error probability for the lognormal approximation. The parameters μ and σ as a function of the SNR and the channel model are estimated by moment matching, maximum likelihood estimation and the ones which result in the smallest Kullback-Leibler distance to the target distribution. We see that the approximation employing the KL distance is more precise in higher SNRs

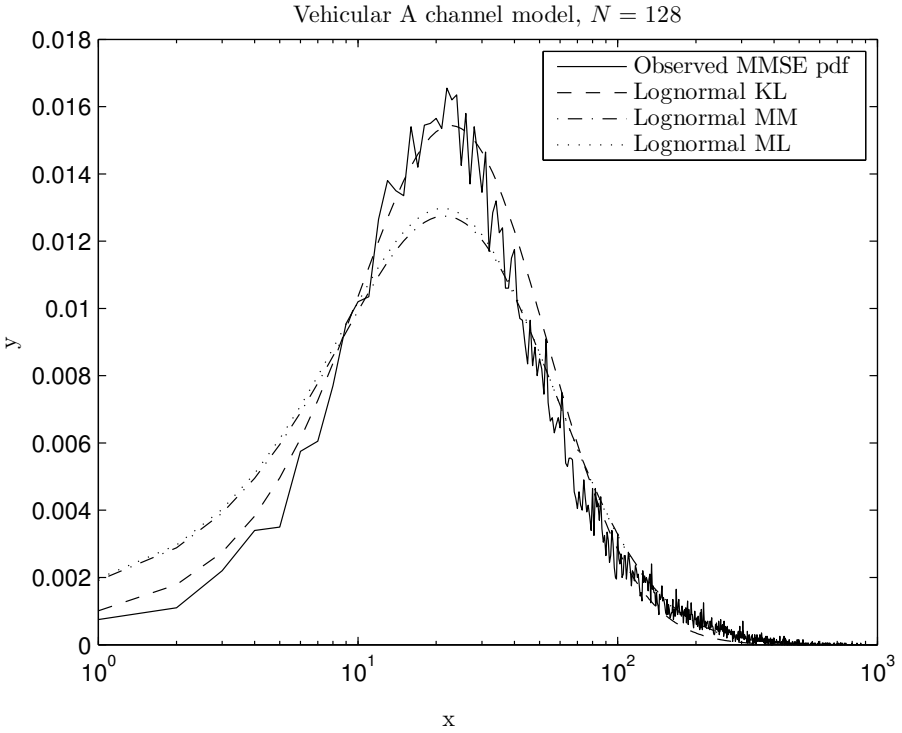

FIGURE 4.7 – A comparison of the true SINR distribution with the approximations at SNR = 25 dB for the Vehicular A channel model.

(> 10 dB) when compared to the other ones using the lognormal distribution in both cases, since it ensures that it will be closer to the real distribution at the left tail of the probability density function curve (as seen in Figures 4.6 and 4.7), which are the significant ones as shown in Figure 4.8.

To validate the novel method presented in Section 4.3, Figure 4.11 compares the results obtained by Monte Carlo simulation with the results from (4.16) using the lognormal approximation (with its parameters obtained by the search for the smallest KL distance), for $N = 512$, the Pedestrian B channel model and code rates R_c of 1/2, 2/3 and 3/4. It is possible to see that the error bounds obtained with the lognormal approximation are very close to the Monte Carlo simulation results.

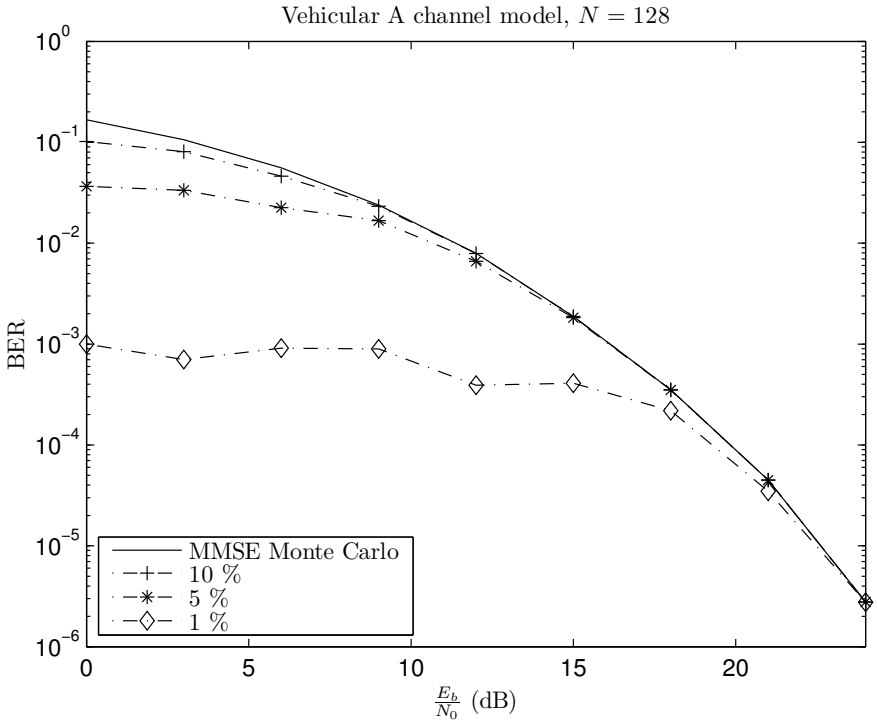

FIGURE 4.8 – Error performance when taking into account different parts of the probability density function curve of the SINR.

4.5 Concluding Remarks

We have presented in this chapter an approximation for the distribution of the SINR in a precoded multicarrier system employing MMSE equalization. This approximation, involving the lognormal distribution and the Kullback-Leibler distance, was shown to be precise when calculating the unconditional uncoded bit error probability even in high signal-to-noise ratios, due to its fidelity in the beginning of the pdf curve. This approximation can also serve as an abstraction for the aforementioned system.

With this abstraction, we have developed a novel method of deriving the analytical coded performance of a precoded multicarrier system employing MMSE equalization. This method allows for a quicker performance evaluation when compared to time-intensive numerical simulations. By using the lognormal approximation to abstract the precoded multicarrier system, an equation for the corresponding PEP was derived. Simulation results have shown that the analysis is accurate when compared to the Monte Carlo simulation

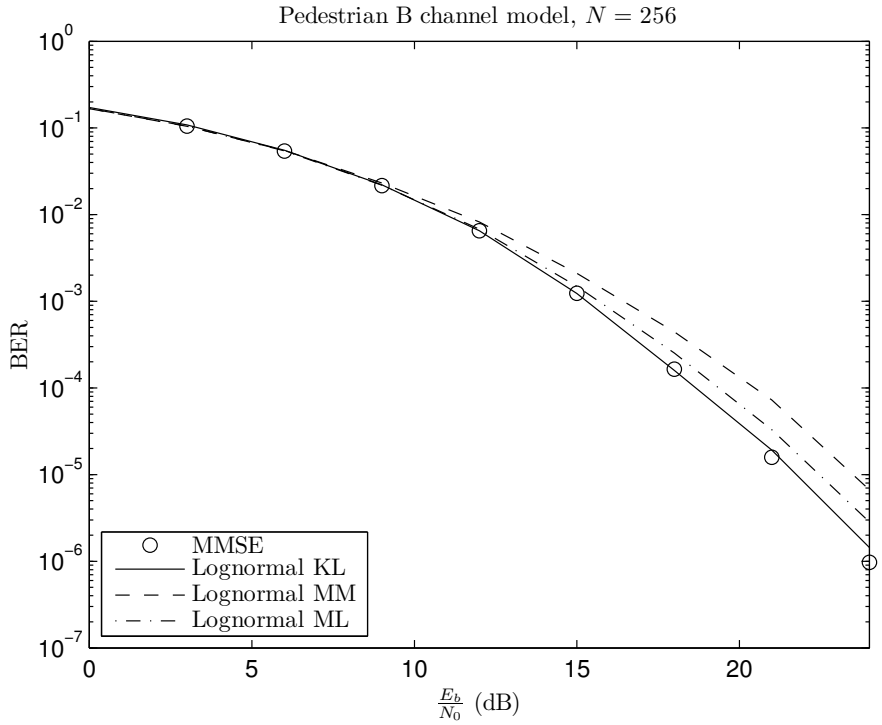

FIGURE 4.9 – Comparison of the error performance using the SINR with the SINR approximations for the Pedestrian B channel model.

results.

The next chapter deals with the application of widely linear processing to precoding and equalization for SC-FDE systems using MMSE equalization.

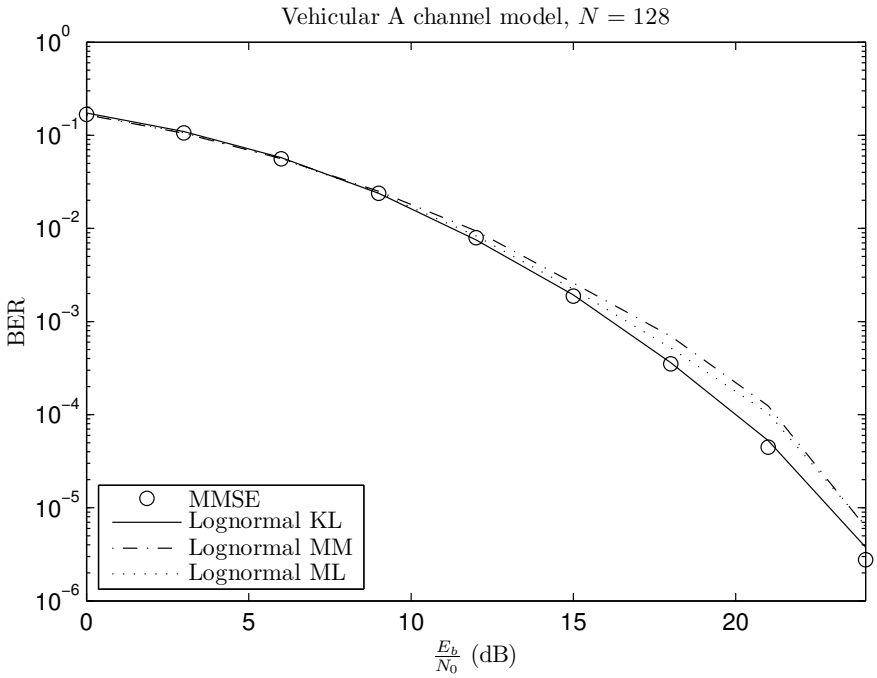

FIGURE 4.10 – Comparison of the error performance using the SINR with the SINR approximations for the Vehicular A channel model.

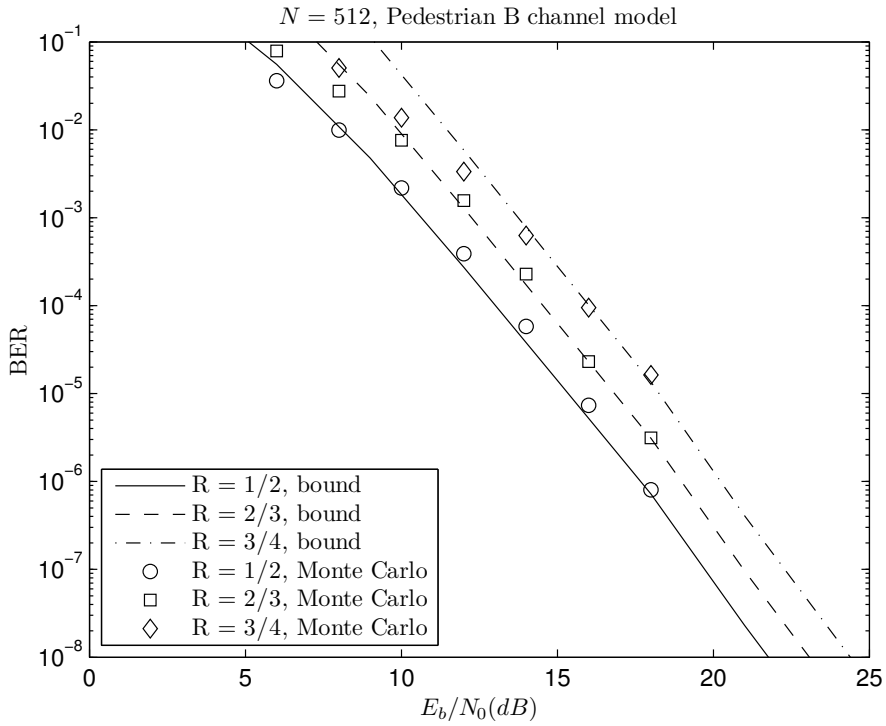

FIGURE 4.11 – Comparison between the bounds and Monte Carlo simulation results for $N = 512$ and the Pedestrian B channel model.

Chapter 5

Widely Linear MMSE Precoding and Equalization Techniques for SC-FDE Systems

5.1 Introduction

We have investigated the use of linear equalization in precoded multicarrier systems in the previous chapters. However, as seen in Section 2.8, if the transmitted signal is improper widely linear processing can be employed with a performance gain.

In this chapter we propose SC-FDE systems using widely linear MMSE-based equalization, decision-feedback equalization and Tomlinson-Harashima precoding. The use of widely linear MMSE-designed equalization and precoding brings a performance advantage with respect to stricly linear systems when improper constellations are transmitted. It also makes the system less sensitive to the feedback filter length (in systems using decision-feedback equalizers) and to channel estimation/channel state information errors (in Tomlinson-Harashima precoded systems) when compared to systems using strictly linear processing. An expression for the Signal to Interference-plus-Noise Ratio (SINR) at the output of the receiver is provided for all cases.

It is divided as follows. Section 5.2 presents the system models used in this work. The derivation of the error performance of SC-FDE systems employing WL-MMSE precoding and equalization is presented in Section 5.3. Simulation results validating the previous sections are shown in Section 5.4. Finally, the concluding remarks are discussed in Section

5.5.

5.2 System Model

On the transmitter side, the block $\tilde{\mathbf{s}} = [\tilde{s}_1\, \tilde{s}_2\, \ldots\, \tilde{s}_N]^T$ of size N is composed by symbols $\tilde{s}_i$ belonging to an improper constellation (such as M-PAM or M^2-OQAM) with unit energy. The transmitted signal, after the RF module, will pass through a channel with an impulse response $\tilde{\mathbf{h}} = [\tilde{h}_1\, \tilde{h}_2\, \ldots\, \tilde{h}_{L_{\tilde{\mathbf{h}}}}]^T$ of size $L_{\tilde{\mathbf{h}}}$. Thus, the cyclic prefix appended to the block $\tilde{\mathbf{s}}$ before transmission must have a length L_{CP} of at least $L_{\tilde{\mathbf{h}}} + 1$, resulting in $\tilde{\mathbf{s}}_{CP}$. Complex proper uncorrelated additional white gaussian noise (AWGN) $\tilde{\mathbf{n}}$ with zero mean and variance σ_n^2 also contaminates the transmitted signal.

Due to the cyclic prefix, the NxN channel matrix $\mathbf{H}_M$ is a circulant one, with its first column containing the impulse response appended by $(N - L_{CP} - 1)$ zeros. Since $\mathbf{H}_M$ is a circulant matrix, we can apply an eigendecomposition to this matrix to obtain $\mathbf{W}^*\mathbf{H}\mathbf{W}$, where $\mathbf{W}$ is the discrete Fourier transform (DFT) matrix and $\mathbf{H}$ is a NxN diagonal matrix with its (k,k)-th entry H_k corresponding to the k-th DFT coefficient of the channel impulse response $\tilde{\mathbf{h}}$.

The signal $\tilde{\mathbf{r}} = [\tilde{r}_1\, \tilde{r}_2\, \ldots\, \tilde{r}_{N+L_{CP}}]^T$ at the entry of the receiver has its cyclic prefix removed and passes to the frequency domain through a Fast Fourier Transform (FFT), whose normalized matrix $\mathbf{W}$ is of size NxN, so that equalization can be done in the frequency domain. This will result in the signal $\mathbf{r}$, expressed as :

$$\begin{aligned} \mathbf{r} &= \mathbf{H}\mathbf{s} + \mathbf{n} \\ &= \mathbf{H}\mathbf{W}\tilde{\mathbf{s}} + \mathbf{n}, \end{aligned} \tag{5.1}$$

where $\mathbf{H}$ corresponds to the channel frequency response of a specific channel realization and $\mathbf{s} = \mathbf{W}\tilde{\mathbf{s}}$. Equalization is performed by an filter based on the minimum mean square error (MMSE) criterion. However, since the equalizer is dealing with a signal from an improper constellation (which has non-zero pseudocorrelation), it has to employ widely linear processing to use all the second-order statistics made available by the received signal. In order to do that, the original version of the signal in the frequency domain together with its conjugate version are processed by the equalizer.

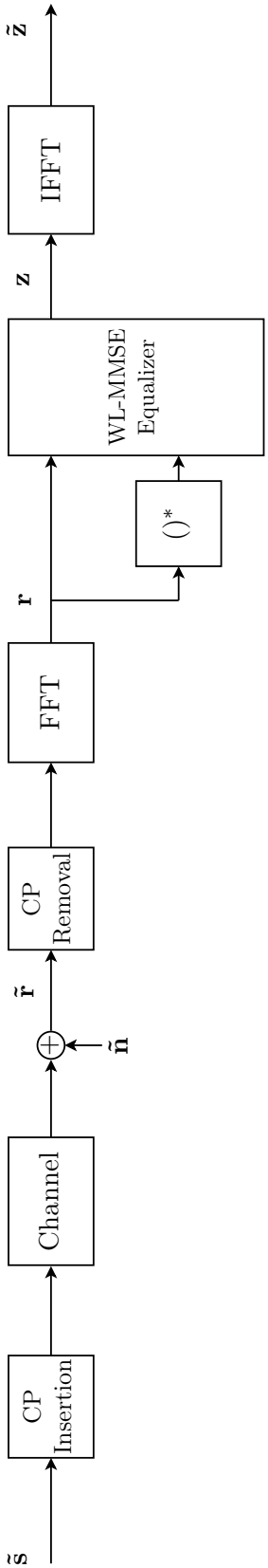

FIGURE 5.1 – A SC-FDE system employing widely linear MMSE equalization.

5.2.1 WL-MMSE Equalizer

The system model for a SC-FDE system employing widely linear MMSE-based equalization is presented in Figure 5.1. The signal at the output of the equalizer $\mathbf{z}$ is given by

$$\mathbf{z} = \mathbf{A}_1^H \mathbf{r} + \mathbf{A}_2^H \mathbf{r}^* = \mathbf{A}^H \mathbf{R}, \tag{5.2}$$

with $\mathbf{A}^H = [\mathbf{A}_1^H \; \mathbf{A}_2^H]$ and $\mathbf{R} = \begin{bmatrix} \mathbf{r} \\ \mathbf{r}^* \end{bmatrix}^T$.

The cost function ϵ_{WL} to derive the equalizer $\mathbf{A}$ based on the WL-MMSE criterion is

$$\begin{aligned} \epsilon_{\text{WL}} &= E[||\mathbf{A}^H \mathbf{R} - \mathbf{s}||^2] \\ &= \mathbf{A}^H \mathbf{C}_{\mathbf{RR}} \mathbf{A} - \mathbf{A}^H \mathbf{C}_{\mathbf{Rs}} - \mathbf{C}_{\mathbf{sR}} \mathbf{A} + \mathbf{I}_N. \end{aligned} \tag{5.3}$$

where

$$\begin{aligned} \mathbf{C}_{\mathbf{RR}} &= E[\mathbf{R}\mathbf{R}^H] \\ &= E\left\{ \begin{bmatrix} \mathbf{r} \\ \mathbf{r}^* \end{bmatrix} \begin{bmatrix} \mathbf{r}^H & \mathbf{r}^T \end{bmatrix} \right\} = \begin{bmatrix} \mathbf{C}_{\mathbf{rr}} & \overline{\mathbf{C}}_{\mathbf{rr}} \\ \overline{\mathbf{C}}_{\mathbf{rr}}^* & \mathbf{C}_{\mathbf{rr}}^* \end{bmatrix} \end{aligned} \tag{5.4}$$

$$\begin{aligned} \mathbf{C}_{\mathbf{rr}} = E\left[\mathbf{r}\mathbf{r}^H\right] &= E\left[(\mathbf{H}\mathbf{s} + \mathbf{n})(\mathbf{n}^H + \mathbf{s}^H \mathbf{H}^H)\right] \\ &= \mathbf{H} E[\mathbf{s}\mathbf{s}^H] \mathbf{H}^H + \sigma_n^2 \mathbf{I} \\ &= \mathbf{H}\mathbf{W} E[\tilde{\mathbf{s}}\tilde{\mathbf{s}}^H] \mathbf{W}^H \mathbf{H}^H + \sigma_n^2 \mathbf{I} \\ &= \mathbf{H}\mathbf{W}\mathbf{W}^H \mathbf{H}^H + \sigma_n^2 \mathbf{I} \\ &= \mathbf{H}\mathbf{H}^H + \sigma_n^2 \mathbf{I}_N \end{aligned} \tag{5.5}$$

$$\begin{aligned} \overline{\mathbf{C}}_{\mathbf{rr}} = E\left[\mathbf{r}\mathbf{r}^T\right] &= E\left[(\mathbf{H}\mathbf{s} + \mathbf{n})(\mathbf{n}^T + \mathbf{s}^T \mathbf{H}^T)\right] \\ &= \mathbf{H} E[\mathbf{s}\mathbf{s}^T] \mathbf{H}^T \\ &= \mathbf{H}\mathbf{W} E[\tilde{\mathbf{s}}\tilde{\mathbf{s}}^T] \mathbf{W}^T \mathbf{H}^T \\ &= \mathbf{H}\mathbf{W}\mathbf{W}^T \mathbf{H}^T \\ &= \mathbf{H}\mathbf{U}\mathbf{H}^T \end{aligned} \tag{5.6}$$

with $\mathbf{U}$ expressed by

$$\mathbf{U} = \begin{bmatrix} 1 & 0 & 0 & \dots & 0 \\ 0 & 0 & 0 & \dots & 1 \\ \vdots & \vdots & \vdots & \vdots & \vdots \\ 0 & 0 & 1 & \dots & 0 \\ 0 & 1 & 0 & \dots & 0 \end{bmatrix}, \tag{5.7}$$

$$\begin{aligned} \mathbf{C_{Rs}} &= E[\mathbf{R}\mathbf{s}^H] = E\left\{ \begin{bmatrix} \mathbf{r} \\ \mathbf{r}^* \end{bmatrix} \mathbf{s}^H \right\} = E\left\{ \begin{bmatrix} \mathbf{r}\mathbf{s}^H \\ \mathbf{r}^*\mathbf{s}^H \end{bmatrix} \right\} \\ &= \begin{bmatrix} \mathbf{H}E[\mathbf{s}\mathbf{s}^H] \\ \mathbf{H}^*E[\mathbf{s}^*\mathbf{s}^H] \end{bmatrix} \\ &= \begin{bmatrix} \mathbf{H}\mathbf{W}E[\tilde{\mathbf{s}}\tilde{\mathbf{s}}^H]\mathbf{W}^H \\ \mathbf{H}^*(\mathbf{W}E[\tilde{\mathbf{s}}\tilde{\mathbf{s}}^T]\mathbf{W}^T)^* \end{bmatrix} \\ &= \begin{bmatrix} \mathbf{H}\mathbf{W}\mathbf{W}^H \\ \mathbf{H}^*(\mathbf{W}\mathbf{W}^T)^* \end{bmatrix} \\ &= \begin{bmatrix} \mathbf{H} \\ \mathbf{H}^*\mathbf{U} \end{bmatrix} \end{aligned} \tag{5.8}$$

and

$$\begin{aligned} \mathbf{C_{sR}} &= E[\mathbf{s}\mathbf{R}^H] = E\left\{ \mathbf{s}^H \begin{bmatrix} \mathbf{r} \\ \mathbf{r}^* \end{bmatrix} \right\} = E\left\{ \begin{bmatrix} \mathbf{s}\mathbf{r}^H \\ \mathbf{s}^*\mathbf{r}^H \end{bmatrix} \right\} \\ &= \begin{bmatrix} E[\mathbf{s}\mathbf{s}^H]\mathbf{H} \\ E[\mathbf{s}^*\mathbf{s}^H]\mathbf{H}^* \end{bmatrix} \\ &= \begin{bmatrix} \mathbf{W}E[\tilde{\mathbf{s}}\tilde{\mathbf{s}}^H]\mathbf{W}^H\mathbf{H} \\ (\mathbf{W}E[\tilde{\mathbf{s}}\tilde{\mathbf{s}}^T]\mathbf{W}^T)^*\mathbf{H}^* \end{bmatrix} \\ &= \begin{bmatrix} \mathbf{W}\mathbf{W}^H\mathbf{H} \\ (\mathbf{W}\mathbf{W}^T)^*\mathbf{H}^* \end{bmatrix} \\ &= \begin{bmatrix} \mathbf{H} \\ \mathbf{U}\mathbf{H}^* \end{bmatrix}, \end{aligned} \tag{5.9}$$

with $E[\mathbf{n}\mathbf{n}^T] = 0$ (since the noise is proper), and $\mathbf{W}\mathbf{W}^H = \mathbf{I}_N$. We obtain the optimal equalizer $\mathbf{A}$ by differentiating ϵ_{WL} with respect to $\mathbf{A}$ and equalling the result to zero, resulting in

$$\begin{aligned} \mathbf{A} &= \mathbf{C}_{\mathbf{RR}}^{-1}\mathbf{C_{Rs}} \\ &= \begin{bmatrix} \mathbf{H}\mathbf{H}^H + \sigma_n^2\mathbf{I}_N & \mathbf{H}\mathbf{U}\mathbf{H}^T \\ \mathbf{H}^*\mathbf{U}\mathbf{H}^H & \mathbf{H}^*\mathbf{H}^T + \sigma_n^2\mathbf{I}_N \end{bmatrix}^{-1} \begin{bmatrix} \mathbf{H} \\ \mathbf{H}^*\mathbf{U} \end{bmatrix}. \end{aligned} \tag{5.10}$$

Using blockwise matrix inversion, $\mathbf{C}_{\mathbf{RR}}^{-1}$ can be expressed by

$$\mathbf{C}_{\mathbf{RR}}^{-1} = \begin{bmatrix} \mathbf{A}\mathbf{A} & \mathbf{B}\mathbf{B} \\ \mathbf{C}\mathbf{C} & \mathbf{D}\mathbf{D} \end{bmatrix}, \tag{5.11}$$

with

$$\mathbf{AA} = \left[\sigma_n^2\left(\mathbf{H}_{mod} + \sigma_n^2\mathbf{I}_N\right)\right]^{-1}\left(\mathbf{UHH}^H\mathbf{U} + \sigma_n^2\mathbf{I}_N\right) \tag{5.12}$$

$$\mathbf{BB} = \left[\sigma_n^2\left(\mathbf{H}_{mod} + \sigma_n^2\mathbf{I}_N\right)\right]^{-1}\mathbf{HUH}^T \tag{5.13}$$

$$\mathbf{CC} = \left[\sigma_n^2\left(\mathbf{H}_{mod} + \sigma_n^2\mathbf{I}_N\right)\right]^{-1}\mathbf{H}^*\mathbf{UH}^H \tag{5.14}$$

$$\mathbf{DD} = \left[\sigma_n^2\left(\mathbf{H}_{mod} + \sigma_n^2\mathbf{I}_N\right)\right]^{-1}\left(\mathbf{UHH}^H\mathbf{U} + \sigma_n^2\mathbf{I}_N\right) \tag{5.15}$$

and

$$\mathbf{H}_{mod} = \mathbf{HH}^H + \mathbf{UHH}^H\mathbf{U}. \tag{5.16}$$

Analysing (5.16), it is possible to see that $\mathbf{H}_{mod}$ is a diagonal matrix with its diagonal equal to $[2|H_1|^2 \quad (|H_2|^2+|H_N|^2) \quad (|H_3|^2+|H_{N-1}|^2)\ldots 2|H_{N/2+1}|^2\ldots(|H_3|^2+|H_{N-1}|^2) \quad (|H_2|^2+|H_N|^2)]$.

This way, the equalizer $\mathbf{A}$ can be expressed as

$$\mathbf{A} = \mathbf{C}_{\mathbf{RR}}^{-1}\mathbf{C}_{\mathbf{Rs}} \tag{5.17}$$

$$= \begin{bmatrix} \mathbf{A}_1 \\ \mathbf{A}_2 \end{bmatrix} \tag{5.18}$$

with

$$\begin{aligned}\mathbf{A}_1 = &\left[\sigma_n^2\left(\mathbf{H}_{mod} + \sigma_n^2\mathbf{I}_N\right)\right]^{-1}\left(\mathbf{UHH}^H\mathbf{U} + \sigma_n^2\mathbf{I}_N\right)\mathbf{H} - \\ &- \left[\sigma_n^2\left(\mathbf{H}_{mod} + \sigma_n^2\mathbf{I}_N\right)\right]^{-1}\mathbf{HUH}^T\mathbf{H}^*\mathbf{U} \\ &= \left[\sigma_n^2\left(\mathbf{H}_{mod} + \sigma_n^2\mathbf{I}_N\right)\right]^{-1}\left(\sigma_n^2\mathbf{H}\right) \\ &= \left(\mathbf{H}_{mod} + \sigma_n^2\mathbf{I}_N\right)^{-1}\mathbf{H}\end{aligned} \tag{5.19}$$

and

$$\begin{aligned}\mathbf{A}_2 = &-\left[\sigma_n^2\left(\mathbf{H}_{mod} + +\sigma_n^2\mathbf{I}_N\right)\right]^{-1}\mathbf{H}^*\mathbf{UH}^H\mathbf{H} + \\ &+ \left[\sigma_n^2\left(\mathbf{H}_{mod} + \sigma_n^2\mathbf{I}_N\right)\right]^{-1}\left(\mathbf{UHH}^H\mathbf{U} + \sigma_n^2\mathbf{I}_N\right)\mathbf{H}^*\mathbf{U} \\ &= \left[\sigma_n^2\left(\mathbf{H}_{mod} + \sigma_n^2\mathbf{I}_N\right)\right]^{-1}\left(\sigma_n^2\mathbf{H}^*\mathbf{U}\right) \\ &= \left(\mathbf{H}_{mod} + \sigma_n^2\mathbf{I}_N\right)^{-1}\mathbf{H}^*\mathbf{U}.\end{aligned} \tag{5.20}$$

When transmitting proper signals, this equalizer is reduced to the strictly linear MMSE one, since with proper signals $E[\mathbf{ss}^T] = 0$. This process is very similar to the one done in [66], but better details $\mathbf{A}_1$ and $\mathbf{A}_2$, showing that $\mathbf{A}_2$ is the conjugate version of $\mathbf{A}_1$.

After equalization, an inverse Fast Fourier Transform (IFFT) is done so that the symbol decision is realized in the time domain. Due to the fact that widely linear processing is employed in the equalizer, the estimated symbols $\tilde{\mathbf{z}}$ at the output of the receiver will be purely real.

5.2.2 WL-MMSE DFE Equalizer

When using a WL-MMSE DFE equalizer, the system model is described in Figure 5.2.

Assuming that correct past decisions are passed along in the feedback filter, the frequency domain representation $\mathbf{q}$ of the symbol estimate $\tilde{\mathbf{q}}$ can be expressed as

$$\mathbf{q} = \mathbf{B}^H\mathbf{R} - \mathbf{D}^H\mathbf{s}, \tag{5.21}$$

where $\mathbf{B}$ is the feedforward filter and $\mathbf{D}$ is a NxN matrix with its main diagonal being the Nx1 sized frequency-domain representation of the time-domain feedback filter $\tilde{\mathbf{d}} = [\tilde{d}_1\, \tilde{d}_2\, \ldots\, \tilde{d}_{L_{\tilde{\mathbf{d}}}}]^T$, with length $L_{\tilde{\mathbf{d}}}$. Thus, the cost function $\epsilon_{\text{WL-DFE}}$ to derive the feedforward filter $\mathbf{B}$ is

$$\begin{aligned}\epsilon_{\text{WL-DFE}} &= E[||\mathbf{B}^H\mathbf{R} - \mathbf{D}^H\mathbf{s} - \mathbf{s}||^2] \\ &= \mathbf{B}^H\mathbf{C_{RR}}\mathbf{B} - \mathbf{B}^H\mathbf{C_{Rs}}\mathbf{D} - \mathbf{B}^H\mathbf{C_{Rs}} - \\ &- \mathbf{D}^H\mathbf{C_{Rs}}\mathbf{B} + \mathbf{D}^H\mathbf{D} + \mathbf{D}^H - \mathbf{C_{sR}}\mathbf{B} + \mathbf{D} + \mathbf{I}_N.\end{aligned} \tag{5.22}$$

Deriving this cost function with respect to the feedforward filter $\mathbf{B}$ and setting it to zero, we obtain the optimal value of $\mathbf{B}$, expressed as

$$\begin{aligned}\mathbf{B} &= \mathbf{C}_{\mathbf{RR}}^{-1}\mathbf{C_{Rs}}(\mathbf{I}_N + \mathbf{D}) \\ &= \mathbf{A}(\mathbf{I}_N + \mathbf{D}).\end{aligned} \tag{5.23}$$

Now, we substitute (5.23) in (5.22) to obtain the new cost function for the optimal value of the feedback filter $\tilde{\mathbf{d}}$, which is

$$\epsilon_{\text{FB}} = \frac{1}{N}\sum_{n=1}^{N}\frac{|1 + D(n,n)|^2}{H_{mod}(n,n) + \sigma_n^2}. \tag{5.24}$$

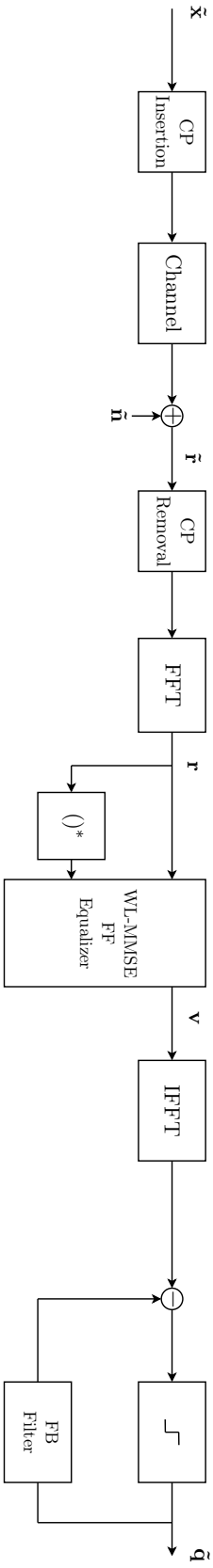

FIGURE 5.2 – A SC-FDE system employing widely linear MMSE equalization and a decision-feedback equalizer.

Using the feedback filter $\tilde{\mathbf{d}}$ in the time domain instead of its frequency domain version $\mathbf{D}$ in 5.24, we have

$$\epsilon_{\text{FB}} = \frac{1}{N}\sum_{n=1}^{N}\frac{\left|1+\sum_{l=1}^{L_{\mathbf{d}}} d_l \exp\left(-j2\pi\frac{ln}{N}\right)\right|^2}{H_{mod}(n,n)+\sigma_n^2}. \tag{5.25}$$

To minimize ϵ_{FB} the feedback filter coefficients $\tilde{\mathbf{d}}$ are given by the solution of the linear system

$$\mathbf{F}\tilde{\mathbf{d}} = -\mathbf{g}. \tag{5.26}$$

The $L_{\tilde{\mathbf{d}}}$x$L_{\tilde{\mathbf{d}}}$ matrix $\mathbf{F}$ and the $L_{\tilde{\mathbf{d}}}$x1 column vector $\mathbf{g}$ are expressed, respectively, as

$$[\mathbf{F}]_{m,l} = \sum_{n=1}^{N}\frac{\exp\left(-j2\pi((n(l-m))/N)\right)}{H_{mod}(n,n)+\sigma_n^2},\ 1\le m,l\le L_{\tilde{\mathbf{d}}} \tag{5.27}$$

and

$$[\mathbf{g}]_m = \sum_{n=1}^{N}\frac{\exp\left(j2\pi(nm/N)\right)}{H_{mod}(n,n)+\sigma_n^2},\ 1\le m\le L_{\tilde{\mathbf{d}}}. \tag{5.28}$$

To initialize the feedback filter, the last $L_{\tilde{\mathbf{d}}}$ symbols of $\tilde{\mathbf{x}}_{CP}$ can be used. Once $\tilde{\mathbf{d}}$ is determined, $\mathbf{B}$ can be calculated by (5.23). To cancel all the ISI from the previous detected symbols, the size of the feedback filter $L_{\tilde{\mathbf{d}}}$ should be equal to the channel length $L_{\tilde{\mathbf{h}}}$.

5.2.3 WL-MMSE Tomlinson-Harashima Precoder

A block diagram for the SC-FDE system using WL-MMSE Tomlinson-Harashima precocding is shown in Figure 5.3.

In this system model, we consider a single carrier block transmission, with the block to be transmitted $\tilde{\mathbf{s}}' = [\tilde{s}_1' \ \tilde{s}_2' \ \dots \ \tilde{s}_{N-L_{\tilde{\mathbf{h}}}}']^T$ of size $N-L_{\tilde{\mathbf{h}}}$ composed by symbols belonging to an improper constellation (such as M-PAM or M^2-OQAM) with unit energy. $\tilde{\mathbf{s}}'$ then goes to the Tomlinson-Harashima precoder, which consists of a $L_{\tilde{\mathbf{d}}}$-sized filter $\tilde{\mathbf{d}}' = [\tilde{d}_1' \ \tilde{d}_2' \ \dots \ \tilde{d}_{L_{\tilde{\mathbf{d}}}}']^T$ and a modulo operator.

The modulo-$2M$ operation to the vector $\tilde{\mathbf{t}}$ in the precoder is done independently on the real and imaginary parts. The output of this modulo operation is given by

$$\begin{aligned}\tilde{\mathbf{x}}'' &= \tilde{\mathbf{t}} - 2M\left\lfloor\frac{Re(\tilde{\mathbf{s}}')}{2M}+\frac{1}{2}\right\rfloor - j2M\left\lfloor\frac{Im(\tilde{\mathbf{s}}')}{2M}+\frac{1}{2}\right\rfloor \\ &= \tilde{\mathbf{t}}+\tilde{\mathbf{a}}.\end{aligned} \tag{5.29}$$

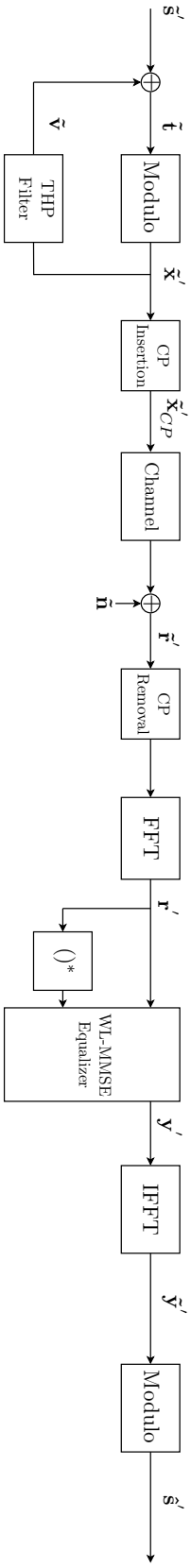

FIGURE 5.3 – A SC-FDE system employing widely linear MMSE equalization and Tomlinson-Harashima precoding.

If the real (imaginary) part of $\tilde{\mathbf{t}}$ is greater than M, $2M$ is (repeatedly) subtracted from it until the result is less than M. If this real (imaginary) part is less than $-M$, $2M$ is (repeatedly) added to it until the result is greater than or equal to $-M$. In other words, $\tilde{\mathbf{t}}$ is reduced modulo $2M$ to the half-open interval $[-M, M)$, limiting the effective dynamic range of the transmitted signal to this interval. This modulo operation is represented by the sequence $\tilde{\mathbf{a}}$. After this operation, $L_{\tilde{\mathbf{h}}}$ zeros are appended to $\tilde{\mathbf{x}}^{''}$ to initialize the state of the precoding filter, resulting in the vector $\tilde{\mathbf{x}}^{'} = [\tilde{x}_1^{'}\, \tilde{x}_2^{'}\, \ldots\, \tilde{x}_N^{'}]^T$ of size Nx1. More power is necessary to transmit the precoded symbols when compared to non-precoded ones (see Table 2.2) ; however, this penalty becomes negligible with an increase in constellation size.

Ignoring the modulo operation, the output of the Tomlinson-Harashima precoder $\mathbf{x}^{'}$ is

$$x_k^{'} = s_k^{'} - \sum_{l=1}^{L_{\tilde{\mathbf{d}}}} d_l^{'} x_{k-l}. \tag{5.30}$$

$\tilde{\mathbf{x}}^{'}$ follows the same path of a SC-FDE WL-MMSE-DFE up to the feedback filter (cyclic prefix insertion, passage through the channel, cyclic prefix removal, FFT, WL-MMSE equalization by the filter $\mathbf{B}^{'}$ and IFFT). The same modulo operation realized in the transmitter is done in the receiver to $\tilde{\mathbf{y}}^{'}$ to map the received data to the interval $(-M, M]$, resulting in the symbol estimate $\hat{\mathbf{s}}^{'}$. Only the first $N - L_{\tilde{\mathbf{h}}}$ elements of $\hat{\mathbf{s}}^{'}$ are used for the decision.

An equivalent linearized scheme of the system model presented in Figure 5.3 is shown in Figure 5.4, following the time domain THP conversion made in [67]. In this Figure, $\mathbf{K} = [\mathbf{H}\, \mathbf{H}^*]^T$ and $\mathbf{D}^{'}$ is a NxN diagonal matrix with its main diagonal being the N-sized Fourier transform of the Tomlinson-Harashima precoder $\tilde{\mathbf{d}}^{'}$.

Figure 5.4 shows that the symbol estimate $\hat{\mathbf{s}}^{'}$ is given by

$$\hat{\mathbf{s}}^{'} = \tilde{\mathbf{s}}_d^{'} + \overline{\mathbf{n}} + \tilde{\mathbf{i}}, \tag{5.31}$$

where $\tilde{\mathbf{s}}_d^{'}$ is the desired symbol vector, $\overline{\mathbf{n}}$ the filtered noise and the remaining interference is expressed by $\tilde{\mathbf{i}}$. This way, the error vector $\tilde{\mathbf{e}}^{'}$ is

$$\begin{aligned} \tilde{\mathbf{e}}^{'} &= \overline{\mathbf{n}} + \tilde{\mathbf{i}} \\ &= \mathbf{W}^{-1}((\mathbf{B}^{'})^H \mathbf{n}) + \mathbf{W}^{-1}((\mathbf{B}^{'})^H \mathbf{K} - \mathbf{D}^{'})\mathbf{x}^{'}. \end{aligned} \tag{5.32}$$

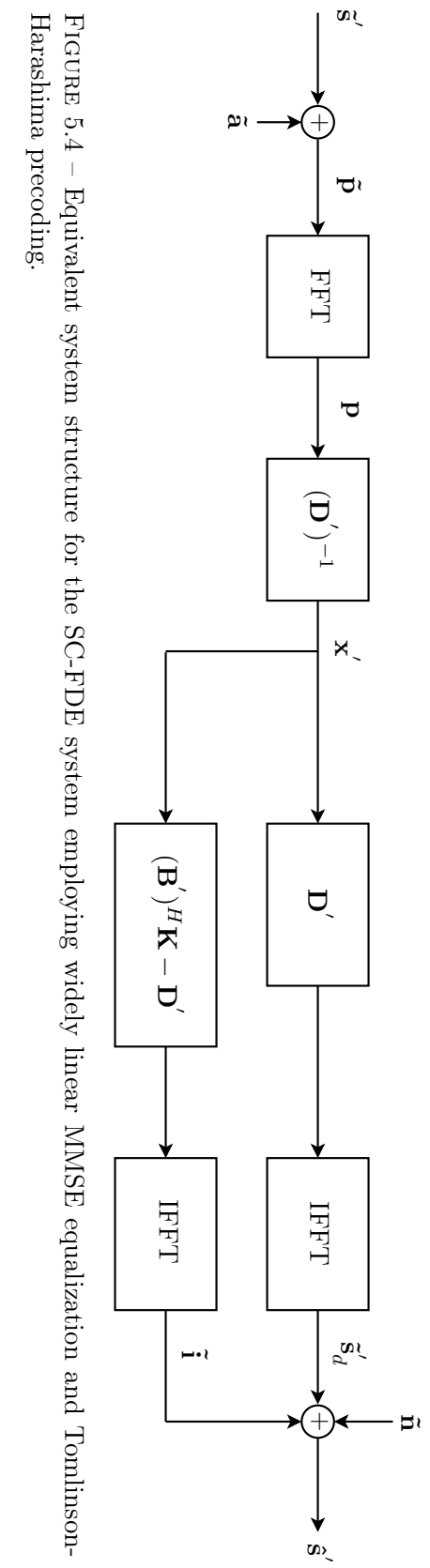

FIGURE 5.4 – Equivalent system structure for the SC-FDE system employing widely linear MMSE equalization and Tomlinson-Harashima precoding.

Using (5.32), we obtain the mean square error $\mathbf{E}^{'}$, given by

$$\begin{aligned}\mathbf{E}^{'} &= E\left\{|\mathbf{e}^{'}|^2\right\} \\ &= E\left\{|\overline{\mathbf{n}} + \tilde{\mathbf{i}}|^2\right\}.\end{aligned} \tag{5.33}$$

Minimizing (5.33) we can find that $\mathbf{B}^{'}$ and $\tilde{\mathbf{d}}^{'}$ are the same as the ones in a SC-FDE system employing a MMSE-based decision-feedback equalizer together with widely linear processing. Thus, the coefficients of the Tomlinson-Harashima precoder $\tilde{\mathbf{d}}^{'} = \tilde{\mathbf{d}}$ are given by (5.26) and the widely linear MMSE equalizer $\mathbf{B}^{'} = \mathbf{B}$ is given by (5.23).

5.3 Error Performance Analysis

5.3.1 SINR for the WL-MMSE Receiver

Let us remember that after the FFT in this system, the received signal and its conjugate version are grouped in the vector $\mathbf{R}$. Both versions are processed together in the frequency domain by the WL-MMSE equalizer $\mathbf{A}$. Thus, the symbol estimate $\tilde{\mathbf{z}}$ is expressed by

$$\begin{aligned}\tilde{\mathbf{z}} &= \mathbf{W^{-1}}\mathbf{A}^{H}\mathbf{R} \\ &= \mathbf{W^{-1}}\mathbf{A}^{H}\begin{bmatrix} \mathbf{HW}\tilde{\mathbf{s}} + \mathbf{n} \\ (\mathbf{HW}\tilde{\mathbf{s}} + \mathbf{n})^{*} \end{bmatrix}\end{aligned} \tag{5.34}$$

is obtained after deprecoding the signal $\mathbf{z}$ at the output of the WL-MMSE equalizer by the IFFT matrix $\mathbf{W}^{-1}$.

We can rewrite $\tilde{\mathbf{z}}$ in the following way :

$$\tilde{\mathbf{z}} = \mathbf{W^{-1}}(\mathbf{A}_1^{H}\mathbf{H} + \mathbf{A}_2^{H}\mathbf{H}^{*}\mathbf{U})\mathbf{W}\tilde{\mathbf{s}} + \mathbf{W^{-1}}\mathbf{A}_1^{H}\mathbf{n} + \mathbf{W^{-1}}\mathbf{A}_2^{H}\mathbf{U}\mathbf{n}^{*}. \tag{5.35}$$

The combined effect of the ISI and the noise in $\tilde{\mathbf{z}}$ is $\mathbf{e}$, given by

$$\begin{aligned}\mathbf{e} = \mathbf{W^{-1}}&(\mathbf{A}_1^{H}\mathbf{H} + \mathbf{A}_2^{H}\mathbf{H}^{*}\mathbf{U} - \mathbf{I}_N)\mathbf{W}\tilde{\mathbf{s}} \\ &+ \mathbf{W^{-1}}\mathbf{A}_1^{H}\mathbf{n} + \mathbf{W^{-1}}\mathbf{A}_2^{H}\mathbf{U}\mathbf{n}^{*}.\end{aligned} \tag{5.36}$$

With $\mathbf{e}$ we can calculate the mean square error $\mathrm{MSE}_{\mathrm{WL}}$, expressed as

$$\mathrm{MSE}_{\mathrm{WL}} = \mathbf{W^{-1}}\left(\mathbf{H}_{mod} + \sigma_n^2\mathbf{I}_N\right)^{-1}\mathbf{W}. \tag{5.37}$$

Since MSE_{WL} is a circulant matrix, its diagonal elements are all the same. Thus, the MSE for all the elements of $\tilde{\mathbf{z}}$ is $\frac{1}{N}\text{tr}[\text{MSE}_{\text{WL}}]$. Note that MSE_{WL} is much lower than the MSE given by the stricly linear equalizer, which is $\frac{1}{N}\text{tr}[\mathbf{W}^{-1}(\mathbf{H}^H\mathbf{H}+\sigma_n^2\mathbf{I}_N)^{-1}\mathbf{W}]$ [39]. The effective SINR after deprecoding when using a WL-MMSE equalizer is

$$\gamma_{\text{WL-MMSE}} = \frac{1}{2}\left(\frac{\gamma N}{\text{tr}[\text{MSE}_{\text{WL}}]} - 1\right), \tag{5.38}$$

with

$$\begin{aligned}\text{tr}[\text{MSE}_{\text{WL}}] = &\frac{1}{2|H_1|^2+\sigma_n^2} + \frac{1}{2|H_{N/2+1}|^2+\sigma_n^2} + \\ &+ \sum_{i=2}^{N/2} \frac{2}{|H_i|^2+|H_{N+2-i}|^2+\sigma_n^2},\end{aligned} \tag{5.39}$$

and $\gamma = E_s/\sigma_n^2$. The division by 2 in (5.38) is because the final symbol decision is only done on the real estimate [68]. Since [66] does not specify well $\mathbf{A}_1$ and $\mathbf{A}_2$, (5.38) clarifies the calculation of the SINR for a SC-FDE system using widely linear MMSE equalization in the SISO case. (5.38)) also does not rely on matrix inversion for its calculation, as is the case for the SINR expression given in [66].

5.3.2 SINR for the WL-MMSE DFE Receiver

For the SC-FDE system using WL-MMSE DFE equalization, its MSE can be expressed, using the method described in [69], as

$$\text{MSE}_{\text{WL-DFE}} = \exp\left(\frac{1}{N}\sum_{n=1}^{N}\log\left(\frac{1}{1+\gamma H_{mod}(n,n)}\right)\right). \tag{5.40}$$

The mean square error expressed in (5.40) does not take into account the error propagation effect that can be caused by erroneous previous decisions. This MSE is lower than the one obtained by the strictly linear solution, given by [41]

$$\text{MSE}_{\text{DFE}} = \exp\left(\frac{1}{N}\sum_{n=1}^{N}\log\left(\frac{1}{1+\gamma|H_n|^2}\right)\right). \tag{5.41}$$

The SINR for the SC-FDE system using WL-MMSE DFE equalization is given by

$$\gamma_{\text{WL-DFE}} = \frac{1}{2}\left(\frac{1}{\text{MSE}_{\text{WL-DFE}}} - 1\right). \tag{5.42}$$

Again, we divide by 2 to obtain the effective SINR for the system using widely linear equalization.

5.3.3 SINR for the WL-MMSE-THP Precoder

The MSE for the WL-MMSE-THP SC-FDE system is the same one from a WL-MMSE DFE one outside of a factor η which will represent the precoding loss. Thus, it can be expressed as

$$\mathrm{MSE}_{\text{WL-THP}} = \exp\left(\frac{1}{N}\sum_{n=1}^{N}\log\left(\frac{1}{1+\frac{\gamma}{\eta}H_{mod}(n,n)}\right)\right), \tag{5.43}$$

with $\eta = \frac{M^2}{M^2-1}$ for one-dimensional constellations and $\eta = \frac{M}{M-1}$ for two-dimensional ones.

Finally, to calculate the error probability P_e conditional to a specific channel realization, the following equation is used :

$$P_e = \alpha Q(\sqrt{\beta\gamma}), \tag{5.44}$$

where α and β are constellation-specific parameters, γ can be $\gamma_{\text{WL-MMSE}}$, $\gamma_{\text{WL-DFE}}$ or $\gamma_{\text{WL-THP}}$ and $Q(x) = \frac{1}{\sqrt{2\pi}}\int_x^\infty \exp\frac{-t^2}{2}\,dt$. The unconditional error probability is obtained by averaging over all the conditional error probabilities corresponding to the channel realizations.

5.4 Simulation Results

Simulation results to validate the use of widely linear MMSE based equalization and precoding for different block sizes and channel models are presented in this section. For the simulations presented in this section, the cyclic prefix size used is the minimum sufficient to eliminate the interblock interference and the power loss caused by the redundance introduced by the cyclic prefix is taken into account in the SNR calculation. A sampling frequency of 10 MHz was used. To calculate the final bit error performance in the Monte Carlo simulations, a minimum of 400 errors were taken into account for each point ; for the method presented in Section 5.3, 5000 independent channel realizations were done to obtain the unconditional error probability. Channel estimation in the receiver is assumed to be perfect (unless noted otherwise), channel fading is considered to be quasistatic (time-invariant during each transmitted block) and other system imperfections are not taken into account. For THP systems, the precoder size is $L_{\tilde{\mathbf{d}}}$. In simulations using channel coding, a mother convolutional code with $R = 1/2$, $K = 7$, $(171, 133)_8$ code followed by a block interleaver is used at the transmitter ; in the receiver, a block de-interleaver followed by a

soft-decision Viterbi decoder is used. Higher code rates are obtained through puncturing.

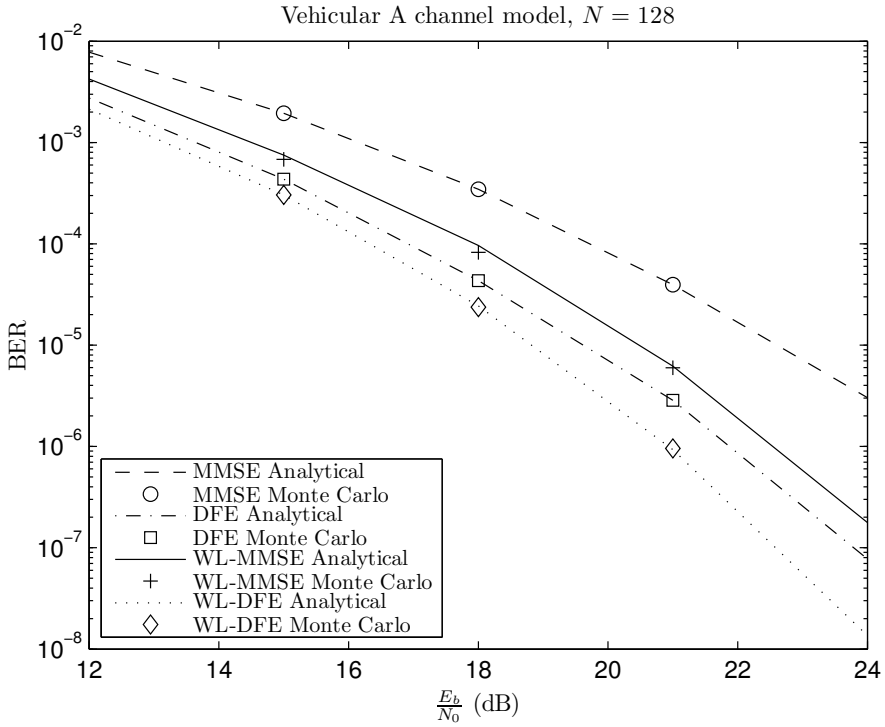

FIGURE 5.5 – Error performance for N = 128 and the Vehicular A channel model in SC-FDE systems.

Figure 5.5 shows the Monte Carlo results for a SC-FDE system using WL-MMSE equalization compared to the results provided by (5.44) for transmission symbols drawn from an BPSK constellation, a block size $N = 128$ and the ITU-T Vehicular A channel model. For the systems employing a DFE, its length $L_{\tilde{\mathbf{d}}}$ is equal to the channel length $L_{\tilde{\mathbf{h}}}$. For reference, the error performance of SC-FDE systems using strictly linear MMSE equalization is also shown. It is possible to see that the use of the analysis presented in this chapter gives consistent results when compared to the Monte Carlo simulation results throughout the E_b/N_0 range. The utilization of the WL-MMSE equalizer brings a performance gain when compared to the strictly linear MMSE one in the entire E_b/N_0 range for systems using or not a DFE, due to the complete use of the second-order statistics made available by the improper signal. Results using a QPSK constellation for the strictly linear receiver and a OQPSK constellation for the widely linear one will be the same as the ones presented in Figure 5.5.

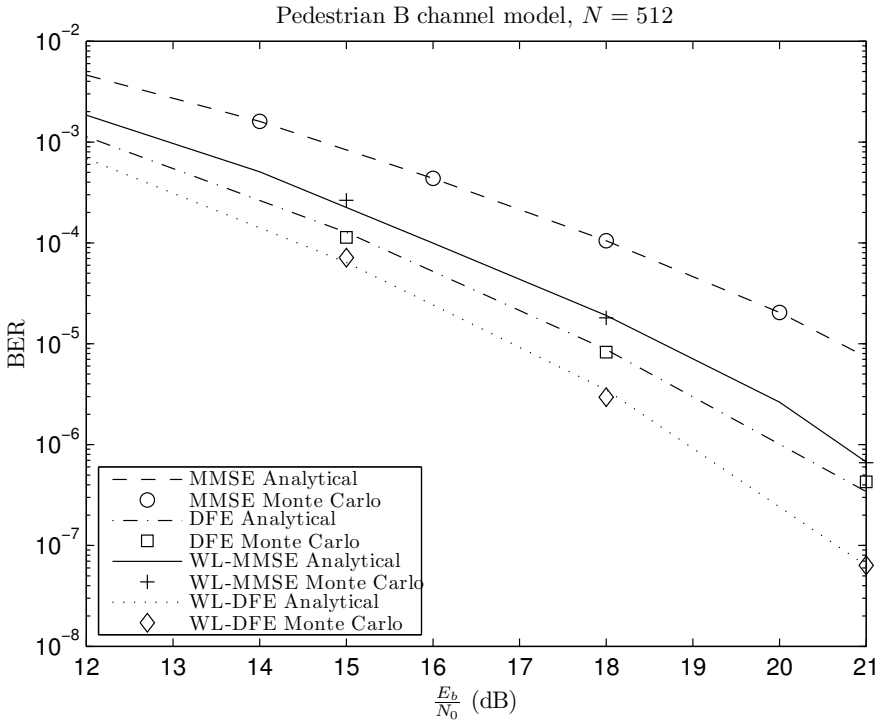

FIGURE 5.6 – Error performance for N = 512 and the Pedestrian B channel model in SC-FDE systems.

Figure 5.6 presents results for $N = 512$, the ITU-T Pedestrian B channel model and again a BPSK constellation. The same conclusions made for the previous case can also be stated for this scenario. For high E_b/N_0 ratios, the Monte Carlo simulation can be very time-consuming for the WL-MMSE receiver, due to low BER values. Thus, the use of the analytical method presented in this chapter allows us to derive the system performance in less time.

Results for the same scenario employed in Figure 5.5, but with 16-QAM/OQAM constellations in Figure 5.7 and 64-QAM/OQAM constellations in Figure 5.8, are shown. It is possible to see that the performance advantage between the widely linear equalizer and the strictly linear one in the case where a DFE is not used increases when the constellation size grows. With a DFE, the advantage for the widely linear equalizer remains the same with the increase of the constellation size. This can be explained by the fact that the WL-MMSE feedforward filter is more effective in eliminating the ISI when compared to the strictly linear MMSE feedforward filter, thus leaving less ISI for its feedback filter to remove. The

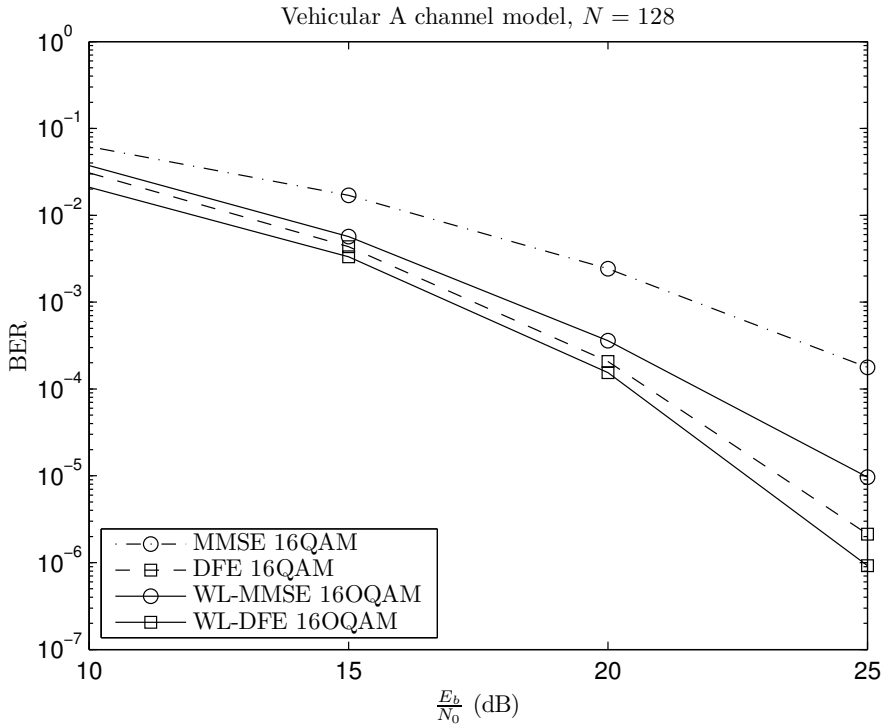

FIGURE 5.7 – Error performance for N = 128 and the Vehicular A channel model for 16-QAM/OQAM in SC-FDE systems.

effect of the linear feedforward filter's lower efficiency in removing the ISI is compensated by its feedback filter. It is interesting to note that the system with a WL-MMSE DFE transmitting symbols from a 64-OQAM constellation has better error performance that the system transmitting symbols from a 16-QAM constellation using regular linear MMSE equalization.

In Figure 5.9, results for $N = 128$, the Vehicular A channel model, but this time using convolutional coding, are presented. In this scenario, the performance gain from using the WL-MMSE equalizer is also observed, with its advantage growing with a weaker code ratio. For systems using a feedback filter, coding is not directly applicable due to the effect of error propagation in the feedback filter, which causes a significant amount of burst errors in the Viterbi decoder [42]. Efforts to overcome this problem in decision-feedback equalizers have been discussed in [70; 71].

The results presented from previous simulations considered that in DFE systems the

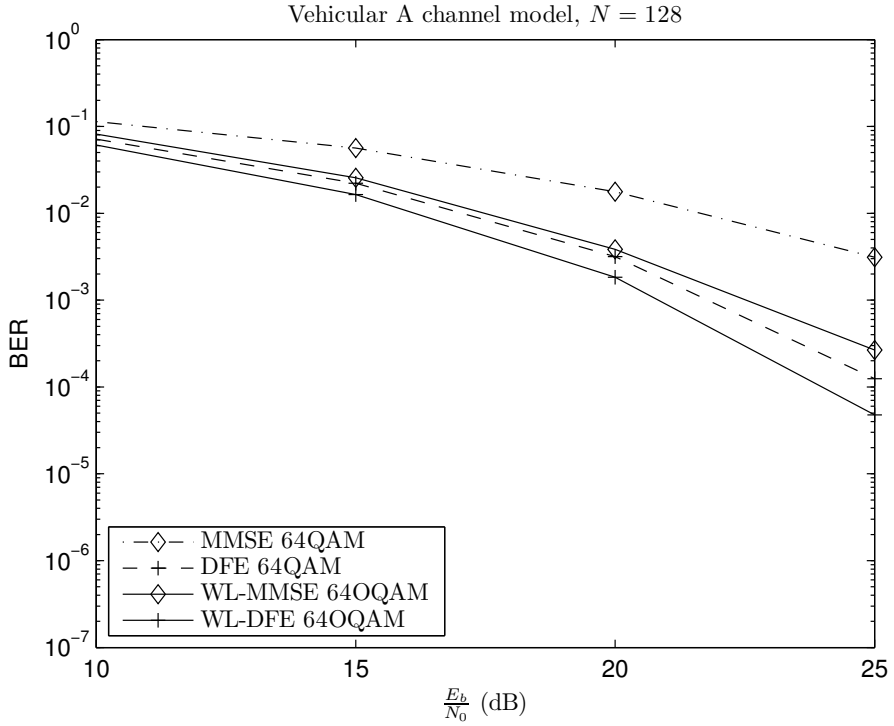

FIGURE 5.8 – Error performance for N = 128 and the Vehicular A channel model for 64-QAM/OQAM in SC-FDE systems.

feedback filter length $L_{\tilde{\mathbf{d}}}$ was equal to the channel impulse response length $L_{\tilde{\mathbf{h}}}$. Figure 5.10 shows the effect of the feedback filter length $L_{\tilde{\mathbf{d}}}$ on the error performance of SC-FDE DFE systems. Feedback filter sizes of $L_{\tilde{\mathbf{h}}}/2$, $L_{\tilde{\mathbf{h}}}/4$ and $L_{\tilde{\mathbf{h}}}/8$ were considered. The system using widely linear equalization has its error performance less sensitive to the error propagation effect caused by the smaller feedback filters when compared to the system using strictly linear equalization, because its feedfordward filter is more effective in removing the ISI. With smaller feedback filters, the computational complexity needed to calculate their coefficients in (5.27) and (5.28) is reduced.

The error performance results of widely linear MMSE Tomlinson-Harashima precoding applied to a SC-FDE system compared to its strictly linear version for a BPSK constellation, $N = 128$ and the ITU-T Vehicular A channel model are shown in Figure 5.11. In these simulations, channel estimation in the receiver and channel state information in the transmitter are assumed to be perfect. It is possible to see that the system using widely linear processing outperforms its strictly linear counterpart. This is due to the complete

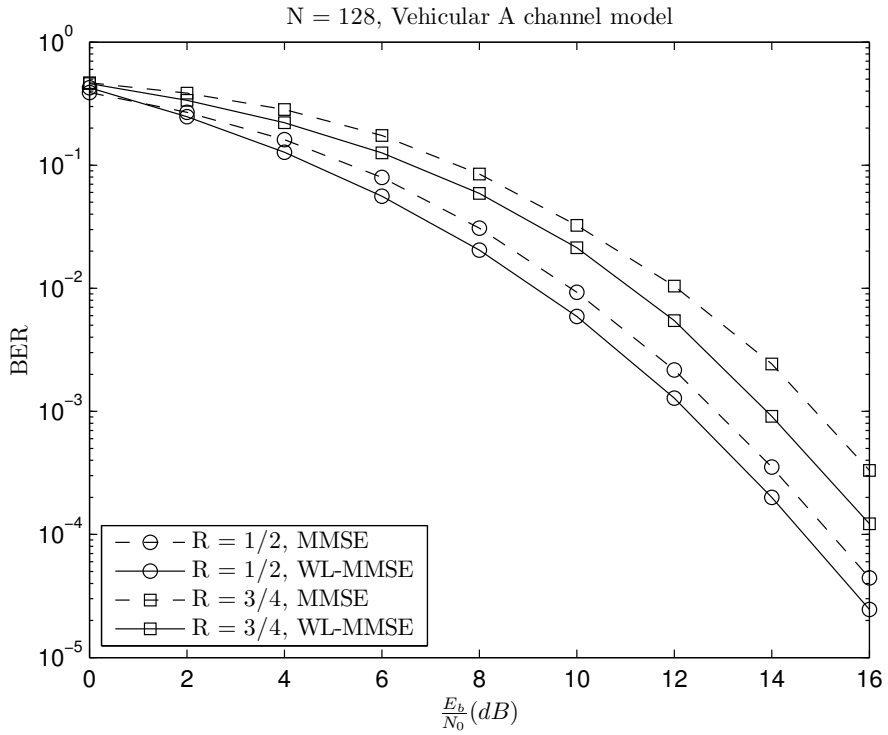

FIGURE 5.9 – Error performance for N = 128 and the Vehicular A channel model using coding in SC-FDE systems.

use of the statistics made available by the transmitted signal.

Results for Tomlinson-Harashima precoded systems using convolutional coding are presented in Figure 5.13. In this scenario, the performance gain from using widely linear-based precoding is also observed, with its advantage growing with a weaker code ratio.

The previous results when using Tomlinson-Harashima precoding assumed perfect channel estimation in the receiver and perfect channel state information at the transmitter ; however, this is an unlikely scenario in real conditions, because of channel variations. As stated before, Tomlinson-Harashima precoded systems rely on complete channel state information in the transmitter, which in turn needs perfect channel estimation in the receiver. A comparison on the impact of channel estimation errors and imperfect CSI in the error performance of MMSE-THP SC-FDE systems using or not widely linear equalization is presented in Figure 5.12 for $\frac{E_b}{N_0} = 19.25$ dB, $N = 128$ and the Vehicular A channel model. The imperfect channel estimates can be expressed as $\mathbf{H}_e = \mathbf{H} + \mathbf{E}_\mathbf{H}$, where $\mathbf{E}_\mathbf{H}$ is the

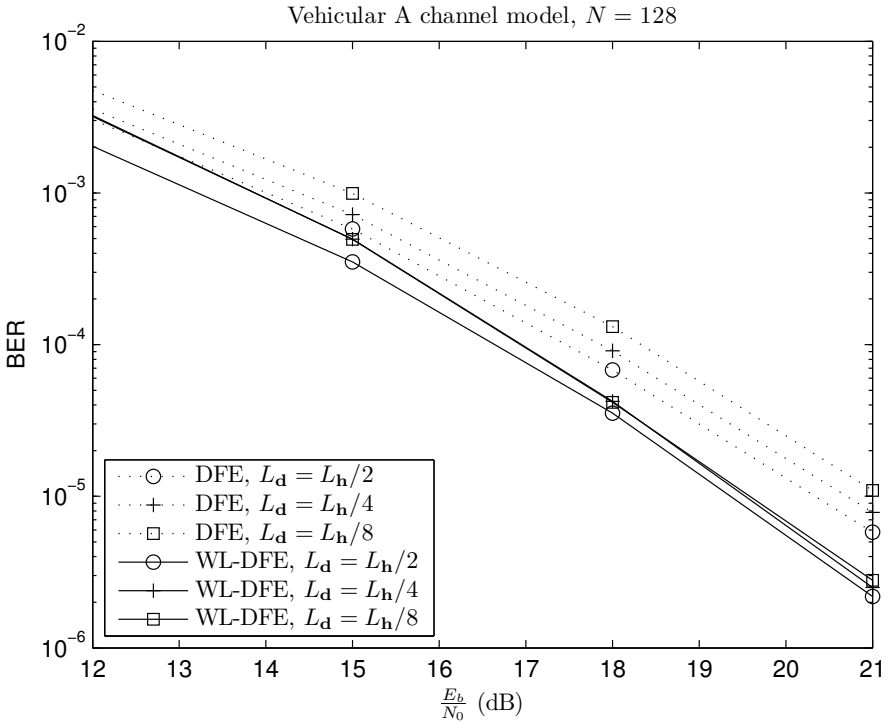

FIGURE 5.10 – Error performance for N = 128 and the Vehicular A channel model with different $L_{\tilde{\mathbf{d}}}$ sizes in SC-FDE DFE systems.

channel estimation error matrix, with its diagonal composed of zero-mean Gaussian distributed random variables with variance σ_e^2 [72]. This imperfect channel estimate is then passed to the transmitter, which will have erroneous CSI. While the error performance of the strictly linear system degrades as the error variance σ_e^2 increases, the widely linear precoded SC-FDE system is nearly insensitive to the increase of the channel estimation error variance.

5.5 Concluding Remarks

This chapter presented SC-FDE systems using widely linear MMSE-based equalization, decision-feedback equalization and Tomlinson-Harashima precoding. The use of widely linear processing brings, when the transmitter uses improper constellations, a performance gain compared to when common strictly linear MMSE processing is used. With respect to SC-FDE systems using MMSE-DFE equalization, together with the performance gain the

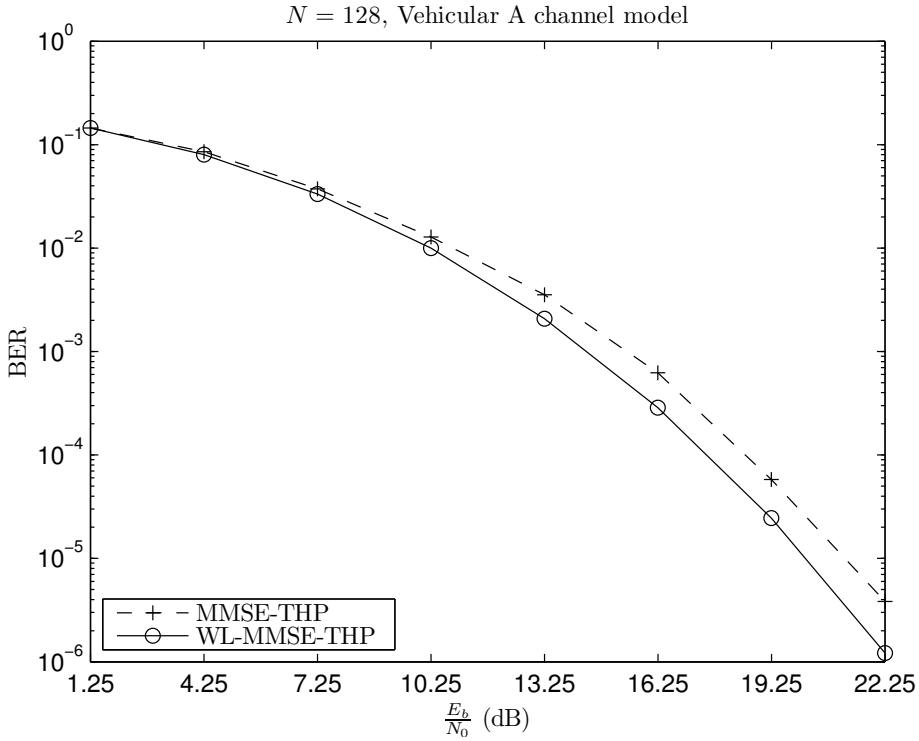

FIGURE 5.11 – Error performance for N = 128 and the Vehicular A channel model in THP SC-FDE systems.

use of widely linear processing also makes the error performance less sensitive to the feedback filter size. The error performance of Tomlinson-Harashima precoded systems using widely linear processing is also much less sensitive to channel estimation/CSI errors than the one from systems using strictly linear processing.

The next chapter brings the concluding remarks and suggestions for future work.

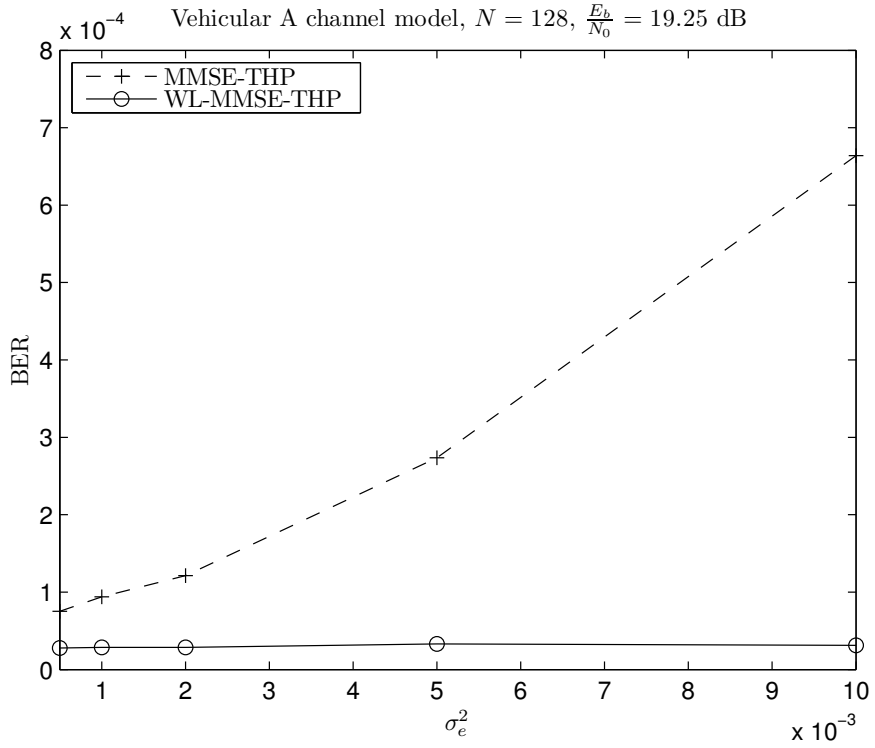

FIGURE 5.12 – The impact of channel estimation/CSI errors on the error performance of THP systems.

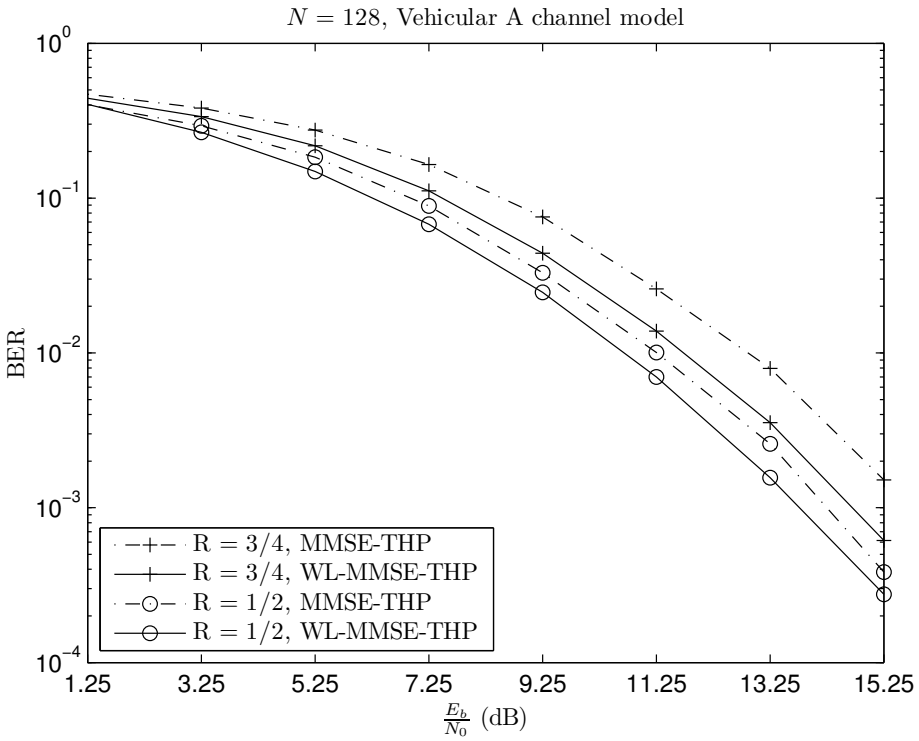

FIGURE 5.13 – Error performance for N = 128 and the Vehicular A channel model using convolutional coding in THP SC-FDE systems.

Chapter 6

Conclusion

In this thesis new precoding and equalization techniques for multicarrier systems were proposed, together with a theoretical analysis of their error performance. First, the error performance of precoded FBMC/OQAM systems was studied in Chapter 3. It was found out that this error performance is highly sensitive to residual ISI stemming from incomplete subchannel equalization. If the subchannel frequency response is flat or if the subchannel equalizer is large enough to compensate the frequency response there will be no residual ISI after equalization and the diversity order will be the same of a SC-FDE system. However, if subchannel equalization is incomplete, the residual interference after equalization will reduce the maximal diversity possible. An expression for the SINR considering these cases was found for uncoded transmissions ; this expression provides results consistent with the Monte Carlo simulation results.

Chapter 4 deals with the probability distribution function of the SINR in a precoded multicarrier system employing linear MMSE equalization. We proposed the lognormal distribution for this SINR as an accurate approximation in the sense of the BER, with its parameters minimizing the Kullback-Leibler distance to the target SINR. By minimizing the Kullback-Leibler distance, we ensure that the approximation will be precise in the lower tail of the pdf, which is the part that counts for the calculation of the BER. With this lognormal distribution as an abstraction for the system we have developed a novel analytical way to determine the error performance of a precoded multicarrier system employing linear MMSE equalization and convolutional channel coding. This method gives results matching

the Monte Carlo simulation results.

MMSE-based equalizers and Tomlinson-Harashima precoders for SC-FDE systems employing widely linear processing were proposed in Chapter 5. Since these equalizers and precoders make full use of the available second-order signal statistics if the transmitted signal is improper, they have a lower mean square error and better error performance. MSE and SINR expressions for all equalizers and precoders presented were developed, and were found to be in agreement with the Monte Carlo simulation results. Widely linear decision-feedback equalizers in SC-FDE systems have their error performance less sensitive to the length of the feedback filter. The error performance of Tomlinson-Harashima precoders using widely linear processing is much less sensitive to erroneous channel state information at the transmitter when compared to their strictly linear counterparts.

Future work to extend the results presented in this thesis could be centered in the following lines :

- We have seen in Chapter 5 that SC-FDE systems using widely linear equalization have less ISI after the feedforward filter when compared to regular linear systems. Thus, iterative widely-linear equalizers for SC-FDE systems (such as the linear ones presented in [73; 74]) could need less iterations to reach the desired error performance when compared to their strictly linear versions.
- Since FBMC/OQAM systems transmit signals from improper modulations, the application of widely-linear equalizers and precoders in linearly precoded FBMC/OQAM systems could increase their error performance. An analysis of their error performance when the subchannel frequency response is selective as the one done in Chapter 3 (if their residual ISI after incomplete equalization also affects the diversity order as much as in precoded FBMC systems using linear equalization) would also be desired.
- In [39] the diversity order of SC-FDE systems using linear equalization is studied. It was found out this diversity order varies with block and constellation sizes. In Chapter 5 it was found that with an increase in the constellation size the error performance advantage of SC-FDE systems using widely linear MMSE equalizers (without DFEs) over their linear counterpart improves. Thus, the mathematical analysis of the diversity order in SC-FDE systems using widely linear processing could bring interesting

results.

- A more fundamental analysis of maximal achievable bit rate of the widely linear decision-feedback equalizer and Tomlinson-Harashima precoder does not exist yet in the literature.
- It was found out in [75] that adaptive multicarrier transmission achieves a bit rate greater than or equal to that of SC-FDE systems using decision-feedback equalization. It remains to be verified if this result holds for SC-FDE WL-MMSE-DFE systems.
- The extension of the analysis presented in Chapter 4 for the case where subchannel equalization is incomplete in precoded FBMC/OQAM systems and for SC-FDE systems using widely linear processing.

Bibliography

[1] Robert F.H. Fischer, *Precoding and Signal Shaping for Digital Transmission.* John Wiley and Sons, 2002.

[2] T. Ahonen, *Tomi Ahonen Almanac 2012 - Mobile Telecoms Industry Review*, 1st ed. Tomi Ahonen, 2012.

[3] R. W. Chang, "Synthesis of band-limited orthogonal signals for multichannel data transmission," Bell Systems Technical Journal, 45 :1755-1796, Tech. Rep., 1966.

[4] S. Weinstein and P. Ebert, "Data Transmission by Frequency-Division Multiplexing Using the Discrete Fourier Transform," *IEEE Transactions on Communication Technology*, vol. 19, no. 5, pp. 628–634, October 1971.

[5] P. Siohan, C. Siclet, and N. Lacaille, "Analysis and design of OFDM/OQAM systems based on filterbank theory ," *IEEE Transactions on Signal Processing*, vol. 50, no. 5, pp. 1170–1183, May 2002.

[6] Hyung G. Myung and Junsung Lim, and David J. Goodman, "Single Carrier FDMA for Uplink Wireless Transmission," *IEEE Vehicular Technology Magazine*, pp. 30–38, Sep. 2006.

[7] H. Sari, G. Karam, and I. Jeanclaude, "Transmission Techniques for Digital Terrestrial TV Broadcasting," *IEEE Communications Magazine*, pp. 100 – 109, feb. 1995.

[8] D. Falconer, S. Ariyavisitakul, A. Benyamin-Seeyar, and B. Eidson, "Frequency Domain Equalization for Single-Carrier Broadband Wireless Systems," *IEEE Communications Magazine*, vol. 40, no. 4, pp. 58–66, Apr. 2002.

[9] Stefania Sesia and Issam Toufik, and Matthew Baker, *LTE "The UMTS Long Term Evolution" : From Theory to Practice*, 2nd ed. John Wiley and Sons, 2011.

[10] B. Picinbono, "On Circularity," *IEEE Transactions on Signal Processing*, vol. 42, no. 12, pp. 3473–3482, 1994.

[11] B. Picinbono and P. Chevalier, "Widely Linear Estimation with Complex Data," *IEEE Transactions on Signal Processing*, vol. 43, no. 8, pp. 2030–2033, 1995.

[12] P. Schreier, L. Scharf, and C. T. Mullis, "Detection and Estimation of Improper Complex Random Signals," *IEEE Transactions on Information Theory*, vol. 51, no. 1, pp. 306–312, Aug. 2005.

[13] P. Chevalier and F. Pipon, "New Insights Into Optimal Widely Linear Array Receivers for the Demodulation of BPSK, MSK, and GMSK Signals Corrupted by Noncircular Interferences - Application to SAIC," *IEEE Transactions on Signal Processing*, vol. 54, no. 3, pp. 870–883, Mar. 2006.

[14] G. Caire and S. Shamai, "On the Capacity of Some Channels with Channel State Information," *IEEE Transactions on Information Theory*, vol. 45, no. 6, pp. 2007–2019, Sep. 1999.

[15] J. J. Sánchez Sánchez, "Analysis of SC-FDMA and OFDMA Performance over Fading Channels," Ph.D. dissertation, Universidad de Málaga, 2011.

[16] H. Wang, X. You, B. Jiang, and X. Gao, "Performance Analysis of Frequency Domain Equalization in SC-FDMA Systems," in *2008 International Communications Conference - ICC 2008*, 2008, pp. 4342–4347.

[17] B. S. Chang, W. L. Lopez, and C. A. da Rocha, "Técnicas de Projeto para equalizadores por subcanal para sistemas FBMC/OQAM," in *XXVII Simpósio Brasileiro de Telecomunicações - SBrT 2009*, 2009.

[18] B. S. Chang, C. A. F. da Rocha, D. L. Ruyet, and D. Roviras, "On the Use of Precoding in FBMC/OQAM Systems," in *2010 International Telecommunications Symposium*, set. 2010.

[19] B. S. Chang and C. A. F. da Rocha, "On the Error Performance of Precoded Filterbank Multicarrier Systems Transmitting Through Highly Frequency Selective Channels," in *XXVIII Simpósio Brasileiro de Telecomunicações - SBrT 2011*, Sep. 2011.

[20] B. S. Chang, C. A. F. da Rocha, D. L. Ruyet, and D. Roviras, "On the Distribution of the SINR in Precoded Multicarrier Systems Using Linear MMSE Equalization," in *2012 16th IEEE Mediterranean Electrotechnical Conference (MELECON 2012)*, May 2012, pp. 703–706.

[21] ——, "On the Effect of ISI in the Error Performance of Precoded FBMC/OQAM Systems," in *The 18th Asia-Pacific Communications Conference (APCC 2012)*, Oct. 2012.

[22] H. Bölcksei, *Advances in Gabor Analysis*. Birkhäuser, 2003, pp. 321–352.

[23] P. Siohan and C. Roche, "Analytical design for a family of cosine modulated filter banks," in *Proceedings of the 1998 IEEE International Symposium on Circuits and Systems - ISCAS '98.*, vol. 5, May-3 Jun 1998, pp. 150–153.

[24] ——, "Cosine-modulated filterbanks based on extended Gaussian functions ," *IEEE Transactions on Signal Processing*, vol. 48, no. 11, pp. 3052–3061, Nov 2000.

[25] M. G. Bellanger, "Specification and design of a prototype filter for filter bank based multicarrier transmission," in *Proceedings of the 2001 IEEE International Conference on Acoustics, Speech, and Signal Processing, 2001 - (ICASSP '01)*, vol. 4, 2001, pp. 2417–2420.

[26] P. Siohan and C. Roche, "Derivation of extended Gaussian functions based on the Zak transform," *IEEE Signal Processing Letters*, vol. 11, no. 3, pp. 401–403, March 2004.

[27] B. Le Floch, M. Alard, and C. Berrou, "Coded orthogonal frequency division multiplex [TV broadcasting]," *Proceedings of the IEEE*, vol. 83, no. 6, pp. 982–996, Jun 1995.

[28] H. G. Feichtinger and T. Strohmer, *Gabor Analysis and Algorithms*. Birkhäuser, 1998.

[29] M. Bellanger and J. Daguet, "TDM-FDM Transmultiplexer : Digital Polyphase and FFT," *IEEE Transactions on Communications*, vol. 22, no. 9, pp. 1199–1205, Sep 1974.

[30] T. Ihalainen, T. Stitz, M. Rinne, and M. Renfors, "Channel Equalization in Filter Bank Based Multicarrier Modulation for Wireless Communications," *EURASIP Journal on Advances in Signal Processing*, Apr 2007.

[31] C. A. F. da Rocha and M. G. Bellanger, "Sub-Channel Equalizer Design Based on Geometric Interpolation for FBMC/OQAM Systems," in *2011 IEEE International Symposium on Circuits and Systems (ISCAS 2011)*, 2011.

[32] S. Nedic and N. Popovic, "Per-bin DFE for advanced OQAM-based multi-carrier wireless data transmission systems," in *2002 International Zurich Seminar on Broadband Communications, 2002. Access, Transmission, Networking.*, Feb. 2002, pp. 38–1–38–6.

[33] D. Waldhauser, L. Baltar, and J. Nossek, "MMSE subcarrier equalization for filter bank based multicarrier systems," in *IEEE 9th Workshop on Signal Processing Advances in Wireless Communications, 2008. SPAWC 2008.*, 2008, pp. 525–529.

[34] G. Cariolaro and F. C. Vagliani, "An OFDM scheme with a half complexity," *IEEE Journal on Selected Areas in Communications*, vol. 13, no. 9, pp. 1586–1599, Dec 1995.

[35] L. Vangelista and N. Laurenti, "Efficient implementations and alternative architectures for OFDM-OQAM systems," *IEEE Transactions on Communications*, vol. 49, no. 4, pp. 664–675, Apr 2001.

[36] ITU-R, "Guidelines for evaluation of radio transmission technologies for IMT-2000 - Recommendation M.1225," ITU, Tech. Rep., 1997.

[37] Lin, Yuan-Pei and Phoong, See-May, "BER minimized OFDM systems with channel independent precoders," *IEEE Transactions on Signal Processing*, vol. 51, no. 9, pp. 2369–2380, Sep. 2003.

[38] Z. Wang, X. Ma, and G. B. Giannakis, "OFDM or Single-Carrier Block Transmis-

sions ?" *IEEE Transactions on Communications*, vol. 52, no. 3, pp. 380–394, Mar. 2004.

[39] A. Tajer and A. Nosratinia, "Diversity Order in ISI Channels with Single-Carrier Frequency-Domain Equalizers," *IEEE Transactions on Wireless Communications*, vol. 9, no. 3, pp. 1022–1032, 2010.

[40] N. Benvenuto and S. Tomasin, "On the Comparison Between OFDM and Single Carrier Modulation With a DFE Using a Frequency-Domain Feedforward Filter," *IEEE Transactions on Communications*, vol. 50, no. 6, pp. 947–955, Jun. 2002.

[41] C. Panazio and A. de Paula, "An uncoded BER comparison between DFE-SCCP and OFDM using a convex analysis framework," in *IEEE International Symposium on Circuits and Systems - IEEE ISCAS 2011*, 2011.

[42] G. Huang, A. Nix, and S. Armour, "Decision Feedback Equalization in SC-FDMA," in *2008 IEEE 19th International Symposium on Personal, Indoor and Mobile Radio Communications*, Sep. 2008.

[43] M. Tomlinson, "New automatic equaliser employing modulo arithmetic," *Electronics Letters*, vol. 7, pp. 138–139, 1971.

[44] H. Harashima and H. Miyakawa, "Matched-transmission technique for channels with intersymbol interference," *IEEE Transactions on Communications*, vol. 20, no. 4, pp. 774–780, Aug 1972.

[45] Y. Zhu and K. B. Letaief, "Frequency Domain Equalization With Tomlinson-Harashima Precoding for Single Carrier Broadband Wireless Communications," in *IEEE Globecom 2006*, Nov. 2006, pp. 1–5.

[46] P. Schreier and L. Scharf, "Second-order analysis of improper complex random vectors and processes," *IEEE Transactions on Signal Processing*, vol. 51, no. 3, pp. 714–725, Mar. 2003.

[47] T. Ihalainen, A. Viholainen, T. H. Stitz, M. Renfors, and M. Bellanger, "Filter Bank

Based Multi-Mode Multiple Access Scheme For Wireless Uplink," in *17th European Signal Processing Conference - EUSIPCO 2009*, aug. 2009.

[48] C. H. G. Yuen, P. Amini, and B. Farhang-Boroujeny, "Single Carrier Frequency Division Multiple Access (SC-FDMA) for Filter Bank Multicarrier Communication Systems," in *CrownCom 2010*, jun. 2010, pp. 1–5.

[49] J. G. Proakis, *Digital Communications*, 4th ed. McGraw-Hill, 2000.

[50] M. Debbah, P. Loubaton, and M. de Courville, "Linear precoded OFDM transmissions with MMSE equalization : facts and results," in *ICASSP 2002*, 2002.

[51] G. Caire, G. Taricco, and E. Biglieri, "Bit-interleaved Coded Modulation," *IEEE Transactions on Information Theory*, vol. 44, no. 3, pp. 927–946, May 1998.

[52] E. Malkamaki and H. Leib, "Evaluating the performance of convolutional codes over block fading channels," *IEEE Transactions on Information Theory*, vol. 45, no. 5, pp. 1643–1646, Jul. 1999.

[53] K.-B. Song, A. Ekbal, S. T. Chung, and J. M. Cioffi, "Adaptive Modulation and Coding (AMC) for Bit-Interleaved Coded OFDM (BIC-OFDM)," *IEEE Transactions on Wireless Communcations*, vol. 5, no. 7, pp. 1685–1694, Jul. 2006.

[54] C. Sung, S. Chung, J. Heo, and I. Lee, "Adaptive bit-interleaved coded OFDM with reduced feedback information," *Communications, IEEE Transactions on*, vol. 55, no. 9, pp. 1649–1655, 2007.

[55] C. Snow, L. Lampe, and R. Schober, "Error Rate Analysis for Coded Multicarrier Systems Over Quasi-Static Fading Channels," *IEEE Transactions on Communications*, vol. 55, no. 9, pp. 1736–1746, Sep. 2007.

[56] C. Shin and H. Park, "A Closed-Form Expression of Instantaneous Bit Error Rate for BIC-OFDM Systems," in *Communications (ICC), 2010 IEEE International Conference on.* IEEE, 2010, pp. 1–5.

[57] D. Rende and T. Wong, "Bit-interleaved space-frequency coded Modulation for OFDM systems," *IEEE Transactions on Wireless Communications*, vol. 4, no. 5, pp. 2256–2266, Sep. 2005.

[58] N. H. Tran, H. H. Nguyen, and T. Le-Ngoc, "Bit-Interleaved Coded OFDM With Signal Space Diversity : Subcarrier Grouping and Rotation Matrix Design," *IEEE Transactions on Signal Processing*, vol. 55, no. 3, pp. 1137–1149, Mar. 2007.

[59] Z. Wang and G. B. Giannakis, "A Simple and General Parameterization Quantifying Performance in Fading Channels," *IEEE Transactions on Communications*, vol. 51, no. 8, pp. 1389 – 1398, aug. 2003.

[60] T. M. Cover and J. A. Thomas, *Elements of Information Theory.* Wiley, 1991.

[61] P. Hall, "On Kullback-Leibler Loss and Density Estimation," *The Annals of Statistics*, vol. 15, no. 4, pp. 1491 – 1519, apr. 1987.

[62] J. Aitchison and J. Brown, *The Log-normal Distribution.* Cambridge University Press, 1957.

[63] M. Simon and M. Alouini, *Digital Communication Over Fading Channels*, 2nd ed. Wiley-Interscience, 2005.

[64] M. Abramowitz and I. Stegun, *Handbook of Mathematical Functions with Formulas, Graphs and Mathematical Tables.* Dover Publications, 1964.

[65] P. Frenger, P. Tony, and A. Svensson, "Multi-rate Convolutional Codes," Chalmers University of Technology, Goteborg, Sweden, Tech. Rep., 1998, tech. Report 21.

[66] Z. Lin, P. Xiao, B. Vucetic, and M. Sellathurai, "Analysis of receiver algorithms for LTE SC-FDMA based uplink MIMO systems," *IEEE Transactions on Wireless Communications*, vol. 9, no. 1, pp. 60–65, Jan. 2010.

[67] R.D. Wesel and J.M. Cioffi, "Achievable Rates for Tomlinson-Harashima Precoding," *IEEE Transactions on Information Theory*, vol. 53, no. 1, pp. 824–831, Mar. 1998.

[68] A. Mirbagheri, K. Plataniotis, and S. Pasupathy, "An enhanced widely linear CDMA receiver with OQPSK modulation," *IEEE Transactions on Communications*, vol. 54, no. 2, pp. 261–272, Feb. 2006.

[69] J. Salz, "Optimum mean-square decision feedback equalization," *Bell System Technical Journal*, vol. 52, pp. 1341–1373, 1973.

[70] M. Eyuboglu, "Detection of coded modulation signals on linear, severely distorted channels using decision-feedback noise prediction with interleaving," *IEEE Transactions on Communications*, vol. 36, no. 4, pp. 401–409, apr. 1988.

[71] Y. Zhu and K. B. Letaief, "Single Carrier Frequency Domain Equalization with Noise Prediction for Broadband Wireless Systems," in *IEEE GLOBECOM 2004 - 2004 IEEE Global Telecommunications Conference*, 2004.

[72] J. Maurer, J. Jalden, and G. Matz, "Multi-threshold TOP-full-diversity vector perturbation precoding with finite-rate feedforward," in *Proc. Asilomar Conf. Signals, Systems Computers*, Oct. 2008, pp. 428–432.

[73] Nevio Benvenuto and Stefano Tomasin, "Iterative Design and Detection of a DFE in the Frequency Domain," *IEEE Transactions on Communications*, vol. 53, no. 11, pp. 1867–1875, Nov. 2005.

[74] F. Sainte-Agathe and H. Sari, "New Results in Iterative Frequency-Domain Decision-Feedback Equalization ," in *14th European Signal Processing Conference - EUSIPCO 2006*, 2006.

[75] Bertrand Devillers and Luc Vandendorpe, "Bit Rate Comparison of Adaptive OFDM and Cyclic Prefixed Single-Carrier with DFE," *IEEE Communications Letters*, vol. 13, no. 11, pp. 838–840, Nov. 2009.

le cnam

Bruno SENS CHANG

Nouvelles Techniques de Précodage et d'Égalisation pour les Systèmes Multiporteuses

UFSC

Résumé :
Dans cette thèse, de nouvelles techniques d'égalisation et de précodage pour des systèmes multiporteuses ont été proposées et analysées. D'abord, la probabilité d'erreurs des systèmes multiporteuses à base de bancs de filtres (FBMC) précodées a été analysée. Il a été montré que cette performance est très sensible à l'égalisation complète des sous-canaux. Lorsqu' il y a de l'interference inter-symbole residuelle qui vient de l'égalisation imparfaite des sous-canaux, il y a une perte de diversité ; cette diversité peut être récuperée avec l'utilisation d'un nombre de sous-canaux assez grand pour que chaque sous-canaux subisse de l'évanouissement plat ou avec l'utilisation d'un égaliseur par sous-canal avec une longueur suffisante pour compenser cette réponse en fréquence. Une approximation pour la distribution du rapport signal/bruit-plus-interfèrence (SINR) des systèmes SC-FDE qui utilisent égalisation MMSE linéaire a été ensuite proposée. Cette approximation utilise la distribution lognormal avec la plus petit distance de Kullback-Leibler vers la vraie distribution, et nous avons montré qu'elle est précise pour estimer la performance d'erreurs ; elle sert aussi comme une abstraction de ce système. Avec cette abstraction, une méthode précise pour obtenir la performance d'erreur analytique codée de ces systèmes a été proposée. Finalement, des précodeurs Tomlinson-Harashima (THP) et égaliseurs (linéaires et à retour de décision) largement linéaires pour des systèmes SC-FDE ont été proposés. Ces précodeurs et égaliseurs ont une meilleures performance comparés aux versions strictement linéaires lorsque les signaux de constellations impropres sont transmises. Aussi, le taux d'erreurs quand des égaliseurs à retour de décision sont utilisés est moins sensible à la longueur du filtre de retour. Quand des précodeurs largement linéaires sont utilisés, cette performance devient moins sensible aux erreurs d'estimation des canaux.

Mots clés :
Systèmes multiporteuses, Précodage, Égalisation, Traitement largement linéaire

le cnam

Bruno SENS CHANG

New Precoding and Equalization Techniques for Multicarrier Systems

UFSC

Abstract :
In this thesis, new precoding and equalization techniques for multicarrier systems were proposed and analyzed. First, the error performance of precoded filterbank multicarrier (FBMC) systems was analyzed. It was found out that this performance is highly sensitive to complete subchannel equalization. When there is residual intersymbol interference (ISI) stemming from imperfect subchannel equalization there is a loss of diversity ; this loss can be prevented with the adoption of a number of subchannels large enough so that each subchannel suffers flat fading or with the utilization of a subchannel equalizer with sufficient length to compensate the subchannel frequency response. After that, an approximation for the signal to interference-plus-noise ratio (SINR) distribution of SC-FDE systems using linear MMSE equalization was proposed. This approximation uses the lognormal distribution with the smallest Kullback-Leibler distance to the true distribution, and was shown to be precise in the error performance sense ; it serves as a system abstraction. With this abstraction, a precise method to obtain the analytical coded error performance of these systems was proposed. Finally, widely linear Tomlinson-Harashima precoders and equalizers (linear and decision-feedback) for SC-FDE systems were proposed. These precoders and equalizers have better error performance when compared to their strictly linear versions if signals coming from an improper constellation are transmitted. Their error performance when decision-feedback equalizers are used is less sensitive to the length of the feedback filter. When widely linear precoders are used, this error performance becomes less sensitive to channel estimation errors.

Keywords :
Multicarrier systems, Precoding, Equalization, Widely linear processing